



**Experimental and Numerical Study for Convective Drying of  
Deformable Rubber Sheet**

**Clement Kehinde Ajani**

**A Thesis Submitted in Fulfilment of the Requirements for the Degree  
of Master of Engineering in Mechanical Engineering**

**Prince of Songkla University**

**2018**

**Copyright of Prince of Songkla University**



**Experimental and Numerical Study for Convective Drying of  
Deformable Rubber Sheet**

**Clement Kehinde Ajani**

**A Thesis Submitted in Fulfillment of the Requirements for the  
Degree of Master of Engineering in Mechanical Engineering  
Prince of Songkla University**

**2018**

**Copyright of Prince of Songkla University**

**Thesis Title**            Experimental and Numerical Study for Convective Drying of  
Deformable Rubber Sheet

**Author**                    Mr. Clement Kehinde Ajani

**Major Program**        Mechanical Engineering

---

**Major Advisor**

.....  
(Assoc. Prof. Dr. Perapong Tekasakul)

**Examining Committee:**

.....Chairperson  
(Prof. Dr. Phadungsak Ratanadecho)

.....Committee  
(Assoc. Prof. Dr. Perapong Tekasakul)

.....Committee  
(Assoc. Prof. Dr. Charoenyut Dechwayukul)

The Graduate School, Prince of Songkla University, has approved this thesis as fulfillment of the requirements for the Master of Engineering Degree in Mechanical Engineering.

.....  
(Prof. Dr. Damrongsak Faroongsarng)

Dean of Graduate School

This is to certify that the work here submitted is the result of the candidate's own investigations. Due acknowledgment been made of any assistance received.

.....Signature

(Assoc. Prof. Dr. Perapong Tekasakul)

Advisor

.....Signature

(Mr. Clement Kehinde Ajani)

Candidate

I hereby certify that this work has neither been accepted in substance for any degree nor is it being submitted in candidature for any degree.

.....Signature

(Mr. Clement Kehinde Ajani)

Candidate

<b>Thesis Title</b>	Experimental and Numerical Study for Convective Drying of Deformable Rubber Sheet
<b>Author</b>	Mr. Clement Kehinde Ajani
<b>Major Program</b>	Mechanical Engineering
<b>Academic Year</b>	2018

### **ABSTRACT**

Natural rubber is one of the major exporting products of Thailand. A few number of research has been carried out on the operating parameters to ensure fast drying of this product. Investigations on the shrinkage of rubber sheets occurring during the drying process have not been conducted so far. Optimization of the operating parameters for the fast drying of rubber is presented in this work. Experimental work was set to vary the velocity, temperature, and relative humidity from 1.5 to 4.0 m /s, 60 to 70°C and 40 to 60% (ideal) respectively. Computational Fluid Dynamics (CFD) approach using the finite element method was used to study the 2D conjugate shrinkage behavior of the rubber sheet thickness under the convective drying condition. An isotropic, linear elastic model was assumed. The Arbitrary Lagrangian-Eulerian (ALE) method was used to solve the two-dimensional problem in accounting for the shrinkage effect. The inference from the experimental studies showed that drying at temperature of 65°C at 2.5 m/s was optimal for best rubber sheet quality as higher temperature affected the rubber sheets quality. Lastly, drying at the lowest possible relative humidity reduces the drying time, equilibrium moisture content and water activity. The optimal operating conditions from the experiment is 65°C, 2.5 m/s for the temperature and velocity. The rubber sheet moisture content was reduced to 0.4% db within 38 hours of drying. The shrinkage percentage was estimated to be 9.1%. The agreement between experimental and simulation results are acceptable in terms of statistical parameters. The formulated predictive model can be used as a quality index evaluation for rubber sheet and for drying process optimization. Water activity can also be used in locating regions that could be prone to microbial spoilage. The drying time was reduced in comparison to the traditional drying of rubber sheets.

**DEDICATION**

*To Jesus Christ my source of inspiration and to my parents*

*Mr. and Mrs. Samson Ajani*

## ACKNOWLEDGMENTS

I would like to express my profound gratitude to my advisor, Assoc. Prof. Dr. Perapong Tekasakul, for his expert guidance, advice, supervision and encouragement through the course of my study.

Also, I would like to appreciate Assoc. Prof. Dr. Stefano Curcio, Department of Computer Engineering, Modelling, Electronics and Systems, University of Calabria, Italy for his invaluable assistance on the CFD modelling. I would like to thank Assoc. Prof. Dr. Anil Kumar, of his guidance on the system design, Dr. Racha Dejchanchaiwong for providing guidance where needed, Assoc. Prof. Dr. Thanansak Theppaya, Assoc. Prof. Dr. Charoenyut Dechwayukul for their tireless guidance and useful suggestions towards the progress of my research. I would like to thank Prof. Dr. Phadungsak Ratanadecho of Thammasat University for COMSOL Multiphysics license use. I also thank the rest of my thesis examination committee members for their valuable time and suggestions in helping me to improve the thesis.

My appreciation goes to the Graduate school of Prince of Songkla University for granting the Thailand Education Hub for ASEAN countries- TEH-AC scholarship. The Natural Rubber Innovation Research Institute, Prince of Songkla University for a research funding grant number NG590305S, Saikao Rubber Cooperative and Department of Mechanical Engineering, Faculty of Engineering, for supporting my study in various aspects. I would like to thank all lecturers in Mechanical Engineering Department, Prince of Songkla University for their assistance. To my energy research group members Sonthawi Sonthikun, Kunchira Thongboon and others, I am grateful for your assistance.

Lastly, I am immensely grateful to my parents, siblings, my family members, friends who endured the long period at home when I was away for study. My pastors, Pastor Kolawole Obaseye (KGM, Nigeria), Pastor Williams Akanmu (Nigeria) and Pastor Chaiyapruck Piwruangnont (HIM Thailand) for your prayers. My friends, brothers and sisters at ICF, PSU for the sweet fellowship and brotherhood.

Clement Kehinde Ajani



## TABLE OF CONTENTS

<b>ABSTRACT.....</b>	<b>V</b>
<b>DEDICATION.....</b>	<b>VI</b>
<b>ACKNOWLEDGMENTS .....</b>	<b>VII</b>
<b>TABLE OF CONTENTS .....</b>	<b>VIII</b>
<b>LIST OF TABLES .....</b>	<b>X</b>
<b>LIST OF FIGURES .....</b>	<b>XI</b>
<b>LIST OF ABBREVIATIONS .....</b>	<b>XIV</b>
<b>CHAPTER 1.....</b>	<b>1</b>
<b>INTRODUCTION.....</b>	<b>1</b>
1.1 Background.....	1
1.2 Research Objectives.....	3
1.3 Scope of Work .....	3
<b>CHAPTER 2.....</b>	<b>4</b>
<b>LITERATURE REVIEW .....</b>	<b>4</b>
2.1 Computational fluid dynamics.....	4
2.2 Simulation Methodology .....	6
2.3 CFD Reviews for rubber sheet drying .....	7
2.4 Continuum Mechanics .....	9
2.5 Thermodynamic equilibrium .....	12
<b>CHAPTER 3.....</b>	<b>15</b>
<b>METHODS AND MATERIALS .....</b>	<b>15</b>
3.1 Numerical methods .....	15
3.1.1 Governing Equations .....	15
3.1.2 Computational domain of a rubber sheet drying chamber.....	19
3.1.3 Mesh Refinement study .....	20
3.1.4 Simulation procedure .....	20
3.2 Experiment and Experimental analysis.....	21
3.3 Statistical analysis.....	24
<b>CHAPTER 4.....</b>	<b>26</b>
<b>RESULTS AND DISCUSSION .....</b>	<b>26</b>

	ix
4.1 Numerical modelling results .....	26
4.2 Experimental results.....	38
<b>CHAPTER 5.....</b>	<b>72</b>
<b>CONCLUSION AND RECOMMENDATION .....</b>	<b>72</b>
5.1 Conclusions.....	72
5.2 Recommendations.....	72
<b>REFERENCES.....</b>	<b>74</b>
<b>APPENDICES .....</b>	<b>82</b>
<b>APPENDIX A .....</b>	<b>83</b>
<b>APPENDIX B .....</b>	<b>86</b>
<b>APPENDIX C .....</b>	<b>94</b>

**LIST OF TABLES**

Table 3.1 Parameters exploited for simulation.	20
Table 3.2 Description of measurement positions of the experimental setup	23
Table 4.1 Mesh refinement study parameters.	26
Table 4.2 Summary of the experimental results.	38
Table 4.3 Influence of velocity variation on drying time and rubber sheet quality at 60°C and 40% RH.	47
Table 4.4 Influence of temperature variation on drying time at 4. m/s and 40% RH.	54
Table 4.5 Influence of velocity at 65°C and 40% RH on drying time.	64
Table 4.6 Influence of relative humidity on drying time.	69
Table 4.7 Summary of all experimental results.	71

## LIST OF FIGURES

Figure 2.1 Diagrammatic representation of the CFD modelling.	6
Figure 2.2 The positions of integer $i$ and nodes of thickness of rubber sheets [45].	7
Figure 2.3 One-dimensional example of Lagrangian, Eulerian and ALE mesh and particle motion [52].	11
Figure 3.1 Schematic diagram of the computational domain and boundary conditions for numerical investigation.	19
Figure 3.2 Experimental setup.	22
Figure 3.3 Experimental set up displaying locations of thermocouples and relative humidity probe.	23
Figure 3.4 Linear fitting of $d_{ex0}$ vs. $d_{Cw}$ for the tested experimental conditions.	25
Figure 4.1 Grid evaluation using the moisture content variation.	27
Figure 4.2 Expansion illustration of the time evolution of flow field and of the calculated streamlines accounting for rubber sheet shrinkage.	29
Figure 4.3 Time evolution of Moisture content variation.	30
Figure 4.4 Moisture content variation across rubber sheet thickness.	30
Figure 4.5 Comparism of numerical simulation and experiment for moisture content.	31
Figure 4.6 Time evolution of temperature developed in the rubber sheet during convective drying along x- axis.	32
Figure 4.7 Temperature variation across rubber sheet thickness along the x- axis.	33
Figure 4.8 Time evolution of (a) first principal shrinkage stress and (b) shrinkage strain tensor in x direction.	36
Figure 4.9 CLSM scan images (a) before drying: position 1 (b) after drying: position 1 (c) after drying: position 2 (d) after drying: position 3.	37
Figure 4.10 Shrinkage model prediction and experimental validation.	38
Figure 4.11 Temperature distribution in the chamber at 1.5 m/s, 40% RH, and 60°C.	39
Figure 4.12 Inside (RH1) and ambient relative humidity (RH2) at 1.5 m/s, 40% RH, and 60°C.	40
Figure 4.13 Moisture content evolution with time at 1.5 m/s, 40% RH, and 60°C.	41
Figure 4.14 Temperature distribution in the chamber at 3.0 m/s, 40% RH, and 60°C.	41

Figure 4.15 Inside (RH1) and ambient relative humidity (RH2) at 3.0 m/s, 40% RH, and 60°C.	42
Figure 4.16 Moisture content evolution with time at 3.0 m/s, 40% RH, and 60°C.	43
Figure 4.17 Temperature distribution in the chamber at 3.5 m/s, 40% RH, and 60°C.	43
Figure 4.18 Inside (RH1) and ambient relative humidity (RH2) at 3.5 m/s, 40% RH, and 60°C.	44
Figure 4.19 Moisture content evolution with time at 3.5 m/s, 40% RH, and 60°C.	45
Figure 4.20 Temperature distribution in the chamber at 4.0 m/s, 40% RH, and 60°C.	45
Figure 4.21 Inside (RH1) and ambient relative humidity (RH2) at 4.0 m/s, 40% RH, and 60°C.	46
Figure 4.22 Moisture content evolution with time at 4.0 m/s, 40% RH, and 60°C.	47
Figure 4.23 Moisture content profile with time at varying velocity.	48
Figure 4.24 Temperature distribution in the chamber at 4.0 m/s, 40% RH, and 65°C.	49
Figure 4.25 Inside (RH1) and ambient relative humidity (RH2) at 4.0 m/s, 40% RH, and 65°C.	49
Figure 4.26 Moisture content evolution with time at 4.0 m/s, 40% RH, and 65°C.	50
Figure 4.27 Rubber sheets with bubbles formed at 4.0 m/s, 40% RH and 65°C.	50
Figure 4.28 Temperature distribution in the chamber at 4.0 m/s, 40% RH, and 70°C.	51
Figure 4.29 Inside (RH1) and ambient relative humidity (RH2) at 4.0 m/s, 40% RH, and 70°C.	52
Figure 4.30 Moisture content evolution with time at 4.0 m/s, 40% RH, and 70°C.	52
Figure 4.31 Rubber sheets with bubbles formed at 4.0 m/s, 40% RH and 70°C.	53
Figure 4.32 Moisture content variation at varying temperature.	54
Figure 4.33 Temperature distribution in the chamber at 2.5 m/s, 40% RH and 65°C.	55
Figure 4.34 Inside (RH1) and ambient relative humidity (RH2) at 2.5 m/s, 40% RH and 65°C.	56
Figure 4.35 Moisture content evolution with time at 2.5 m/s, 40% RH, and 65°C.	56
Figure 4.36 Temperature distribution in the chamber at 3.0 m/s, 40% RH and 65°C.	57
Figure 4.37 Inside (RH1) and ambient relative humidity (RH2) at 3.0 m/s, 40% RH and 65°C.	58
Figure 4.38 Moisture content evolution with time at 3.0 m/s, 40% RH and 65°C.	59
Figure 4.39 Temperature distribution in the chamber at 3.5 m/s, 40% RH and 65°C.	60

Figure 4.40 Inside (RH1) and ambient relative humidity (RH2) at 3.5 m/s, 40% RH and 65°C.	60
Figure 4.41 Moisture content evolution with time at 3.5 m/s, 40% RH and 65°C.	61
Figure 4.42 Temperature distribution in the chamber at 4.0 m/s, 40% RH and 65°C.	62
Figure 4.43 Inside (RH1) and ambient relative humidity (RH2) at 4m/s, 40% RH and 65°C.	62
Figure 4.44 Moisture content evolution with time at 4m/s, 40% RH and 65°C.	63
Figure 4.45 Moisture content variation with varying velocity at 65°C.	64
Figure 4.46 Temperature distribution in the chamber at 4.0 m/s, 50% RH, and 60°C.	65
Figure 4.47 Inside (RH1) and ambient relative humidity (RH2) at 4.0m/s, 50% RH, and 60°C.	66
Figure 4.48 Moisture content evolution with time at 4.0 m/s, 50% RH, and 60°C.	67
Figure 4.49 Temperature distribution in the chamber at 4.0 m/s, 60 RH, and 60°C.	68
Figure 4.50 Inside (RH1) and ambient relative humidity (RH2) at 4.0 m/s, 60% RH, and 60°C.	68
Figure 4.51 Moisture content evolution with time at 4.0 m/s, 60% RH, and 60°C.	69
Figure 4.52 Moisture content variation at varying relative humidity.	70

## LIST OF ABBREVIATIONS

NR	Natural Rubber
RSS	Ribbed Smoked Sheet
ADS	Air Dried Sheet
% db	% Dry basis
CFD	Computation Fluid Dynamics
RH	Relative Humidity
MC	Moisture Content
$D_{eff}$	Effective diffusion coefficient of water in the air )m <sup>2</sup> /s(
$C_2$	Water concentration in air (mol/m <sup>3</sup> )
$C_{pa}$	Air specific heat J/(kg K)
$C_{ps}$	Rubber specific heat J/(kg K)
$C_v$	Vapor concentration in rubber sheet mol/m <sup>3</sup>
$D_a$	Diffusion coefficient of water in air m <sup>2</sup> /s
$D_v$	Effective diffusion coefficient of vapor in rubberm <sup>2</sup> /s
$D_w$	Capillary diffusion coefficient of water in rubberm <sup>2</sup> /s
$I$	Volumetric rate of evaporation mol/(m <sup>3</sup> s)
$p_v$	Vapor pressure of water Pa
$p_{vs}$	Saturated vapor pressure of water Pa
$R$	Gas constant J/(mol K)
$T$	rubber sheet temperature K

$T_2$	Air temperature K
$T_{air}$	Air temperature at the drier inlet K
$u_0$	Air velocity at the drier inlet (m/s)
$U_r$	Relative humidity of air
$X_b$	Moisture content on a dry basis kg water/kg dry solid
$a_w$	Activity coefficient of water (liquid phase)
$n$	unity vector normal to the surface
$X_{b0}$	Initial moisture content
$d\varepsilon_x$	Variation of rubber sheet thickness
$dC_w$	Variation of water concentration
CSLM	Confocal Laser Scanning Microscope
$R^2$	Coefficient of determination
RMSE	Root-Mean-Square Error
$C_w$	Concentration of water in the rubber sheet (mol/m <sup>3</sup> )
$D_w$	Moisture diffusion coefficient in rubber sheet (m <sup>2</sup> /s)
$T$	Temperature of rubber sheet (K)
$\rho_s$	Density of rubber sheet (kg/m <sup>3</sup> )
$C_{ps}$	Specific heat of rubber (J/kg K)
$K_{eff}$	Effective thermal conductivity of the natural rubber (W/m K).
$\rho_a$	Air density (kg/m <sup>3</sup> )



$P$  Drying chamber pressure (N/m<sup>2</sup>)

$u$  Velocity vector (m/s)

$t$  Time (s),

$\mu$  Dynamic viscosity.

$E_y$  Young modulus

$\nu$  Poisson ratio,

$\sigma$  Stresses

$t_x$  Instantaneous thickness

#### Subscript

0 Initial condition (t=0)

atm Atmospheric conditions

w water

2 water concentration in the air

#### Superscript

$T$  Transpose

## CHAPTER 1

### INTRODUCTION

#### 1.1 Background

Thailand is a leading producer of natural rubber (NR) sheet in the world, exporting about 3.8 million tons, which accounted for 37% of global natural rubber production in 2017. Natural rubber is commercially produced in four forms among which are the Block rubber (STR), ribbed smoked sheet (RSS), concentrated latex and other forms [1-3].

The factors affecting the drying process optimization and quality of dried products such as rubber sheets include the relative humidity, temperature, air velocity, material size, initial moisture content, energy and drying time. Drying process optimization is aimed at production cost minimization while maintaining the quality of the products. The drying time alongside the energy consumption are parameters needed to be minimized [4]. The limitations associated with fuel usage in RSS production is the effect of the moisture of combusted gas from firewood burning that retards the rubber sheet drying time, color and could also affect the ecosystem [5-6]. Also, the drying process is energy consuming, hence, parameters optimization is pertinent for the enhancement of the drying process efficiency in terms of the production time and energy usage, without compromising the product quality [7]. Drying shrinkage is defined as the contracting of a porous materials as a result of capillary water removal. This shrinkage engenders increase in the tensile stress, which results in warping internally, cracking and deflection externally [8].

Computational fluid dynamics (CFD) technique is increasingly becoming popular in modelling of fluid flow, heat and mass transfer. This is because CFD is an accurate, effective and cost-efficient method [9]. The flow and temperature behavior in the drying system can be studied by using CFD. It involves discretization of the conservation of mass, momentum and energy [10]. It also has a wide usage in many industrial processes. Simultaneous heat and mass transfer under transient conditions is common in drying processes and CFD simulations have been widely used to analyse problems of fluid flow in drying processes [10-12]. Understanding fluid flow and heat

transfer in the natural rubber drying process will help improve rubber drying process, quality, production time, energy and efficiency. Previous studies have reported the use of the CFD modelling of single-phase fluid flow and heat transfer in rubber-smoking rooms [9, 13]. Others used a conjugate approach to solve the heat and mass transfer in the rubber sheet without the effect of the shrinkage [14-15]. However, the shrinkage models in CFD simulation are presented by Curcio and Avaser [16] by investigating shrinkage and transport phenomena during convective drying of vegetables. The Finite Elements Method (FEM) was exploited. The system of PDEs was referred to a time dependent deformed mesh, accounting for food shrinkage.

Shrinkage coefficient is pertinent for modelling of the drying shrinkage field, and hence, an accurate estimation of the coefficient is important [8]. Drying shrinkage occurs because of the moisture migration due to the drying process [17]. It takes place during the simultaneous heat and mass transfer of porous and composite materials (Rubber, concretes, wood). However, current literatures on drying of rubber solely considers the drying models with no particular consideration of the rubber shrinkage during the drying process [9, 14-15, 18-19]. Hence, the investigation of the optimal operating parameters for rubber sheet drying with the shrinkage effect is considered in the present study.

Perspective of the present study is to reduce the drying time and improve the quality of the dried rubber sheet by evaluating the shrinkage, enhancing heat and mass transfer through forced convection at high air velocity using CFD and experimental validation. The concept of fast drying is primarily related to the operating velocity of the drying air and the optimization objective is to determine best operating conditions for the drying rubber sheets. According to the international standard and quality packaging for natural rubber grades, shrinkage characteristics and bubble formation (A result of uneven shrinkage stresses in the rubber sheet) during drying are key quality evaluation criteria for the determination of the marketability of the dried products [20-21]. Shrinkage of rubber sheet takes place simultaneously with moisture diffusion during drying. Hence, understanding the shrinkage phenomena in rubber sheet plays an important role in the drying process. This research will then be focused on study of CFD simulation of rubber shrinkage and optimizing operating parameters for rubber sheet fast drying.

## **1.2 Research Objectives**

In this research, CFD technique is applied to analyze the flow fields, and heat and mass transfer during the rubber sheet drying period. The main objectives of this research are:

1. To determine the optimal condition of the operating parameters (velocity, temperature, RH) for rubber sheet fast drying.
2. To study the flow field, heat and mass transfer of the rubber sheet using the CFD simulation, validated with the experimental results.
3. To formulate predictive model to investigate the effect of shrinkage on the rubber sheet drying by the CFD simulation and experiment for the evaluation of the rubber sheet product quality and optimization of rubbers sheet drying process.

## **1.3 Scope of Work**

Flow, heat and mass transfers of the rubber sheet in the rubber sheet fast drying process with the shrinkage effect alongside the experimental validation are studied. The scope of the work includes:

1. Design the drying chamber with maximum capacity of 4 sheets.
2. Parametric study of the rubber sheet drying and determine the optimum conditions for fast drying (velocity varied from 1.5-4.0 m/s, temperature varied from 60 to 70oC and relative humidity regulated at (ideal) average value as from 40 to 60 %).
3. Numerically simulate shrinkage behavior of a rubber sheet using a 2D model with experimental validation.

## CHAPTER 2

### LITERATURE REVIEW

#### 2.1 Computational fluid dynamics

CFD is a method to study heat transfer, fluid flow, mass transfer and other phenomena using computer-based simulation. It is a powerful and versatile technique used for several industrial and non-industrial applications [22]. Numerical algorithms are the bedrock for the building of CFD codes used in solving problems of fluid flow. A pre-processor, solver and post-processor are the three basic elements of all CFD codes [22]. CFD codes such as ANSYS FLUENT software using finite volume approach is employed for the simulation of the interaction of fluid flow inside the drying chamber [23]. Other codes such as COMSOL Multiphysics, ANSYS CFX use finite element approach and are used for handling of more complex problems [24]. Dryer performance can be improved, and dried materials can be analyzed and improved by the use of CFD modelling. It is employed in the study of various ventilation systems and used in the determination of the distribution of temperature and flow [14-15, 18, 25].

Applications of fluid flow, heat, momentum and mass transfer in the design of drying process have received a remarkable attention and development within the last few decades. Problems involving complex geometry, heat, momentum and mass transfer, chemical reactions and phase change, which hitherto involves the use of expensive experimental rigs can presently be modelled using high level temporal and spatial accuracy on personal computers [26]. Various thermal-hydraulic phenomena can be easily quantified using CFD. Several billions of production costs are saved across several disciplines [27-28].

##### 2.1.1 Finite difference Method

The basic concept of finite difference method (FDM) is to replace the partial derivatives by approximations obtained by Taylor expansions near the point of interests. FDM underlines principles involving the replacement of the domains where the independent variables in the partial differential equations (PDEs) are defined by a

finite grid or mesh of points where the approximation of the dependent variable is done. The partial derivatives of each grid point are approximated from the neighboring values in the PDEs [29]. Several FDM commercial softwares exist such as Diffpack, ELLPACK, Cogito and COMPOSE [30, 31].

### **2.1.2 Finite Volume method**

The finite volume method (FVM) is a numerical method for solving partial differential equations that calculate the values of the conserved variables averaged across the volume. FVM uses Stokes theorem to obtain its formula approximating the differential operators [32]. The conservation law in the integral form is satisfied for control volume on the domain of interest to an appreciable degree of approximation. FVM's popularity is due to its advantages when compared to the FDM [33]. FLUENT is a very popular CFD whose implementation is based on discretization using the FVM and is used in the simulation of 3D and viscous flows [34]. It is used in aerospace, chemical and automotive industries among others. In ANSYS FLUENT there are no room for the modification of the codes not implemented by default. The User Defined Functions (UDFs) can be used to add other codes using C programming language and loaded in the solver [35].

### **2.1.3 Finite element method**

The name "finite element method (FEM)" was derived by Clough [36]. In history, NASTRAN, ASKA, and SAP are most prominent FEM programs with applications in automotive and aerospace industries [37]. Finite element programs are versatile programs with various usage in engineering and science [38]. Initially used for structural analysis, it has gained more popularity in multiphysics problems such as fluid structure interactions and other fluid flow problems [39-40]. The principle of virtual displacements (work) is employed to formulate FEM. The finite element analysis of complex systems usually requires the solution of a large number of algebraic equations based on the multiphysics problems and types of analysis [41-42]. FEM gives an easier flexibility of modelling geometries that are complex compared to the FDM and FVM. It has a wide usage in the resolution of many flow related phenomenon such as mechanical, structural, fluid dynamics and heat transfer problems [43]. Also due to advancement in hardware and software, FEM can be used

in handling viscoelastic and hyper elastic material models. FEM packages include COMSOL Multiphysics, ANSYS CFX, ABAQUS [24]. Commercially available COMSOL Multiphysics package is used in the present study because of its flexibility and ease in handling complex fluid problems.

## 2.2 Simulation Methodology

Generally, numerical algorithm is made of these steps: integrating the governing equations of the fluid flow over the domains control volume, changing of the integrated equation to algebraic equation, discretization, solving of the algebraic equations using the method of iteration [44]. In defining fluid flow problems ranging from a point, angles, lines, surfaces and solids inside a drying chamber, CFD fills the volume of the dryer with fluid. The mesh (uniform or non-uniform) is defined and the appropriate solvers is used to solve the problem. Several post processing of the results is then carried out. Fig. 2.1 shows a diagrammatic representation of the CFD modelling methods.

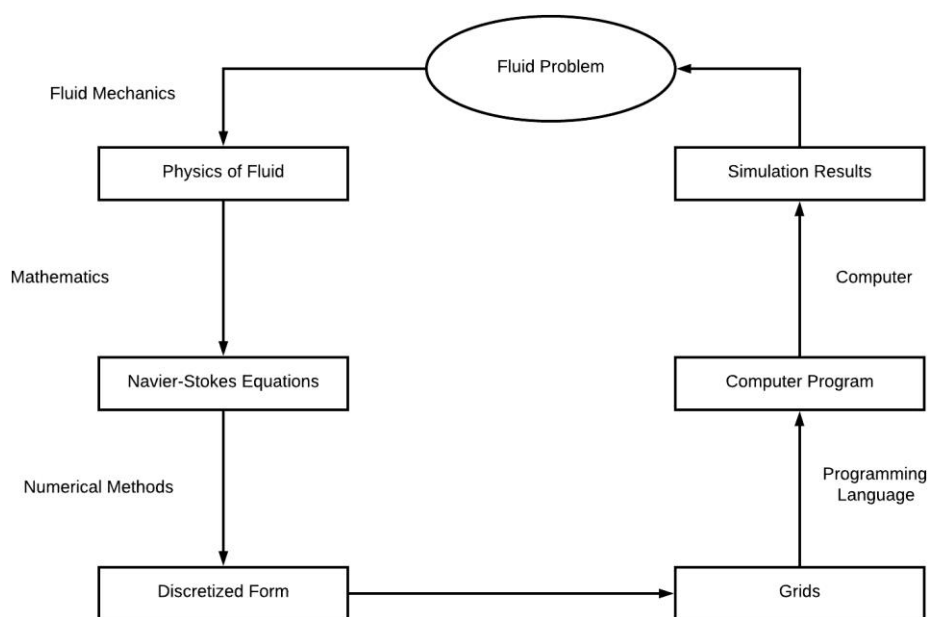


Figure 2.1 Diagrammatic representation of the CFD modelling.

Jitjack et al. [45] applied the finite difference method, in determining the reduction rate of the moisture content in the rubber sheet on dry basis. The diagrammatical representation of the finite difference scheme is shown in Fig. 2.2.

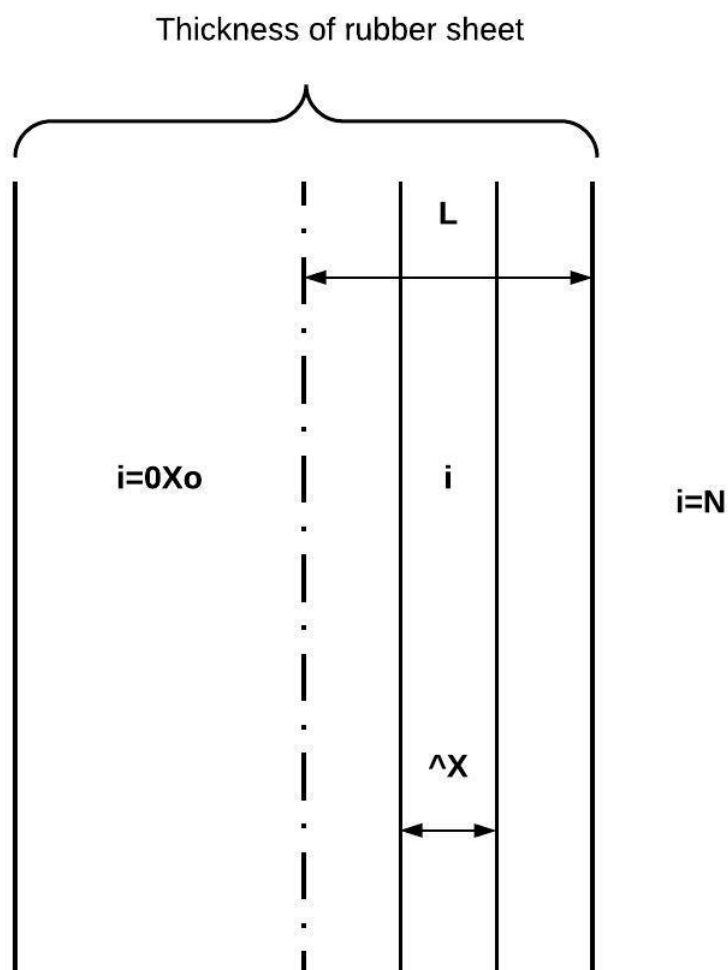


Figure 2.2 The positions of integer  $i$  and nodes of thickness of rubber sheets [45].

### 2.3 CFD Reviews for rubber sheet drying

In the last few decades, several researchers have used CFD for the design and evaluation of the NR sheet drying systems. Promtong and Tekasakul [9] studied the temperature distribution of rubber smoking room using the finite volume method and compared with experiment. The simulation was conducted using a CFD program FLOVENT V5.2 to study at near steady period. Temperature measurements were carried out in an empty room and compared with CFD simulation. With an efficiency of 65%, it established a benchmark for NR smoke room optimization subsequently



Tekasakul and Promtong [13] investigated the temperature and velocity using CFD. It was discovered that the ventilating lids, gas supply ducts and size need to be optimized. Sonthikun et al. [19] achieved drying of natural rubber sheet to reduce moisture content from 34.26% to 0.34% (db) within 48 hours using a solar-biomass dryer. In order to optimize the circulating fan, CFD technique was employed for the simulation of the system distribution of air flow and temperature. Dejchanchaiwong et al., (2014) used CFD modelling of single-phase and multicomponent flows for the simulation of the relative humidity and temperature at different points in an empty NR drying chamber. In all planes, unlike the single-phase model, the multicomponent model temperature distribution is relatively uniform. Thus, the multiphase model is deemed superior. The inclusion of water vapor in the multiphase model increases the agreement between model and experimental temperature data. Clearly, the multicomponent model is more appropriate for simulating chambers containing rubber sheets [18].

Tekasakul et al. [46] computationally investigated the effects of moisture and heat transfer on NR drying using a 3-D modelling. A temperature range from 4.0 to 7.7°C was observed to be the disparity between experimental and simulated work. As a base for the design of an effective NR drying system, the predicted temperature and moisture content revealed an agreement between the simulation and experiment. 3D computational fluid dynamics model of rubber sheet drying using a conjugate approach was presented by Dejchanchaiwong et al. [15]. Velocity, air temperature, concentration of water in the rubber sheets were studied. The experimental and simulation results are in good agreement in terms of statistical parameters. The drying time was significantly reduced from 72 hours in a conventional natural-flow smoking room to 48 hrs in this new design room.

Somsila and Teeboonma [47] used 3D model to study the flow of air inside a dryer. The CFD study was used for the prediction of the air circulation and temperature distribution inside rubber solar greenhouse dryer and the results formed a basis for the design and development of a high efficiency solar greenhouse dryer for rubber.

In an effort to improve the air and aerosol distribution in a rubber smoke house, Purba and Tekasakul [48] computationally studied the temperature, velocity,

aerosol concentration and particles trajectories in an RSS sheet factory. The simulation was performed using turbulent free convection flows with mesh volume of 2,159,347 generated by GAMBIT 2.2. The modification made as a result considerably improved the ventilation thereby decreasing the aerosol particle concentration in the factory. The distance of 200 m was observed to be the travelling length of the thick cloud smoke in the factory. The CFD study helps in designing smoke house to prevent the exposure of the factory workers to smoke related ailments.

Pianroj et al. [49] experimented using the finite elements method to simulate a steady state drying kinetics of natural rubber sheet convective drying at 40, 50, and 60°C for 10 hours. The simulation was validated with experiment and found to be well fitted with the experimental results for moisture ratio of dried natural rubber sheets.

Kaewnok and Thepa [50] conducted a CFD modelling of the solar assisted NR smoking room using FEM. The simulation results revealed that smoking room with dimension 2x2.5x2.5 m<sup>3</sup> and greenhouse cover of 4x6.5x3 m<sup>3</sup>, with collector zone of 1 m and a channel width for rubber wheelbarrow of 2 m provides the best flow characteristics to increase efficiency and decreases fuel usage.

## **2.4 Continuum Mechanics**

In this section, continuum mechanics is briefly explained because it is the bedrock for the Eulerian and Arbitrary Lagrangian-Eulerian method used in the present study. The algorithms of continuum mechanics usually make use of the following descriptions of motion: the Lagrangian, the Eulerian and/or Arbitrary Lagrangian Eulerian (ALE) descriptions. These descriptions of motion form the major theory behind the CFD simulation of conjugate problems such as that employed in the present study. The descriptions are explained to understand the fluid-structure interaction occurring in the conjugate drying of rubber sheets

Continuum is the mathematical description of deformation and related stresses. In mechanics, it is a branch that involves the mechanical behavior and kinematic with the analysis of materials modelled not as a discrete particle but as a continuous mass. Continuum mechanics is the fundamental basis upon which several

phenomena such as elasticity, plasticity, viscoelasticity, and mechanics are founded [51]. The simulation of complex problems in CFD and solid mechanics that are highly nonlinear usually needs to cope with massive distortions of the continuum being considered while, at the same time, allow a clear delineation of free surfaces, and fluid–solid, solid–solid, or fluid–fluid interfaces [52]. The fundamental assumption inscribed in the name is that materials are assumed to be homogeneous, isotropic, continuous and independent of any particular coordinates system [51].

#### **2.4.1 Lagrangian algorithms,**

In Lagrangian formulation the coordinates are glued to and move with a material point through space and time. Therefore, the coordinates of both the material point and the attached variables, such as temperature, do not change along their trajectory [51]. The computational mesh of each node follows the material particle associated with it during motion (Fig.2.3) [52]. The description of the Lagrangian approach gives room for easily tracking the various interface between the materials interface and free surfaces. It equally enhances a history dependent, constitutive treatment of the material relations. The frequent remeshing operation is needed because it cannot cope with a large distortions of the computational domain [51]. This formulation has the disadvantage that it is difficult to know the state of the fluid at a given point in space and time [53].

#### **2.4.2 Eulerian algorithms**

Fluid dynamics usually works with the Eulerian formulation. Here, as shown in Fig. 2.3, a fixed computational mesh, and a continuum moves by taking the grid as a reference. The advantage with the Eulerian description is that, the massive distortions in the motion continuum can be easily handled, but the accuracy of the interface definition and the details of the flow suffer [52]. On the other hand, entanglements of the elements are easily solved using the Eulerian formulation methods [54-55].

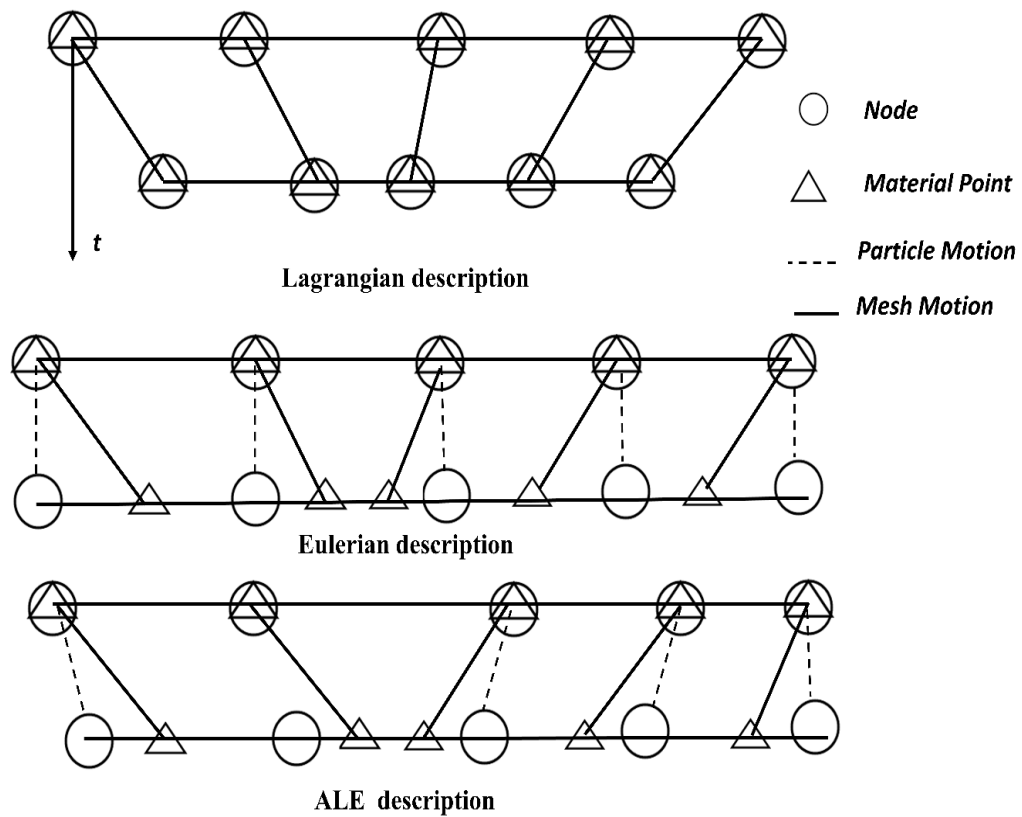


Figure 2.3 One-dimensional example of Lagrangian, Eulerian and ALE mesh and particle motion [52].

### 2.4.3 Arbitrary Lagrangian Eulerian (ALE)

A novel numerical approach with multiple advantages used in solving a wide variety of multidimensional problems in fluid dynamics that are time-dependent is presented. The Arbitrary Lagrangian Eulerian (ALE) uses a conjugate kinematic approach by using a classical combination of the Eulerian and Lagrangian reference frames. It is a technique that automatically and continuously re-joins the mesh. It is carried out by displacing the mesh based on the displacement of the moving body [56]. The method employs the finite difference mesh with vertices that can either be fixed (Eulerian), moved with the fluid (Lagrangian), or having the advantage of being moved in all manner of direction (Arbitrary Lagrangian Eulerian) [55, 57]. In the

ALE description, the nodes in the computational mesh are free to move in normal Lagrangian manner with the continuum, or in a stationary Eulerian mode. It can also be moved in specific arbitrary manner as shown in Fig. 2.3, to be able to continuously rezone. The massive freedom offered by ALE description in the movement of the computational mesh makes it easier to handle the large distortions of the continuum which cannot be done by a pure Lagrangian method, and with greater resolution than obtained by pure Eulerian method [52, 58]. Hence, it is pertinent to conclude that the ALE description which combines the best features of the pure Lagrangian approach and the Eulerian methods provides a more accurate simulation than the individual methods. Hence, it is most appropriate for finite solid forming and strain deformation problems.

#### ***2.4.3.1 ALE kinematics***

In the description of motion with the ALE method, the spatial configuration or the material configuration are not taken as reference. Thus, another domain (third) is added and it is denoted by the configuration of reference, where the identification of the grid point is done by the reference coordinates [59]. Since an arbitrary choice of the reference configuration is made, the immense advantages of both Lagrangian and Eulerian descriptions can be maximized while playing down on their drawbacks.

### **2.5 Thermodynamic equilibrium**

#### **2.5.1 Isotherms and Equilibrium**

The amount of water that can be removed from food, rubber sheets and other porous materials are limited irrespective of the prevailing conditions applied to the porous materials. The equilibrium moisture content (EMC) is the amount of moisture content in a porous material when it is in equilibrium with the surrounding partial pressure of water vapor. Different materials have different EMC after they have been dried. Sorption isotherms can be calculated and developed when the equilibrium moisture content is measured at varying conditions of relative humidity and temperature as a function of water activity [60].

### 2.5.2 Water Activity

The primary way by which the moisture content of food and other porous materials such as agricultural product are measured and expressed is in terms of water activity [61]. Water activity  $a_w$  is a function of the water vapor partial pressure ( $p_w$ ) above the porous media/food surface per unit of the pure component vapor pressure of water ( $p'_w$ ) at the same temperature as the given sample, thus [60]

$$a_w = p_w / p'_w \quad (2.1)$$

Provided that a solution that is aqueous is maintained at a constant temperature, Raoult's law states that the product of the mole fraction of water and the pure component vapor pressure of water is equal to the partial pressure above the liquid surface and hence is given by [62],

$$p_w = x_w \cdot p'_w \quad (2.2)$$

Clearly when the liquid phase is pure water, and  $x_w = 1$ , then  $p_w = p'_w$  and the partial pressure is equal to the vapor pressure. Equally, when the water content is zero ( $x_w = 0$ ) there can be no partial pressure of water in the vapor phase. However, Raoult's law applies to ideal systems and water is not an ideal material. It is therefore necessary to introduce an activity coefficient  $\gamma$  such that

$$p_w = \gamma x_w \cdot p'_w \quad (2.3)$$

However, activity coefficients are complex functions of both temperature and moisture content and cannot be readily determined. Substituting into the definition of water activity gives

$$a_w = \gamma x_w \cdot p'_w / p'_w \quad (2.4)$$

therefore

$$a_w = \gamma x_w \quad (2.5)$$

which for an ideal system reduces to

$$a_w = x_w \quad (2.6)$$

Raoult's law generally holds only at relatively high values of  $x_w$ . Thus, for both an ideal system and high moisture contents, water activity is effectively nothing more than the mole fraction of water in the liquid phase within the materials. It is important to realize that  $x_w$  is defined in relation only to the soluble constituents within a food and ignores the insoluble components.

Humidity is related to saturation conditions and is expressed in terms of partial pressures:

$$RH = p_w / p_{ws} * 100 \quad (2.7)$$

The limitation in calculating the water activity with Eq. (2.5) leads to the formation of another equation. If there is a thermodynamic equilibrium between rubber and the surrounding air then, from the definition of relative humidity Eq. (2.7), water activity is equal to the fractional relative humidity. That is

$$a_w = \%RH / 100 \quad (2.8)$$

The right hand side of Eq. (2.8) is also represented by equilibrium relative humidity (ERH) which is the relative humidity obtained when RH in the rubber sheet and surrounding air are equal. The formulation is the basis used in the water activity measurement.

## CHAPTER 3

### METHODS AND MATERIALS

#### 3.1 Numerical methods

The numerical modelling of the shrinkage behavior and transport phenomena of a natural rubber sheet under convective drying is conducted using CFD. The conjugate time dependent analysis of the heat and mass transfer in rubber sheet drying process is considered. The directional shrinkage in the thickness is correlated to the time evolution of the water concentration variation in the rubber sheets. The concentration and temperature in the fluid domain are coupled to the flow field. The solid mechanics, moisture diffusion and temperature in the material domain are equally coupled together and the virtual work principle was applied to control the domain displacement. Finally, the Arbitrary Lagrangian Eulerian (ALE) method is used to combine both domains together. The theoretical formulations and relevant numerical methods used are presented in this section.

##### 3.1.1 Governing Equations

###### 3.1.1.1 Modelling of external flow, mass and temperature of drying air

Assumptions for the drying air modelling are: (i) 2-D geometry is used for evaluation because of the symmetry of the chamber (ii) the coupled external flow fields are assumed to be uniform in the drying chamber (iii) physical and thermal properties are assumed to be constant (iv) no-slip condition (v) negligible gravity effect. The governing equations of a drying fluid in a two-dimensional domain are the mass, momentum and energy conservation equations, as follows [63-66]:

Continuity equation

$$\partial \rho_a / \partial t + \nabla \cdot \rho_a (u) = 0 \quad (3.1)$$

Momentum equation

$$\rho_a \partial u / \partial t + \nabla \cdot \rho_a (uu) = -\nabla P + \mu \nabla^2 u = 0 \quad (3.2)$$



where  $\rho_a$  is air density (kg/m<sup>3</sup>),  $P$  is the drying chamber pressure (N/m<sup>2</sup>),  $u$  is the velocity vector (m/s) and  $t$  is the time (s),  $\mu$  is the dynamic viscosity (Pa.s).

Energy balance

$$\rho_a C_{pa} \partial T_1 / \partial t - \nabla \cdot (K_a \nabla T_1) + (\rho_a C_{pa} u \cdot \nabla T_1) = 0 \quad (3.3)$$

Where  $T_1$  is the air temperature (K),  $C_{pa}$  is the specific heat (J/kg K) and  $K_a$  is the thermal conductivity (W/m K).

The mass balance of the drying air for the water vapor diffusion can be described as:

$$\partial C_1 / \partial t + \nabla \cdot (D_a \nabla C_1) + u \cdot \nabla C_1 = 0 \quad (3.4)$$

where  $C_1$  is the concentration of water vapor in the drying air (mol/m<sup>3</sup>) and  $D_a$  is the diffusion coefficient of water vapor in the drying air (m<sup>2</sup>/s).

### 3.1.1.2 Modelling of internal moisture, temperature fields and shrinkage of the rubber sheets.

Heat and mass transfer inside the rubber sheet during drying is predicted based on assumptions: (i) linear elasticity (ii) isotropic shrinkage or deformation (iii) no heat generated inside the rubber sheet (iv) negligible radiation effect (v) hygroscopic porous media (vi) shrinkage along the thickness only (vii) shrinkage relating to variation in the water concentration. The following governing 2-D heat and moisture transfer equations can be described:

Heat transfer equation

$$\rho_s C_{ps} \partial T / \partial t + \nabla \cdot (-K_{eff} \nabla T) + \lambda I = 0 \quad (3.5)$$

where  $T$  is the temperature of rubber sheet (K),  $\rho_s$  is the density of rubber sheet (kg/m<sup>3</sup>),  $C_{ps}$  is the specific heat of rubber (J/kg K),  $K_{eff}$  is the effective thermal

conductivity of the natural rubber (W/m K),  $\lambda$  is the water latent heat of vaporization (J/mol) and  $I$  is the rate of evaporation (mol/(m<sup>3</sup> s)).

Mass transfer equation

*liquid water*

$$\partial C_w / \partial t + \nabla \cdot (D_w \nabla C_w) + I = 0 \quad (3.6)$$

*water vapor*

$$\partial C_v / \partial t + \nabla \cdot (D_v \nabla C_v) - I = 0 \quad (3.7)$$

where  $C_w$  is the concentration of water in the rubber sheet (mol/m<sup>3</sup>),  $C_v$  is the concentration of water vapor (mol/m<sup>3</sup>)  $I$  is the rate of evaporation (mol/(m<sup>3</sup> s)),  $D_v$  is the effective diffusion coefficient of vapor in rubber sheet (m<sup>2</sup>/s) and  $D_w$  is the moisture diffusion coefficient in rubber sheet (m<sup>2</sup>/s) obtained from [67]:

$$D_w = 4 \times 10^{-5} \exp(-615847/T) \quad (3.8)$$

The water vapor pressure ( $P_v$ ) is a function of rubber sheet temperature and moisture content ( $X_b$ ) can be defined as:

$$P_v / P_{vs} = -146.211 \exp(-12.777 X_b) / (T - 311.650) \quad (3.9)$$

where  $P_{vs}$  is the saturated vapor pressure of water (Pa). Regards to the equilibrium at the interface between the air and rubber sheet, the thermodynamic equilibrium expression with the assumption of an ideal gas behavior is given by:

$$a_w x_w P_{vs} = y_w P \quad (3.10)$$

where  $P$  is the atmospheric pressure (Pa),  $x_w$  and  $y_w$  are the mole fractions of water in the rubber sheet and drying air, respectively and  $a_w$  is the water activity coefficient.

The relationship between the stress and strain can be expressed through the elastic stress–strain matrix, accounting for the young modulus ( $E_y$ ), the Poisson ratio ( $\nu$ ), and the stresses ( $\sigma$ ) given by:

$$\begin{Bmatrix} d\sigma_x \\ d\sigma_y \\ d\sigma_{xy} \end{Bmatrix} = \begin{Bmatrix} E_y(1-\nu)/(1+\nu)(1-\nu) \\ E_y(1-\nu)/(1+\nu)(1-\nu) \\ 0 \end{Bmatrix} \begin{bmatrix} 1 & \nu/(1-\nu) & 0 \\ \nu/(1-\nu) & 1 & 0 \\ 0 & 0 & (1-2\nu)/2(1-\nu) \end{bmatrix} \begin{Bmatrix} d\varepsilon_x \\ d\varepsilon_{sy} \\ d\gamma_{xy} \end{Bmatrix} \quad (3.11)$$

Where  $\varepsilon_{sy}$  is the uniaxial yield stress. The young modulus and the poisson ratio are assumed constant [68-69].

The time variation of the free shrinkage strain,  $\{d\varepsilon_{x0}\}$  was assumed to be proportional to the water concentration variation [16, 70-71]:

$$\{d\varepsilon_{x0}\} = K_{ds} \cdot C_w \quad (3.12)$$

where  $K_{ds}$  is the hydrous compressibility factor estimated from experiment.

The structural changes of the rubber sheet during drying period are correlated to the moisture removal in the rubber sheet. An isotropic shrinkage model is assumed for the rubber. The local total strain or total displacement  $\{d\varepsilon\}$  is a function of the mechanical strain  $\{d\varepsilon_s\}$  and the shrinkage strain  $\{d\varepsilon_0\}$  due to the moisture loss [16].

$$\{d\varepsilon\} = \{d\varepsilon_s\} + \{d\varepsilon_0\} \quad (3.13)$$

The changes in stress  $\{d\sigma\}$  is a function of changes in mechanical strain  $\{d\varepsilon_s\}$ .

$$\{d\sigma\} = [D]\{d\varepsilon_s\} \quad (3.14)$$

The changes in stress is a function of changes mechanical strain. Here  $[D]$  is the stress-strain matrix containing the Young Modulus

The formulated virtual work principle is used to obtain the equilibrium equation necessary to complete the structural mechanics model which is written as:

$$\int_V \delta \{d\varepsilon_s\}^T \{d\sigma\} dV = 0 \quad (3.15)$$

$\delta$  is the displacement variation,  $V$  is the rubber sheet volume and the superscript  $T$  represents the transpose of matrix.

### 3.1.2 Computational domain of a rubber sheet drying chamber

The flow fields, and heat and mass transfer of rubber sheet in a rubber sheet drying chamber model using conjugate approach are studied. Computational domain used for numerical investigation with the boundary conditions in the chamber is presented in Fig. 3.1. The initial conditions are shown in Table 3.1.

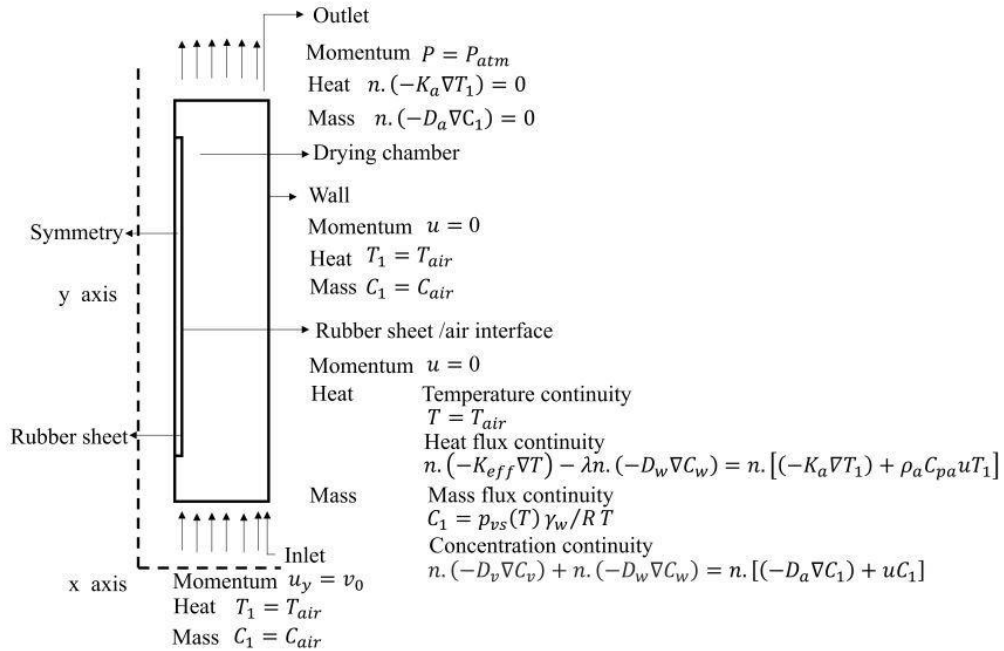


Figure 3.1 Schematic diagram of the computational domain and boundary conditions for numerical investigation.

Table 3.1 Parameters exploited for simulation.

Name	Value
rubber density	920 (kg/m <sup>3</sup> )
Operating pressure $P_o$	101325
Rgas	8.314472
Porosity	0.3
Young modulus	1e7 Pa
Poison Ratio	0.498
Heat capacity	1888 J/(kg.K)
Thermal conductivity	0.13
Coefficient of thermal expansion	1.52e-6 1/K
Temperature ( $T_0$ )	289 K
Moisture content on a dry basis ( $X_{b0}$ )	0.4
Temperature ( $T_0$ )	333 K
Relative humidity ( $U_{x0}$ )	50%
Velocity in x and y directions ( $u_{x0}$ , $u_{y0}$ )	0, 2.5 m/s

### 3.1.3 Mesh Refinement study

The mesh refinement study is done using four physics-controlled (default mesh sizes generated by the software) mesh sizes: normal, fine, extra fine and extremely fine. The quality of the mesh is dependent on the average element quality [61]. Because of the computational requirement (Large memory) for the conjugate problem, the extra fine mesh was exploited.

### 3.1.4 Simulation procedure

The 2D time dependent model is solved. The flow in the drying chamber (Eq. 3.1 and 3.2) are solved using the laminar flow module. The fluid inside drying

chamber occur at the transition to turbulence with Reynolds number of 3519.4, which falls in the transition regime. However, the problem is simulated under the laminar flow condition. This is because of the complexity of the domain under study. Equations (3.3) and (3.4) refer to the energy and mass balance, respectively. They are solved using heat transfer in fluid and transport of dilute species module. In accounting for the shrinkage in the rubber sheet, solid mechanics module, transport of diluted species in porous media and heat transfer in solid module are employed Eq. (3.5) to (3.14). A second order discretization was assumed for the material and spatial domains. The relative and absolute tolerance of 0.01 and 0.001 was assumed. Implicit time stepping scheme is used in the solution of the PDEs systems [16]. The simulation was done using COMSOL multiphysics V. 4.4.

### 3.2 Experiment and Experimental analysis

Natural rubber sheets are obtained from Saikao rubber cooperative (N 7° 10' 32'' : E 100° 36' 52'') situated in the Muang District, Songkhla Province, Thailand. The average area of each sample rubber sheet is about 0.5 m×1.0 m. The ASABE 1988 method was used in the determination of the moisture content [72]. The drying chamber with dimension of 1.5 m×0.8 m×0.2 m is used for the experiments and is shown in Fig. 3.2. Three (800-W each) and one (500-W) electrical heaters are used to heat the inlet air and water inside the water compartment, respectively. The water compartment with dimension of 0.7 m×0.4 m×0.4 m is used to control the relative humidity of the hot air.

A 400-W blower is installed at the exhaust duct to control the air flow inside the drying chamber and continuously remove the humid air from the chamber. The exhaust hot air is also recirculated through the recirculation duct for waste heat recovery. Experimentations have been conducted in a drying chamber for 4 rubber sheets. The temperatures at nine locations (T1 to T9) as shown in Fig. 3.3 and Table 3.3 are measured by Type-K thermocouples and recorded by a data logger (Data-Taker, DT 605) with an accuracy of  $\pm 1^\circ\text{C}$ . Relative humidity is measured by a humidity sensor at the inlet (RH1) and outside the drying chamber (RH2) (Fig. 3.3). The velocity inside the chamber (V1) is measured by the vane type anemometer in the position as shown in Fig. 3.3.

Weight of four rubber sheets samples are measured by a load cell (A&D Company, AD-4329A) of accuracy  $\pm 1\text{g}$  to calculate the average moisture content of rubber sheet. To investigate the time evolution of the shrinkage behavior based on a previous experimental study on rubber sheet shrinkage [73], the thickness of the rubber sheets samples are monitored using a micrometer screw gauge (Mitutoyo, MES4117/3) of accuracy  $\pm 0.01\text{ mm}$ . Moreover, the variation in the thickness of the dried sheets are measured by a confocal laser scanning microscope or CLSM (FV300, Olympus, JAPAN) to obtain image and calculate the corresponding thickness of the rubber sheet samples before and after the drying process. Three rubber sheet samples (#1, #2, #3) at different vertical positions are cut from one rubber sheet for CLSM testing, as shown in Fig. 3.3 and the weights are measured by a precision balance (Shimadzu, accuracy of  $\pm 0.01\text{ g}$ ). To achieve the validation of the present model, the experimentations have been conducted under operating conditions of air temperature, inlet velocity, average relative humidity of 333K, 2.5 m/s, 60%, respectively.

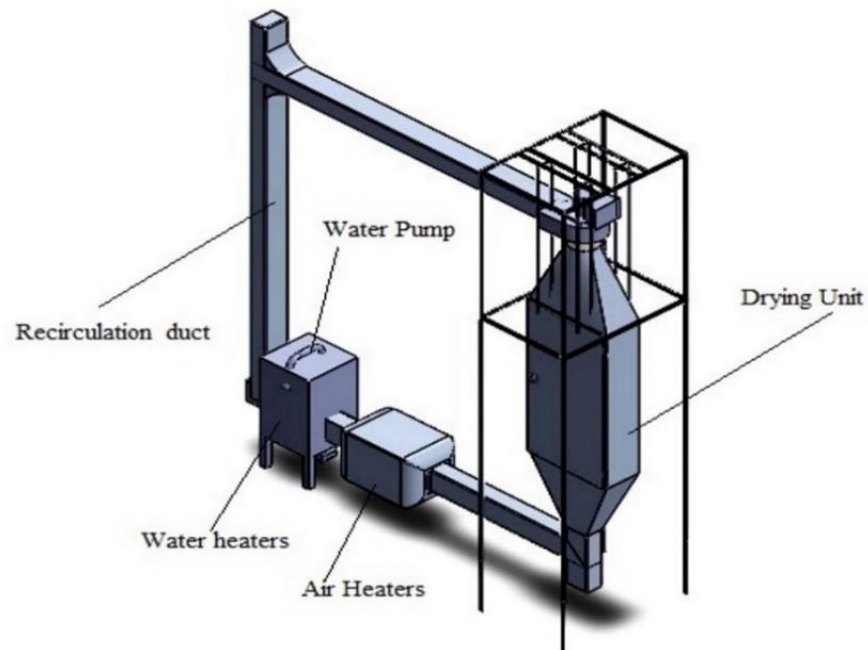


Figure 3.2 Experimental setup.

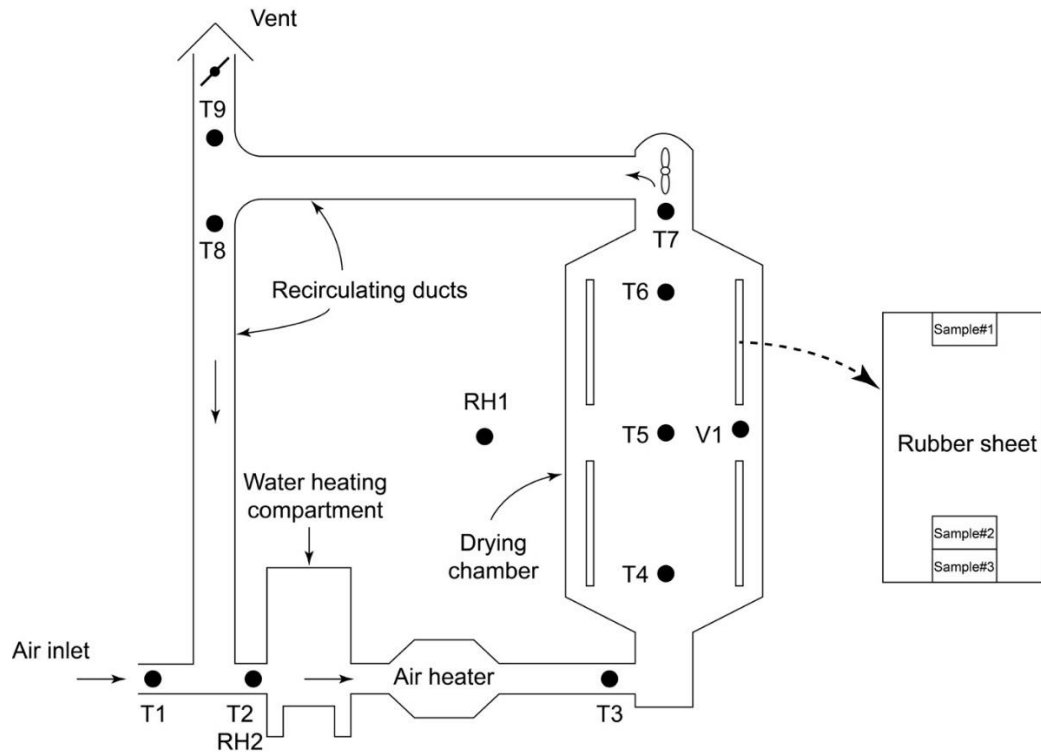


Figure 3.3 Experimental set up displaying locations of thermocouples and relative humidity probe.

Table 3.2 Description of measurement positions of the experimental setup

Position	Description
T1	Thermocouple base inlet
T2	Thermocouple at water heater compartment inlet
T3	Thermocouple at drying chamber inlet
T4	Thermocouple at bottom plane inside the drying chamber
T5	Thermocouple at middle plane inside the drying chamber
T6	Thermocouple at Top plane inside the drying chamber
T7	Thermocouple at drying chamber outlet
T8	Thermocouple at recirculated air position
T9	Thermocouple at exhaust air position
RH1	Ambient Relative humidity sensor
RH2	Inside Relative humidity sensor



### 3.3 Statistical analysis

The assessment of the simulated results with experimental values are evaluated using the coefficient of determination ( $R^2$ ) and root-mean-square error (RMSE) [74]. The collected experimental data are used to ascertain the validity of Eq. (3.10) and to estimate the value of hydrous compressibility factor  $K_{ds}$  to be exploited. The free drying shrinkage strain components  $d\varepsilon_{x0}$  of the thickness is calculated as:

$$d\varepsilon_{x0} = (t_x - t_{x0}) / t_{x0} \quad (3.16)$$

Where  $t_{x0}$  indicates the values of rubber sample thickness measured at the beginning of the drying process and  $t_x$  is the instantaneous thickness [16]. Assuming that the decrease in natural rubber weight could be ascribed to water evaporation, the corresponding time variation of water concentration,  $dC_w$  is estimated on the basis of the difference between the measured value of sample weight and its initial weight. The final percentage of shrinkage of the rubber sheet sample is defined from [73]:

$$\text{Shrinkage (\%)} = (\text{initial thickness} - \text{final thickness}) / (\text{final thickness}) \times 100 \quad (3.17)$$

The experimental and linear fitting of  $d\varepsilon_{x0}$  vs  $dC_w$  are shown in Fig. 3.4. The calculated slopes suggest a nearly constant value of  $K_{ds}$ . The estimated value of  $1.52 \times 10^{-5}$  was used in the numerical simulations to predict the shrinkage behavior of rubber samples during convective drying./

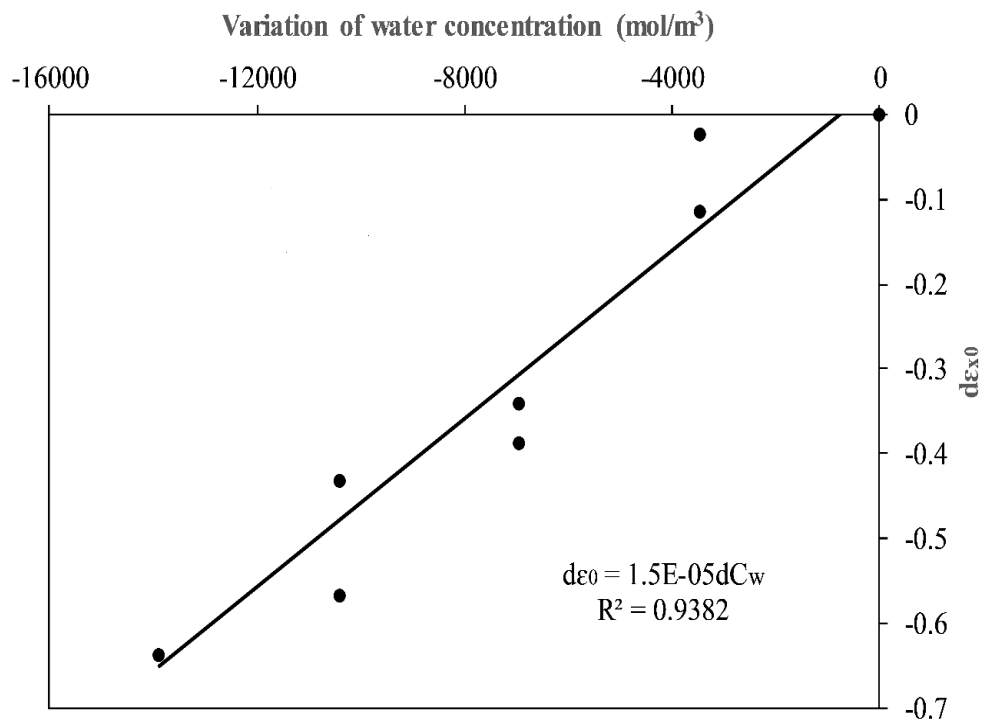


Figure 3.4 Linear fitting of  $d\epsilon_{x0}$  vs.  $dC_w$  for the tested experimental conditions.

## CHAPTER 4

### RESULTS AND DISCUSSION

#### 4.1 Numerical modelling results

In this section, comprehensive results generated from the numerical simulation using COMSOL Multiphysics version 4.4 including mesh refinement and results of velocity, temperature, moisture content, shrinkage stress and strain profiles are presented. Finally, validation with experimental data where needed is also included in this section.

##### 4.1.1 Mesh refinement results

Summary of the mesh sizes, the corresponding degree of freedom and average element quality used in the simulation are outlined in Table 4.1. The evaluation of each mesh sizes using the variation in the moisture content is also shown in Fig. 4.1. Mesh refinement study was carried out using four physics-controlled mesh sizes: normal, fine, extra fine and extremely fine. The quality of the mesh is dependent on the average element quality (a criterion for grid dependence check in COMSOL) of the elements [61]. That is, the higher the average quality, the more accurate the solution and more memory and computational time required.

Table 4.1 Mesh refinement study parameters.

Mesh	Number of Elements	Degree of Freedom	Average Element Quality
Normal	11804	160976	0.8916
Fine	20496	278974	0.9089
Extra fine	94252	1277948	0.9287
Extremely fine	178424	2331554	0.9576

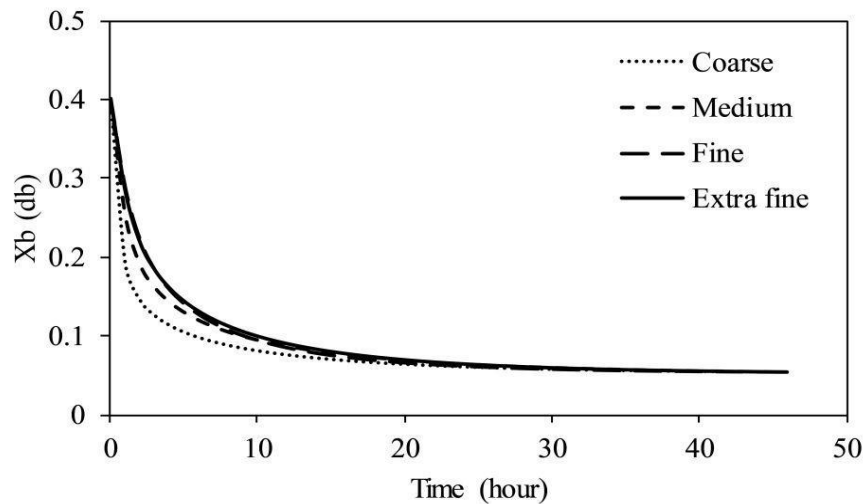


Figure 4.1 Grid evaluation using the moisture content variation.

#### 4.1.2 Flow field distribution with shrinkage inside drying chamber

The conjugate time evolution of the flow field with the proportionate shrinkage is shown in Fig. 4.2. The streamlines of the flow field are represented by white lines while the initial surface of the rubber sheet before drying is represented by a single black line and a symbol  $\Omega$  (Fig. 4.2). The progressive displacement of the rubber sheet is a ratio of shrinkage per unit of the original thickness ( $\tau = \delta/t$  where  $\delta$  is the displacement and  $t$  is the original thickness) at different time steps as shown in Fig. 4.2. The rubber sheet thickness was zoomed at three locations as shown in Fig. 4.2 for clarity. At the initial time (0 hour), the flow as represented by the streamline patterns (in white color) are scattered in different directions in relation to other time (1 hour, 12 hours, and at the end 46 hours). It is assumed that at the initial time, the flow is not fully forced convective but more of natural convection as a result of the initial starting of the blower. From the surface plot, the velocity at the initial time was almost zero and hence,  $\tau$  is approximately zero.

At 1st hour, it can be seen that shrinkage has increased progressively (with  $\tau = 0.057$ ) since it is in the constant drying rate period when the moisture content reduced rapidly. Also, at the 12th and 46th hours (the end of drying)  $\tau$  becomes 0.079 and 0.089, respectively. The shrinkage variation with time is slower because the moisture removal at this period (falling drying rate period) is gradually decreased. On a closer

examination, air streamlines profile at the 1st to 46th hours changed significantly especially around the rubber sheet interface with the surrounding air

From the 1st to 46th hour, air flow at the leading edge of the rubber sheet interface with the air is rapid (from the surface plot profile) and is reduced gradually as the flow moves up to the trailing edge (Fig. 4.2). These flow patterns could be attributed to the drag forces developed along the rubber sheet interface with the drying air. On the actual domain, it is observed that the velocity distribution inside the drying chamber is almost constant at an average value of 2.5 m/s (estimated value from experiment). The thickness reduces progressively as the rubber sheet is being dried in the drying chamber. The initial interface (black line) of the rubber sheet is gradually replaced by the flow field of air streamlines. The heat and mass transfer at the rubber sheet surface is strongly affected by isotropic modification of the shape of rubber sheet and the consequent variation of the velocity profile. This approach thus provides a reliable basis for the prediction of the actual structural changes occurring during rubber sheet drying. The maximum shrinkage percentage of 8.9% obtained from simulation was achieved at the final drying time.

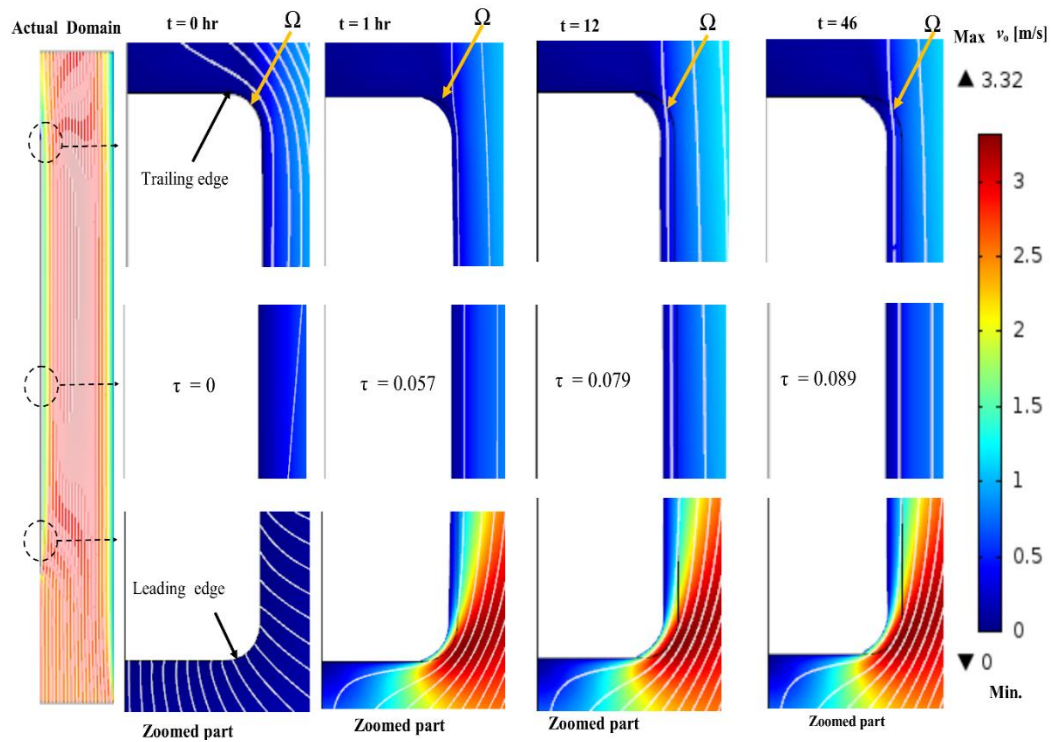


Figure 4.2 Expansion illustration of the time evolution of flow field and the calculated streamlines accounting for rubber sheet shrinkage.

#### 4.1.3 Moisture content distribution of rubber sheet

The time evolution of moisture content distribution developed within the rubber sample during the drying process is shown in Fig. 4.3. The moisture content  $X_b$  is on dry basis, initial MC ( $X_{b0}$ ) is 0.4 kg of water/kg dried rubber sheet. At the initial stage of drying (0 hr), the moisture content variation across the rubber sheet is assumed to have a negligible difference between the core and the outer surfaces. Moisture content is highest at the core and it reduces in the direction toward the edges. Drying at the external surfaces exposed to free air, is more rapid than that in the inner regions. This implies that the water movement from the center to the surface is lower than the rate of evaporation on the external surfaces. The variation of water from the outer to the inner core as shown in Fig. 4.4. shows that more water are trapped at the core than at the outer region of the rubber sheet.

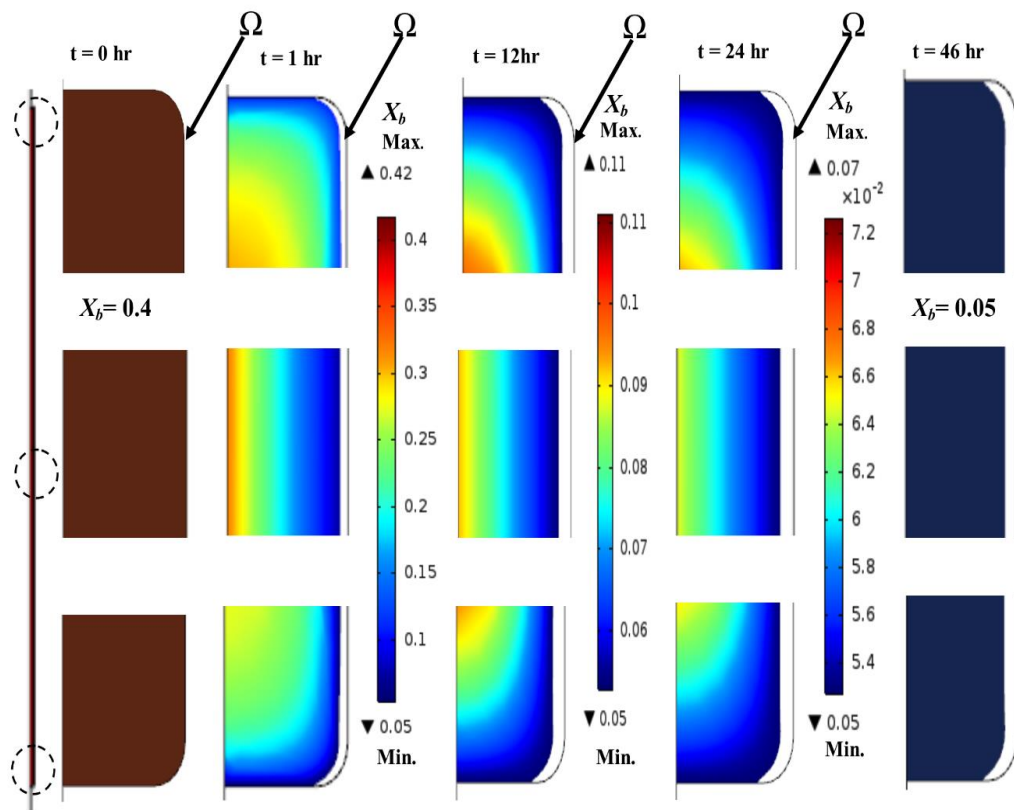


Figure 4.3 Time evolution of moisture content variation.

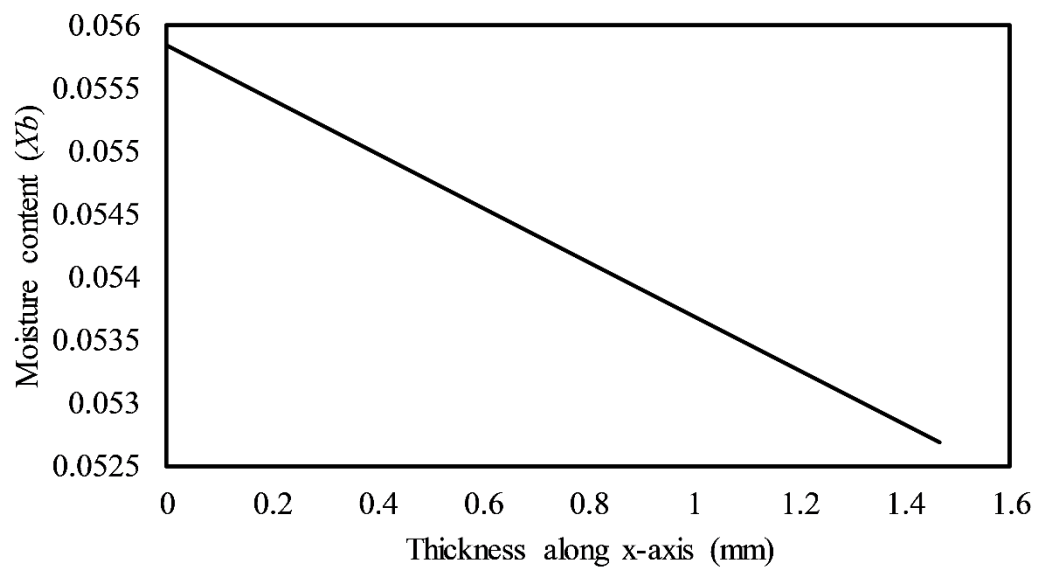


Figure 4.4 Moisture content variation across rubber sheet thickness.

Experimental and simulation results of the  $X_b$  are in a good agreement, as shown in Fig. 4.5. In terms of statistical analysis, the maximum error, average error,  $R^2$  and RSME are 3.31%, 0.65%, 0.9809 and 0.0196, respectively. Hence, the shrinkage approach shows an improvement in the formulated predictive model for the MC profile (Fig. 4.3) when compared to earlier study with no consideration of shrinkage effect.

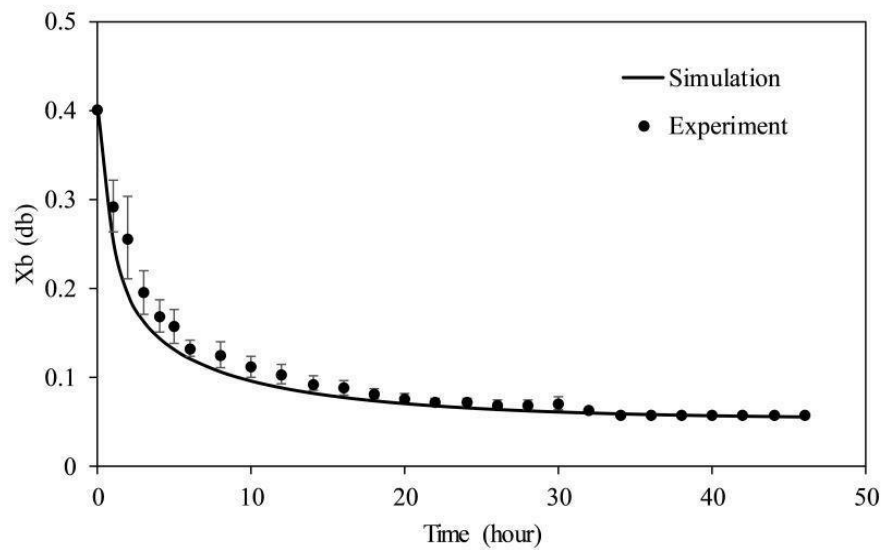


Figure 4.5 Comparison of numerical simulation and experiment for moisture content.

#### 4.1.4 Temperature distribution across rubber sheet

The time evolution of the temperature developed in the rubber sheet during drying is shown in Fig. 4.6. At the initial period of drying the temperature in the rubber sheet rose drastically and then became relatively constant at 333K which the set temperature for is the drying. The temperature variation across the rubber sheet thickness (x-direction) at the end of drying (46th hour) is shown in Fig. 4.7. It is observed that the outer temperature is higher. This is largely due to the direct impact of the operating conditions (applied velocity, temperature and RH) on the outer surface than the inner core.



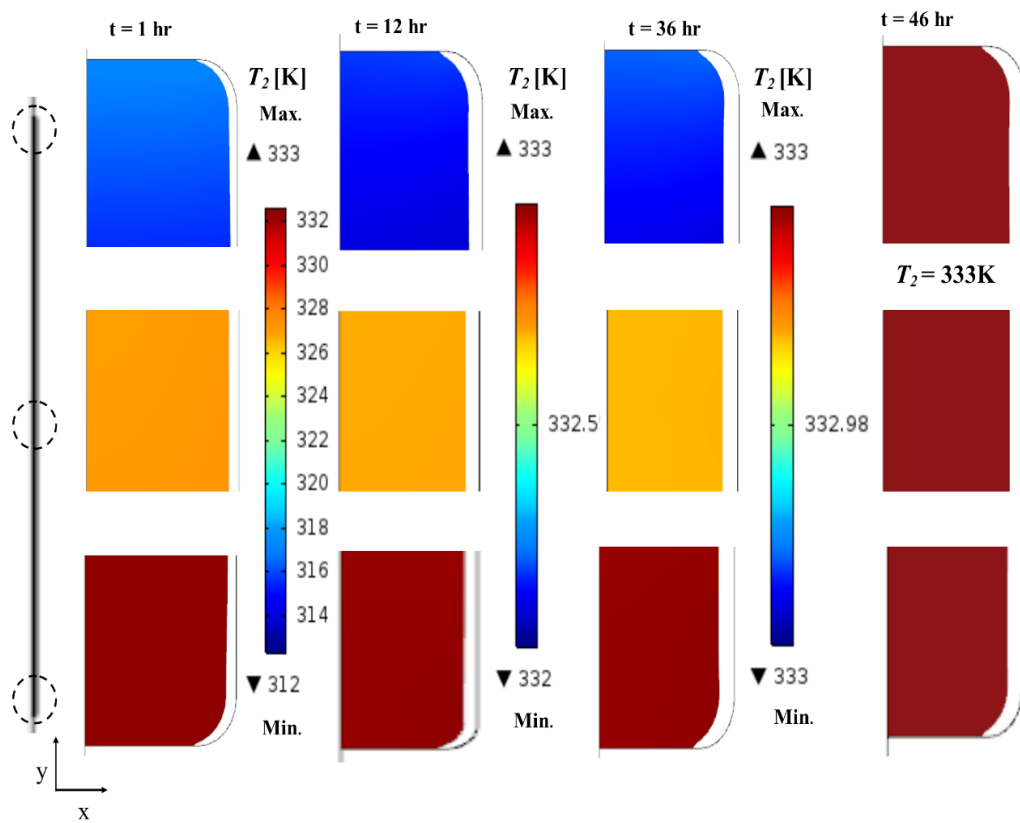


Figure 4.6 Time evolution of temperature developed in the rubber sheet during convective drying along x- axis.

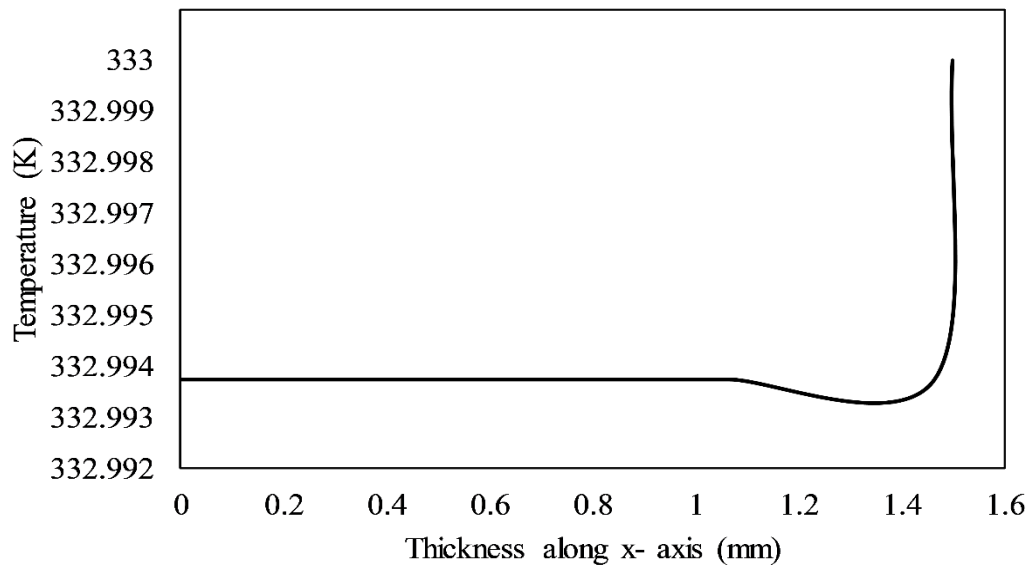


Figure 4.7 Temperature variation across rubber sheet thickness along the x- axis.

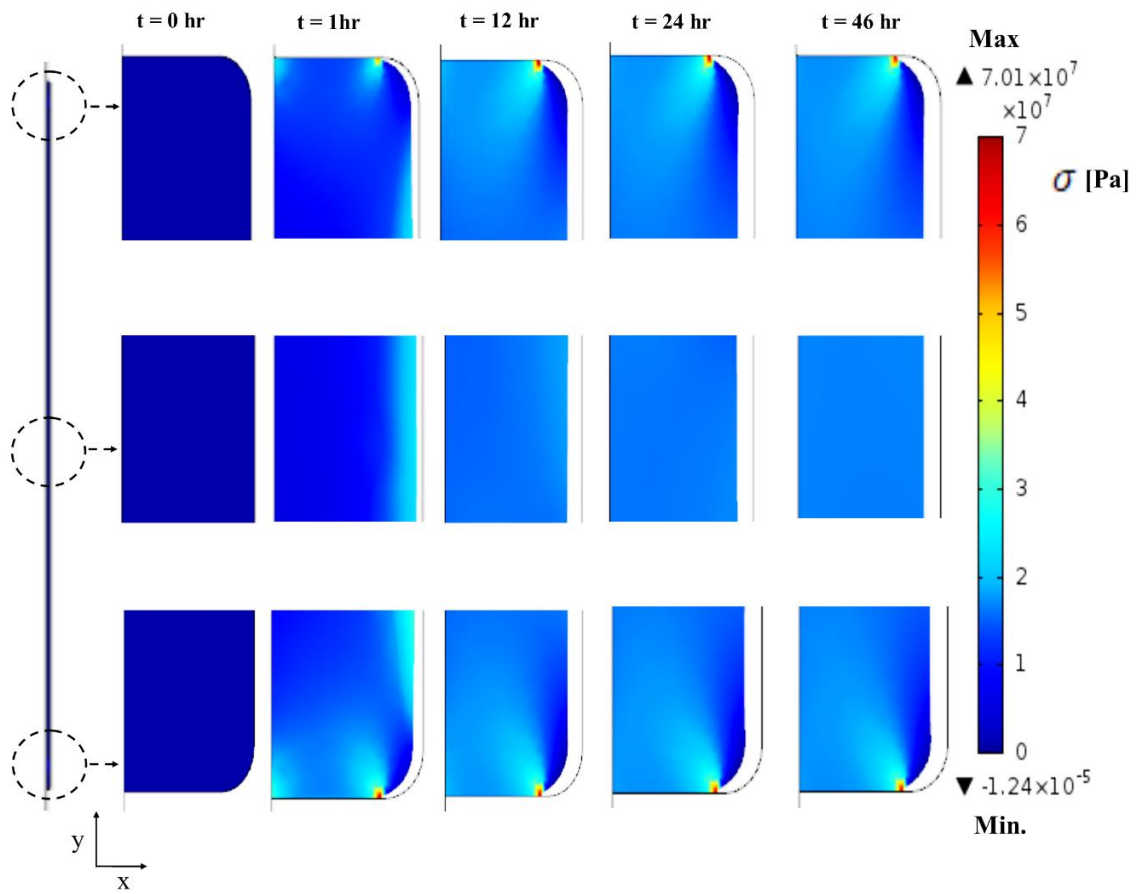
#### 4.1.5 Shrinkage deformation

The time evolutions of the first principal shrinkage stress and strain tensor developed within the rubber sample are shown in Figs. 4.8(a) and (b), respectively. The methodology and equations used to obtain the profile of the rubber sheet shrinkage are as detailed in section 3.1.4. During the initial stages of drying, the stress and strain distributions are almost zero except on the outer edges which were constantly impinged by air. Hence, external surface of the rubber sheet has faster moisture removal and consequently larger shrinkage rate. The increased moisture gradients (Fig. 4.3) lead to a non-uniform distribution of the strain and is responsible for the corresponding decrease in the structural mobility of natural rubber and further engenders the development of either tensional stresses or compressive stresses in the natural rubber. With progression in drying, the rubber sample surfaces attempted to shrink but with restriction from the wet core.

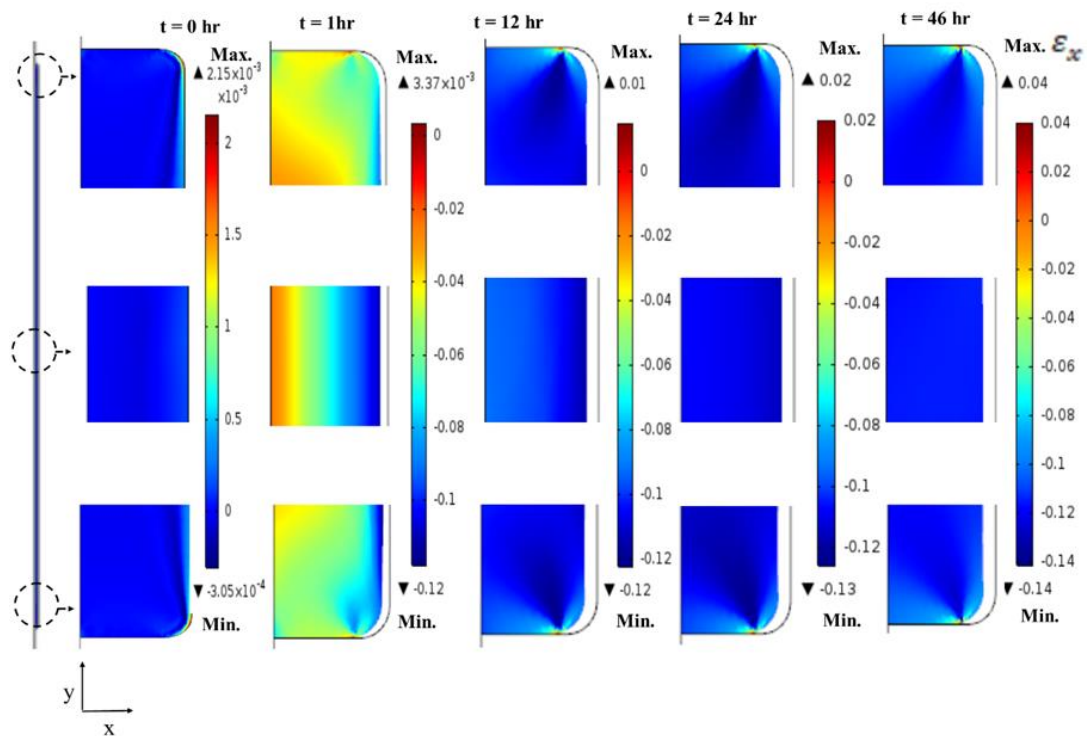
The stresses developed in the rubber sheet as shown in Fig. 4.8(a) can be seen to be largely a compressive force, which in essence shows why shrinkage is occurring in the rubber sheet. From Fig. 4.8(b), the outer surfaces were subjected to tension (positive sign), while the wet core was subjected to compression (negative sign). The

extensive tensile stresses might lead to the formation of possible crack on natural rubber surface, which could consequently cause damage with an improper operating condition during drying. It could also be observed that during the falling drying rate period, rapid moisture content decrease led to a significant shrinkage in the natural rubber [16, 75].

The strains and stresses developed within natural rubber samples as a result of moisture removal may provide useful insights on the mechanical properties of the natural rubber sheet. These can be used as evaluation criteria for natural rubber sheet quality. It can also pave way for optimization of the natural rubber sheet drying process and prevent the formation of bubbles and cracks as a result of the variation in the stresses developed in the rubber sheet [73]. In addition, the numerical model formulated can be used in locating regions where water activity could engender microbial spoilage.



(a)



(b)

Figure 4.8 Time evolution of (a) first principal shrinkage stress and (b) shrinkage strain tensor in x direction.

#### 4.1.6 Shrinkage verification

The rubber sheet thickness was investigated using confocal laser scanning microscope (CLSM). The CLSM images of rubber sheet samples before and after drying are shown in Fig. 4.9. Figs. 9(a) and (b) show the rubber sheet thickness of sample #1 before and after drying while Figs. 9(c) and (d) show the thickness of sample #2 and #3 only after drying as outlined in Fig. 3.3. The CLSM images after drying further justify that cracks formed after drying could be because of the uneven stresses in the dried rubber sheet as displayed in Figs. 4.9 (b)–(d). It can be observed that the different cracks formed after the drying could result in the damage and bubbles developed in those regions. The initial and final thickness was also calculated from the CLSM scan image.

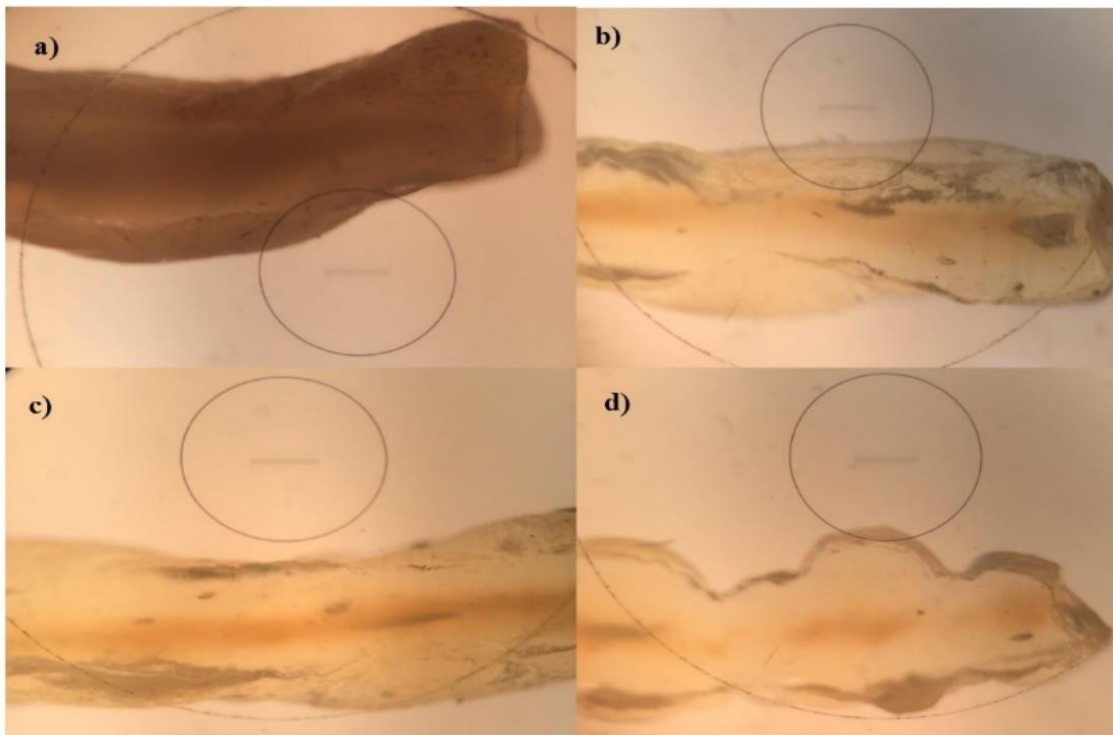


Figure 4.9 CLSM scan images (a) before drying: position 1 (b) after drying: position 1 (c) after drying: position 2 (d) after drying: position 3.

Experimental validation of the numerical simulation was carried out for the considered operating conditions. The model prediction and the corresponding experimental points expressing the time evolution of rubber sheet thickness are shown in Fig. 4.10. Agreement between experimental and simulation results is good with slight difference in the thickness variation. The regions with the big differences are due to the rapid evolution of the water out of the rubber sheet at the constant drying rate period. In terms of statistical analysis, the maximum error,  $R^2$  and RSME are 0.006%, 0.9991 and 0.0091, respectively. The percentage shrinkage from the experiments, simulation (Eq. 17) and CLSM scan are found to be 9.1%, 8.9% and 13.6%, respectively. This confirms the significance of rubber sheet shrinkage when being dried.

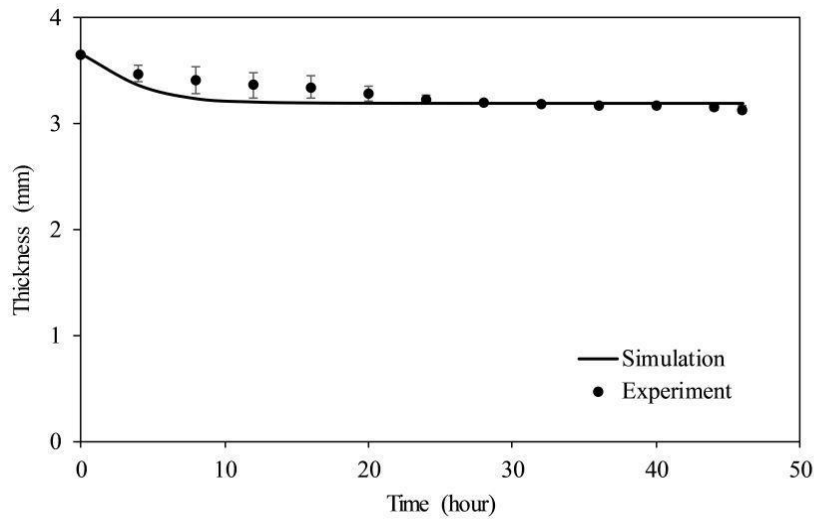


Figure 4.10 Shrinkage model prediction and experimental validation.

## 4.2 Experimental results

Summary of the designed experimental results obtained at different operating conditions is shown in Table 4.2. The experiments conducted have been sectioned into four groups to study the effect of the different parameters. Velocity was varied from 1.5 m/s to the maximum value of 4.0 m/s in Experiment 1 while temperature and inlet air relative humidity were kept constant at 60°C and 40%, respectively, to study effects of air velocity. In Experiment 2, the temperature was increased over regularly operated 60°C to investigate the highest possible operating temperature. Elevated temperature at 65 °C was set in Experiment 3 and the velocity was varied. Finally, the best condition was confirmed and relative humidity was varied.

Table 4.2 Summary of the experimental conditions.

Experiment	Experiment	Temperature °C	Ideal inlet RH	Velocity
Exp. 1	1.1	60	40	1.5
	1.2	60	40	3.0
	1.3	60	40	3.5
	1.4	60	40	4.0
Exp. 2	2.1	65	40	4.0
	2.2	70	40	4.0

Exp. 3	3.1	65	40	2.5
	3.2	65	40	3.0
	3.3	65	40	3.5
	3.4	65	40	4.0
Exp. 4	4.1	60	50	4.0
	4.2	60	60	4.0

### Experiment set 1: Effects of velocity at 60°C and 40% RH

#### #1.1 Velocity at 1.5 m/s

The temperature distribution, relative humidity (RH) and moisture content profile are presented in Figs. 4.11, 4.12, and 4.13, respectively. The average temperature at T6, T5 and T4, were 55.8°C, 58.3°C and 58.9°C, respectively. Differences in the of average temperatures between any planes were negligible. The total average temperature was 57°C.

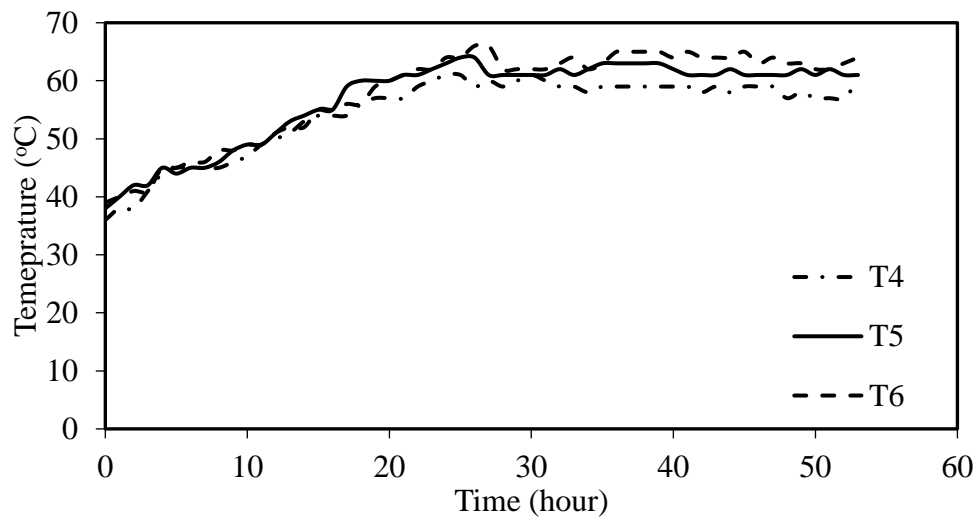


Figure 4.11 Temperature distribution in the chamber at 1.5 m/s, 40% RH, and 60°C.

The relative humidity in the forced convective dryer (RH1) and ambient (RH2) is shown in Fig. 4.12. Relative humidity inside drying room was set to 40% RH but with the limitation in keeping the relative humidity constant which can be



seen from the wavelike profile of the RH, the average RH obtained is 39%. The value of the RH obtained could be due to the high initial moisture in the rubber sheets. The heated water and the recirculation duct were used in regulating the inside RH. Average RH2 was 62%.

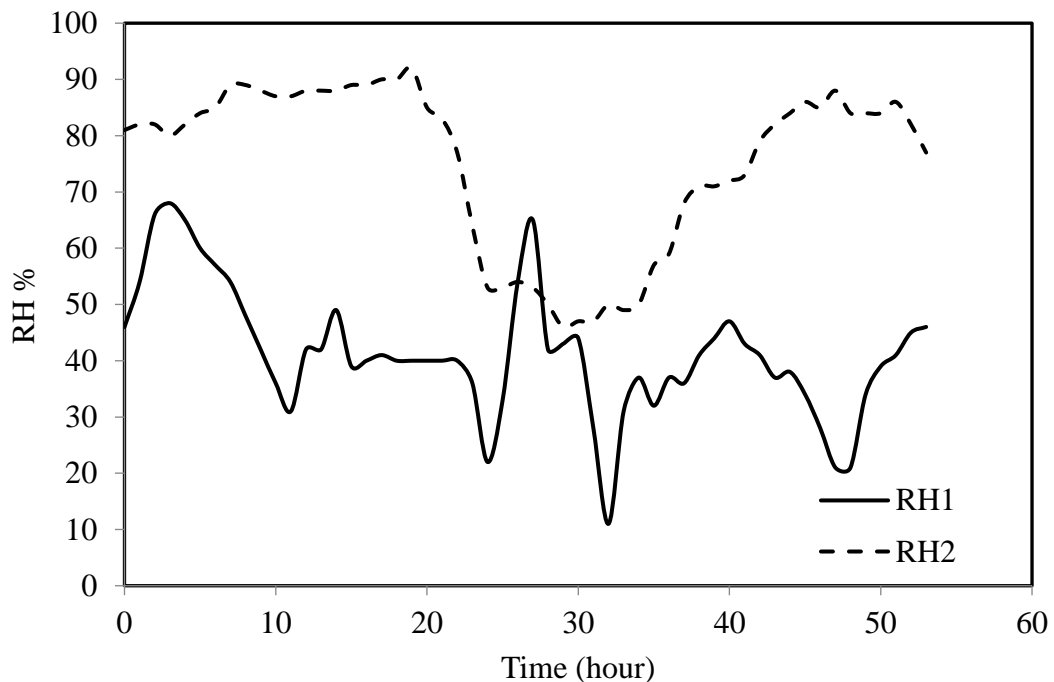


Figure 4.12 Inside (RH1) and ambient relative humidity (RH2) at 1.5 m/s, 40% RH, and 60°C.

Average percentage dry basis moisture content (MC) of four samples of rubber sheets is shown in Fig. 4.13. The MC decreased in an exponential manner from an initial 43 % db to a final 3% db in 53 hours. The final moisture content obtained was largely due to the regulation of the inside RH in the dryer, hence, the moisture content could not be reduced further. The dried samples of rubber sheets had bright gel texture, brown yellow color and without air bubble and granule. The rubber sheet quality was good.

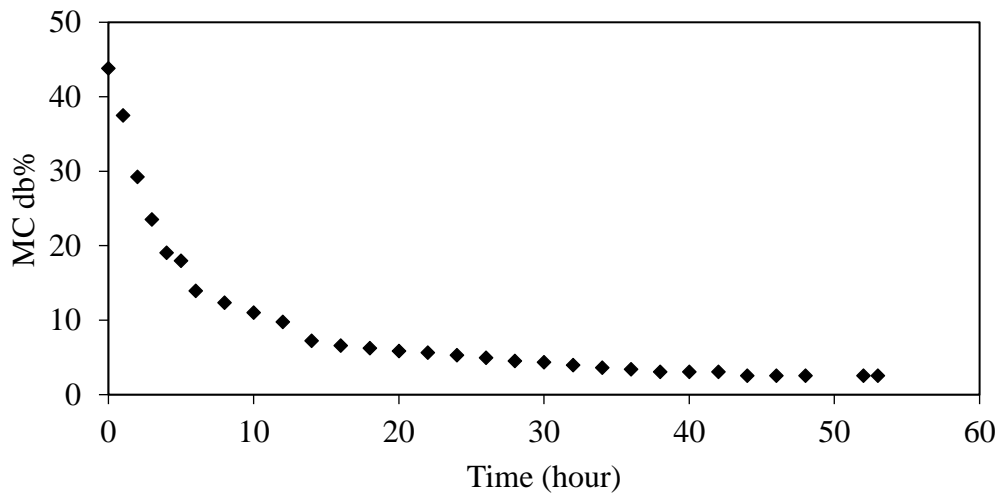


Figure 4.13 Moisture content evolution with time at 1.5 m/s, 40% RH, and 60°C.

### #1.2 Velocity at 3.0 m/s

The temperature distribution, relative humidity and moisture content profile are presented in Figs. 4.14, 4.15, and 4.16, respectively. The average temperature at the top, middle and bottom plane were 55.2°C, 55.5°C and 55.5°C respectively. Differences in the of average temperatures between any planes are negligible. The total average temperature is 55°C. The temperature variations were minimized largely due to the temperature control systems installed in the dryer.

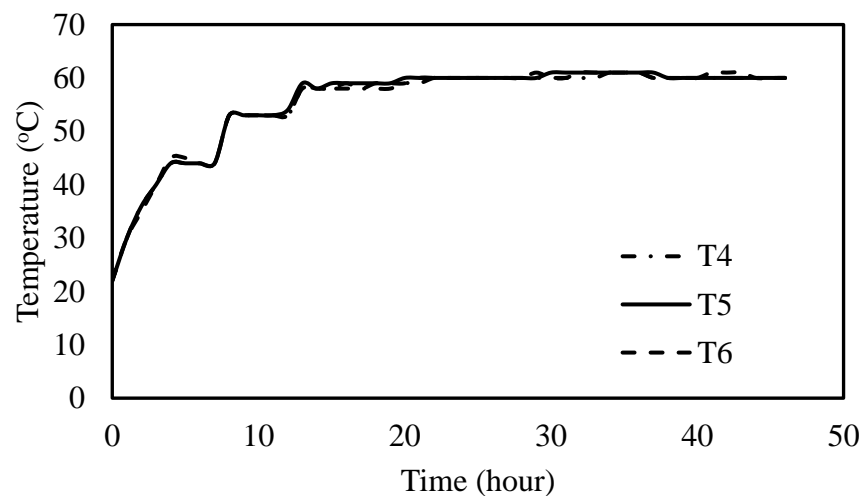


Figure 4.14 Temperature distribution in the chamber at 3.0 m/s, 40% RH, and 60°C.

The relative humidity in the forced convective dryer (RH1) and ambient (RH2) are shown in Fig. 4.15. Relative humidity inside drying room was set to 40% RH but the average obtained value of RH1 was 31%. The heated water and the recirculation duct were used in regulating RH1. Average RH2 was 79% due to the prevalence of rainfall during the period of the experiment.

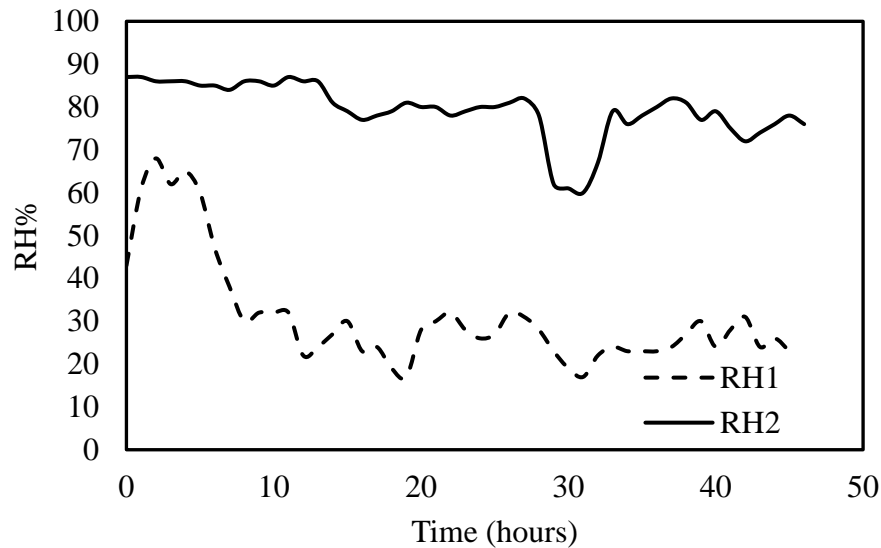


Figure 4.15 Inside (RH1) and ambient relative humidity (RH2) at 3.0 m/s, 40% RH, and 60°C.

Average percentage dry basis MC of four samples of rubber sheets is shown in Fig. 4.16. The MC decreased from an initial 37.3% db to a final 0.5% db in 46 hours. The reduced final moisture content was due to reduction in the holding relative humidity inside the chamber. The rubber sheet quality was good.

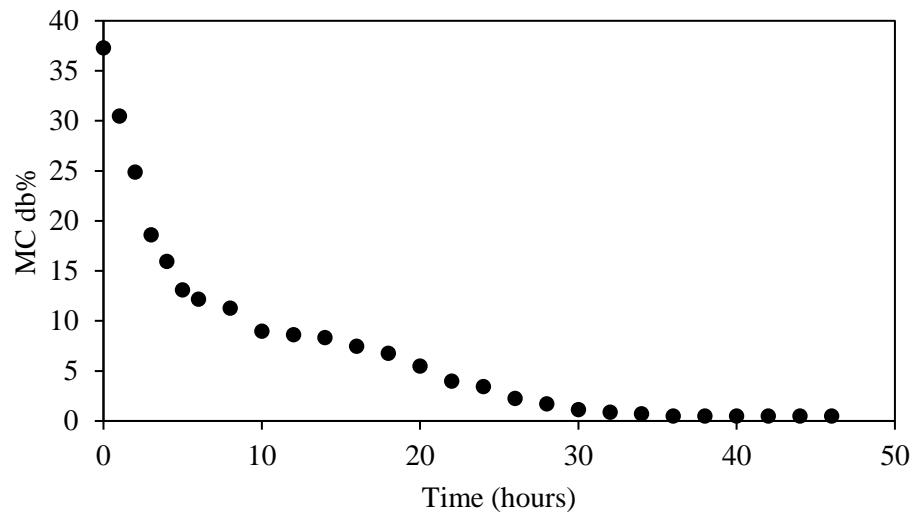


Figure 4.16 Moisture content evolution with time at 3.0 m/s, 40% RH, and 60°C.

### #1.3 Velocity at 3.5 m/s

The temperature distribution, relative humidity and moisture content profile are presented in Figs. 4.17, 4.18, and 4.19, respectively. The average temperature at the top, middle and bottom plane were 56.2°C, 56.6°C and 56.5°C, respectively. Differences in the of average temperatures between any planes were almost same. The total average temperature was 56°C.

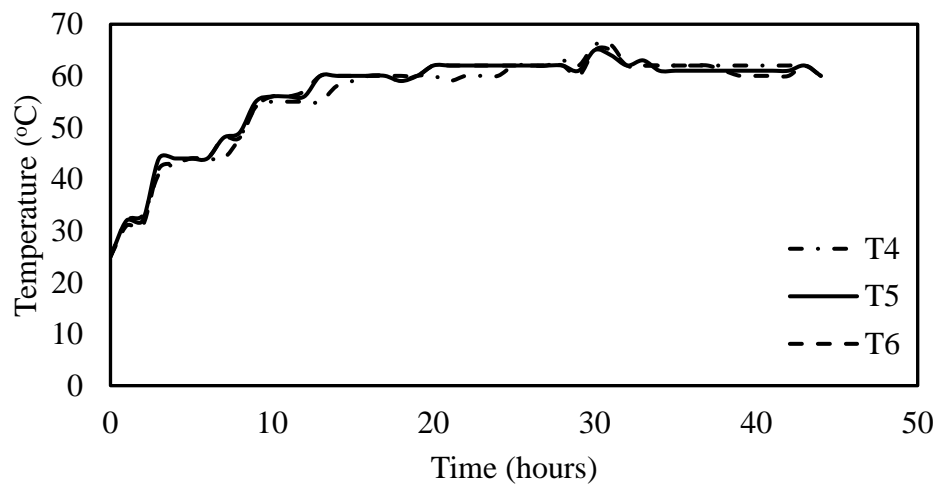


Figure 4.17 Temperature distribution in the chamber at 3.5 m/s, 40% RH, and 60°C.

The relative humidity in the forced convective dryer (RH1) and ambient (RH2) are shown in Fig. 4.18. RH1 was set to 40% RH but the average obtained value was 33%. The heated water and the recirculation duct were used in regulating RH1. Average RH2 was 75%.

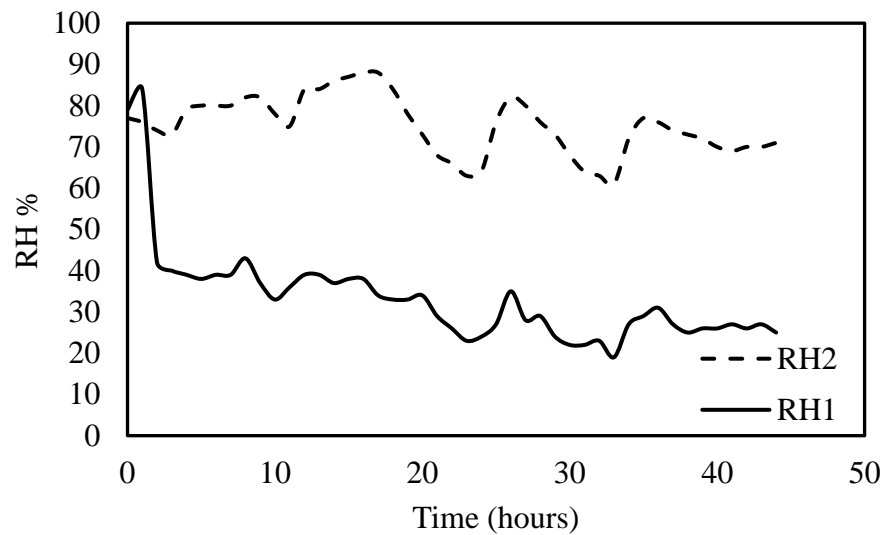


Figure 4.18 Inside (RH1) and ambient relative humidity (RH2) at 3.5 m/s, 40% RH, and 60°C.

Average percentage dry basis MC is shown in Fig. 4.19. The MC decreased from an initial 35.1% db to a final 1% db in 43 hours. The dried samples of rubber sheets were of good quality.

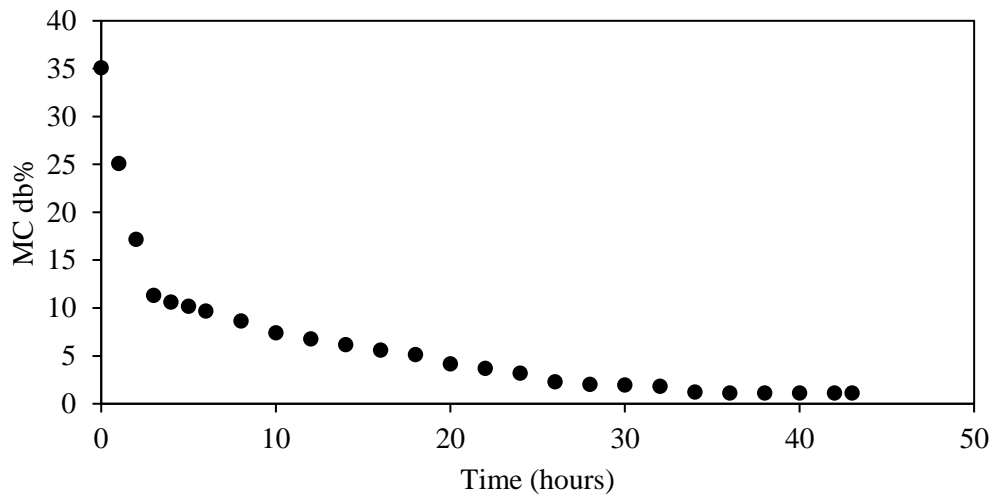


Figure 4.19 Moisture content evolution with time at 3.5 m/s, 40% RH, and 60°C.

#### #1.4 Velocity at 4.0 m/s

The temperature distribution, relative humidity and moisture content profile are presented in Figs. 4.20, 4.21, and 4.22, respectively. The average temperature at the top, middle and bottom plane were 55.2°C, 55.1°C and 55.4°C, respectively. Differences in the of average temperatures between any planes were negligible. The total average temperature was 55°C.

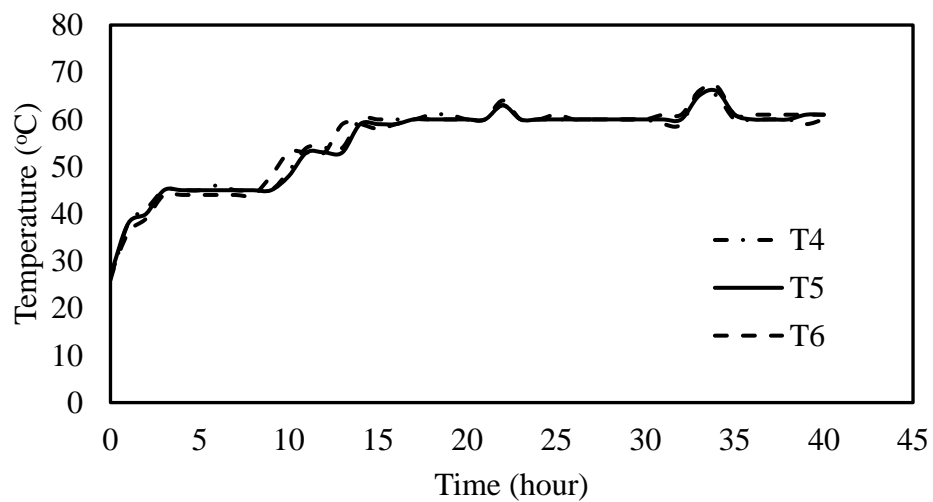


Figure 4.20 Temperature distribution in the chamber at 4.0 m/s, 40% RH, and 60°C.

The relative humidity in the forced convective dryer (RH1) and ambient (RH2) are shown in Fig. 4.21. RH1 was set to 40% RH but an average RH 31% was actually obtained. The heated water and the recirculation duct were used in regulating RH1. Average RH2 was 70%.

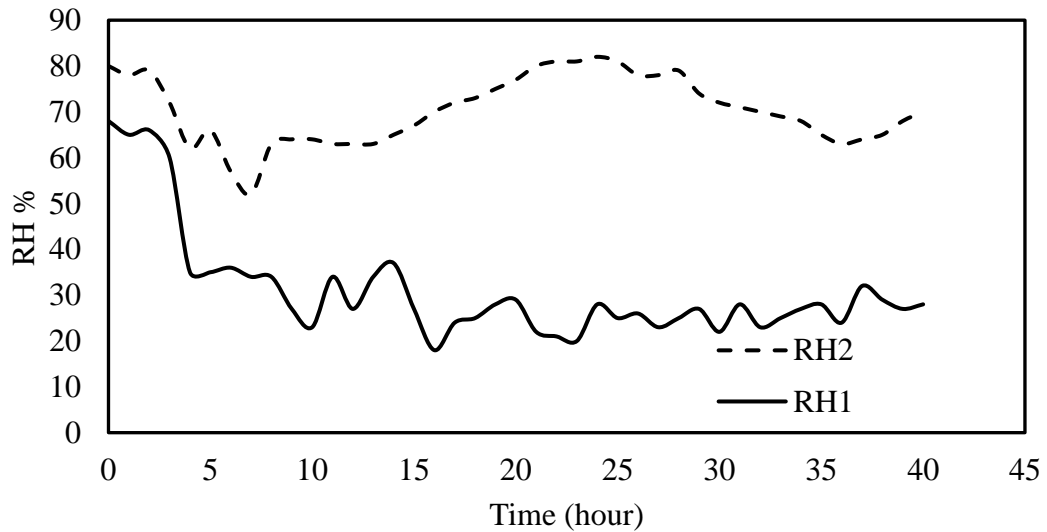


Figure 4.21 Inside (RH1) and ambient relative humidity (RH2) at 4.0 m/s, 40% RH, and 60°C.

Average percentage dry basis MC of four samples of rubber sheets is shown in Fig. 4.22. The MC reduced progressively from an initial 32.9% db to a final 0.6% db in 40 hours. The dried samples of rubber sheets have bright gel texture, brown yellow color and without air bubble and granule.

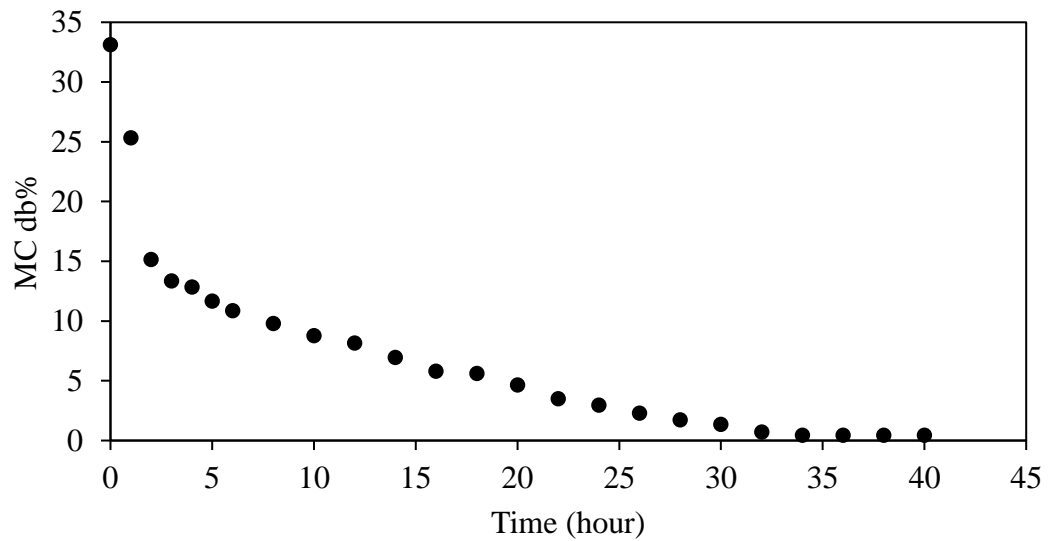


Figure 4.22 Moisture content evolution with time at 4.0 m/s, 40% RH, and 60°C.

Effects of the drying air velocity at 40% RH, and 60°C are summarized in Table 4.3 and Fig. 4.23. High drying air velocity lowered the drying time. The quality of the dried sheets for all the conditions were good. Hence, drying at the highest obtainable velocity of 4.0 m/s from the system gave the optimal drying time as one could expect. From Table 4.3, it was observed that the least drying time was 40 hours at the highest obtainable velocity of 4.0 m/s. Fig. 4.23 shows that the MC evolution was more drastic for velocity of 4.0 m/s compared to the lower values of velocities and hence, the least drying time.

Table 4.3 Influence of velocity variation on drying time and rubber sheet quality at 60°C and 40% RH.

Exp.			Ideal inlet RH	Velocity m/s	Time (hours)	Realized Average Inlet RH%	Final MC db%	Quality
	S/N	T °C						
Exp. 1	1.1	60	40	1.5	53	39	3	Good
	1.2	60	40	3.0	46	31	0.5	Good
	1.3	60	40	3.5	43	33	1	Good
	1.4	60	40	4.0	40	31	0.6	Good



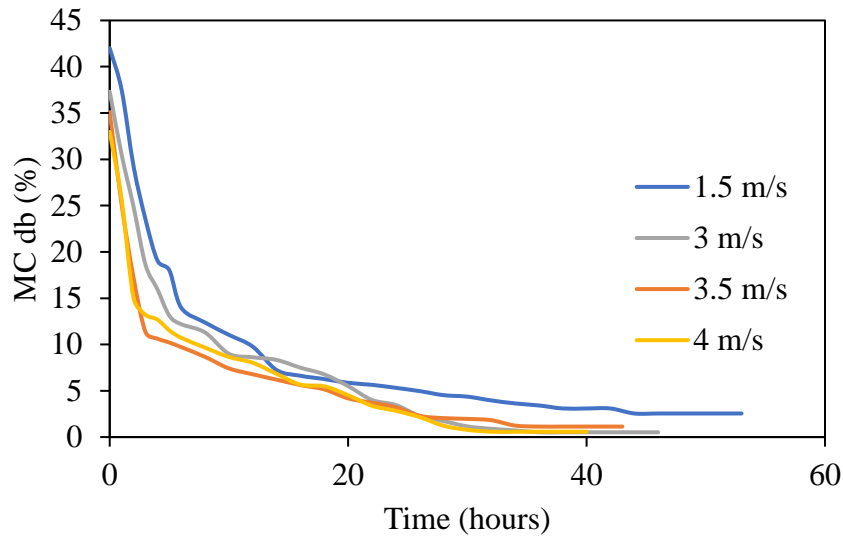


Figure 4.23 Moisture content profile with time at varying velocity.

### Experiment set 2: Effects of Temperature at 4.0 m/s and 40% RH

In the preceding experiments, temperature and relative humidity were kept constant at 60°C and 40%, respectively. It was found that velocity can be increased to the maximum capacity of the dryer at 4.0 m/s without deteriorating quality of the rubber sheets under drying process. In this section, the velocity is kept maximum at 4.0 m/s and relative humidity was maintained at 40%. Temperature was increased to determine the maximum temperature allowed.

#### #2.1 Temperature at 65°C.

The temperature distribution, relative humidity and moisture content profile are presented in Figs. 4.24, 4.25, and 4.26, respectively. The average temperature (Fig. 4.24) at the top, middle and bottom plane were 59.9°C, 60.3°C and 58.6°C, respectively. However, the differences in the average temperatures between any planes were negligible. The total average temperature was 60°C.

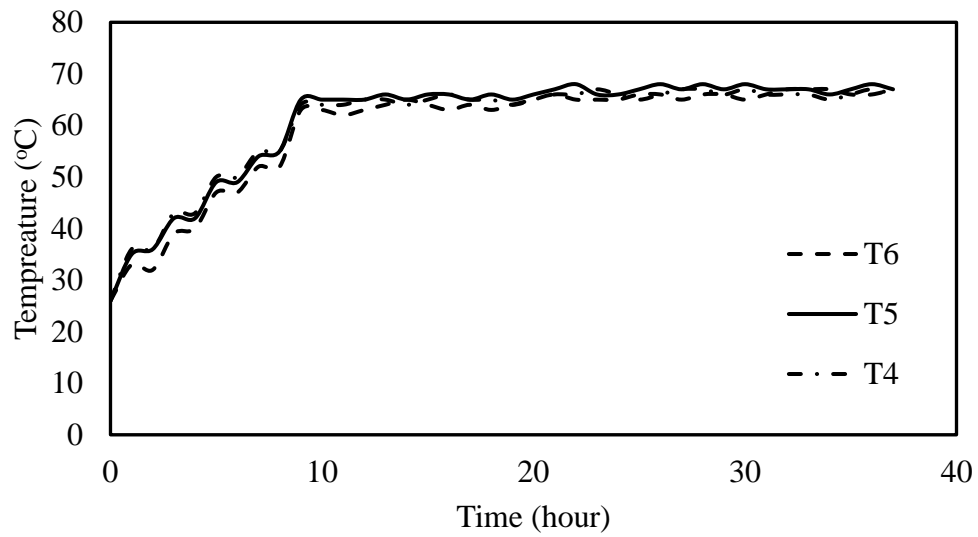


Figure 4.24 Temperature distribution in the chamber at 4.0 m/s, 40% RH, and 65°C.

The relative humidity in the forced convective dryer (RH1) and ambient (RH2) are shown in Fig. 4.25. The average RH1 of 22.3% was actually obtained. The heated water and the recirculation duct were used in regulating the inside RH. Average RH2 was 79.9%.

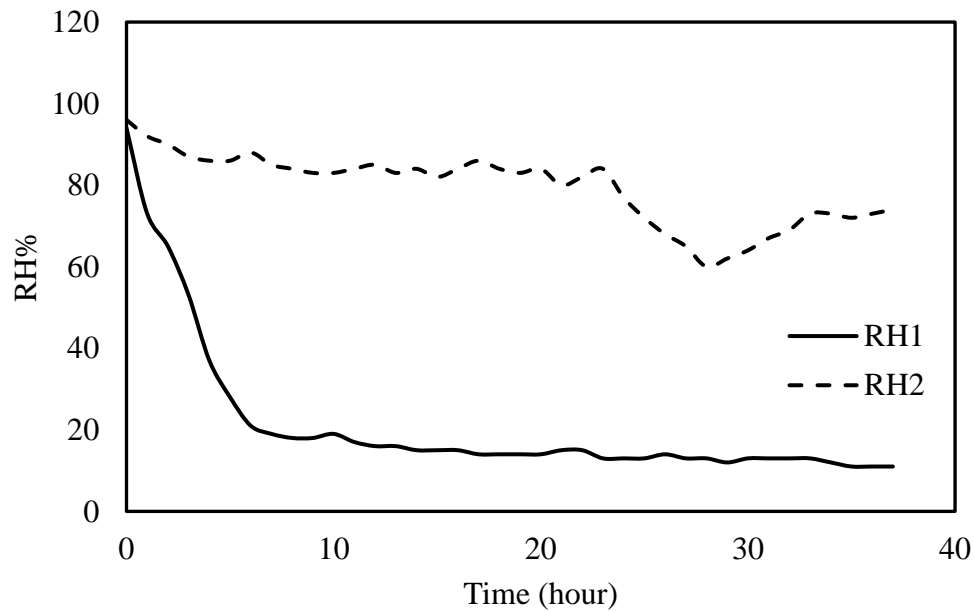


Figure 4.25 Inside (RH1) and ambient relative humidity (RH2) at 4.0 m/s, 40% RH, and 65°C.

Average percentage dry basis MC of four samples of rubber sheets is shown in Fig. 4.26. The MC decreased from an initial 29.2% db to a final 0.4% db in 37 hours. The dried samples of rubber sheets have large bubbles formed on them as shown in Fig. 4.27. Hence, this is unsuitable condition for drying.

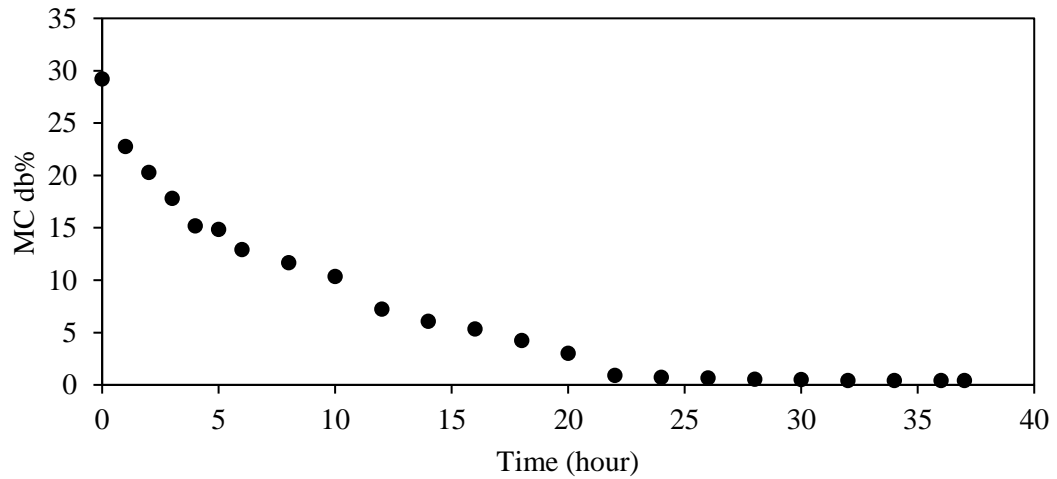


Figure 4.26 Moisture content evolution with time at 4.0 m/s, 40% RH, and 65°C.



Figure 4.27 Rubber sheets with bubbles formed at 4.0 m/s, 40% RH and 65°C.

## #2.2 Temperature at 70°C.

The temperature distribution, relative humidity and moisture content profile are presented in Figs. 4.28, 4.29, and 4.30, respectively. The average temperature at the top, middle and bottom plane were 58.7 °C, 59.8 °C and 61.6 °C, respectively. However, the differences in the of average temperatures between any planes were negligible. The total average temperature was 60 °C.

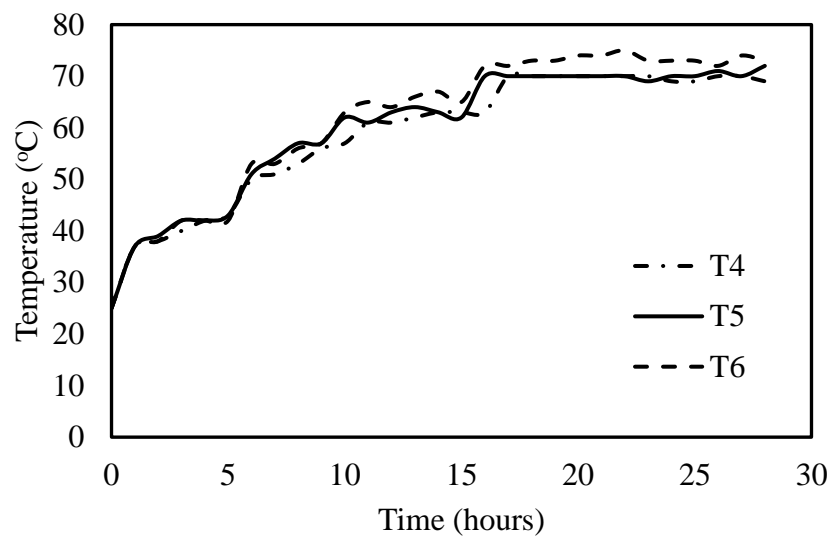


Figure 4.28 Temperature distribution in the chamber at 4.0 m/s, 40% RH, and 70°C.

The relative humidity in the forced convective dryer (RH1) and ambient (RH2) are shown in Fig. 4.29. RH1 was set to the lowest possible RH with an average RH1 of 21% actually obtained. The heated water and the recirculation duct were used in regulating RH1. Average RH2 obtained was 75%.

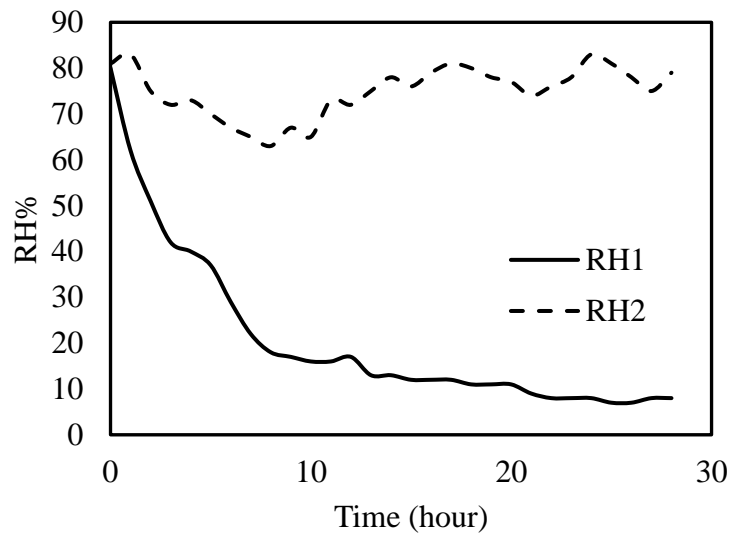


Figure 4.29 Inside (RH1) and ambient relative humidity (RH2) at 4.0 m/s, 40% RH, and 70°C.

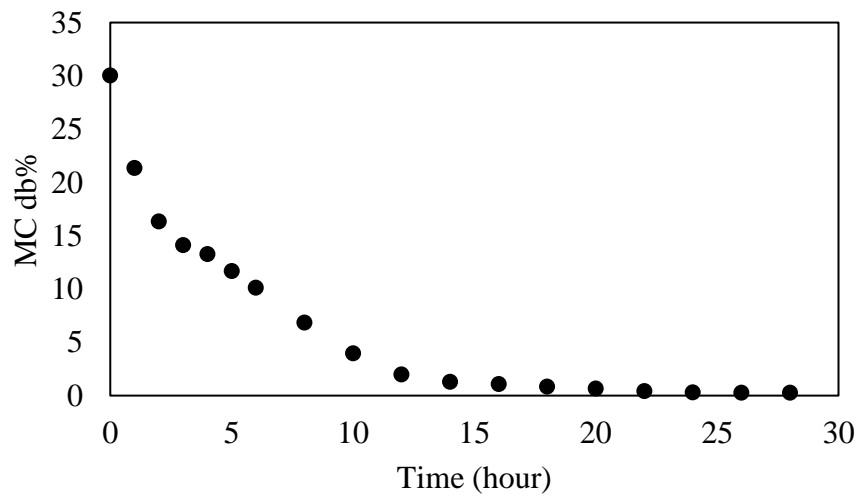


Figure 4.30 Moisture content evolution with time at 4.0 m/s, 40% RH, and 70°C.

Average percentage dry basis MC of four samples of rubber sheets is shown in Fig. 4.30. The MC decreased from an initial 30.1 % db to a final 0.3% db in 28 hours. The lowest time achieved in all the experiment, but with the large bubbles developed as shown in Fig. 31. The condition is unsuitable for the quality of the rubber sheets.



Figure 4.31 Rubber sheets with bubbles formed at 4.0 m/s, 40% RH and 70°C.

The influence of temperature on the drying time at the highest velocity obtainable in the experiment 4.0 m/s and the RH of 40% are summarized in Table 4.4 and Fig. 4.32. The falling drying rate period at 70°C was the most drastic and thus have the least drying time of 28h. However, the quality of the rubber sheets at 70°C was bad and hence drying at 70°C is unsuitable for rubber sheets. At 65°C and 4.0 m/s velocity, the drying time is 37 hours and the rubber sheets quality are equally compromised. Lastly, from the two experimental results, it can be concluded that drying at temperature of 65°C and 70°C at the highest system velocity of 4 m/s are unsuitable rubber sheet due to bubble formation on the rubber sheets due to excessively high temperature. The numbers of bad sheets from the experiments were 2 and 3 for temperatures 65°C and 70°C, respectively.

Table 4.4 Influence of temperature variation on drying time at 4. m/s and 40% RH.

Exp.	T °C	Ideal	Velocity (m/s)	Time (hours)	Realized	Final	Quality
		inlet RH			Average Inlet RH%	MC db%	
2.1	65	40	2.5	38	18	0.4	Not good (2 sheets)
2.2	65	40	3.0	39	18	0.4	Not good (3 sheets)

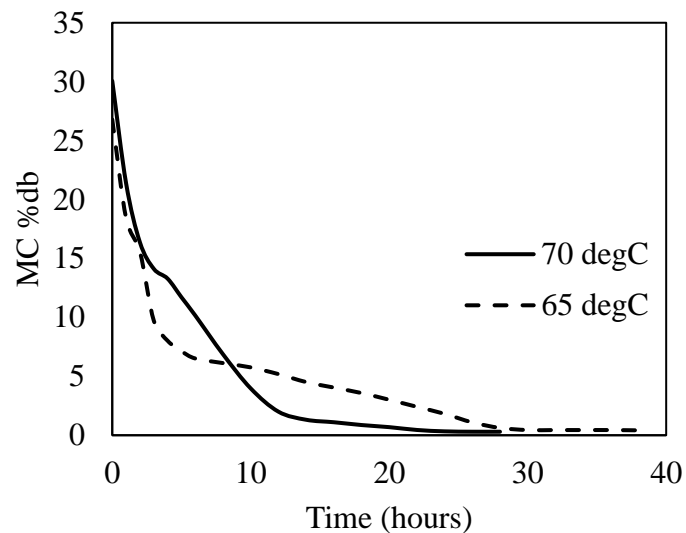


Figure 4.32 Moisture content variation at varying temperature.

### Experiment set 3: Effects of velocity at 65°C and 40% RH

From preceding two sets of experiments, the fastest drying condition that maintains good quality of the rubber sheets was 60°C, 4.0 m/s and 40% RH. Drying time was 40 hours. In this section, the temperature 65°C and relative humidity was maintained at 40% to double check if the elevated temperature is suitable at lower velocity. Velocity was increased to determine the maximum velocity allowed for quality rubber sheet at 65°C

### #3.1 Velocity at 2.5 m/s.

The temperature distribution, relative humidity and moisture content profile are presented in Figs. 4.33, 4.34, and 4.35, respectively. The average temperature at the top, middle and bottom plane were 58.7°C, 58.9°C and 59.4°C, respectively. Differences in the of average temperatures between any planes were negligible. The total average temperature was 59°C.

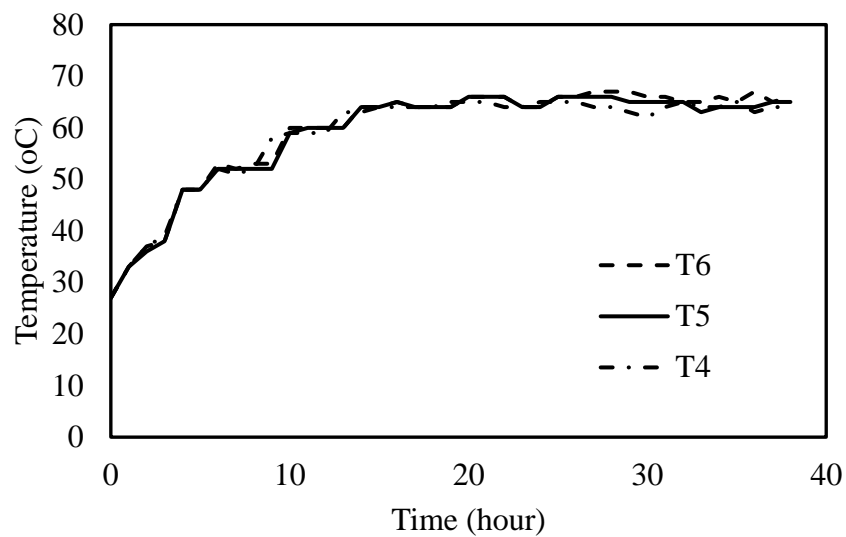


Figure 4.33 Temperature distribution in the chamber at 2.5 m/s, 40% RH and 65°C.

The relative humidity in the forced convective dryer (RH1) and ambient (RH2) are shown in Fig. 4.34. Average RH1 is 17.8%. The heated water and the recirculation duct were used in regulating the RH1. Average RH2 was 63.7%.



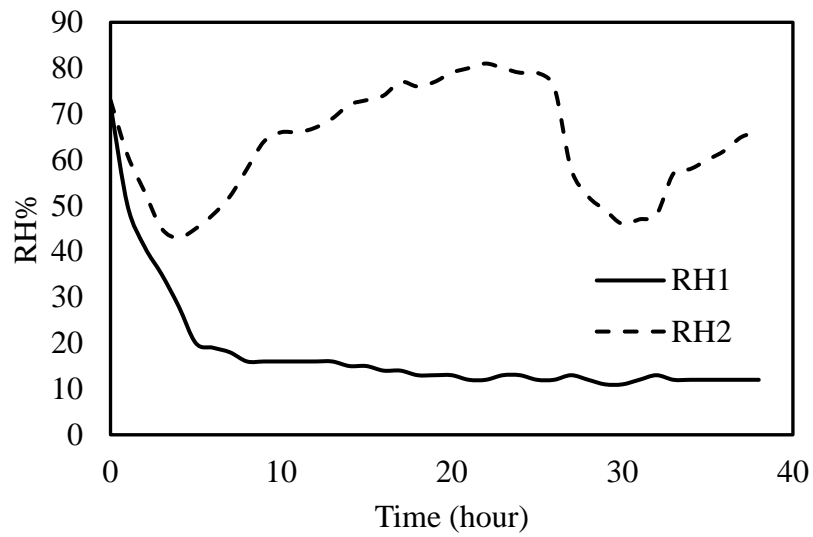


Figure 4.34 Inside (RH1) and ambient relative humidity (RH2) at 2.5 m/s, 40% RH and 65°C.

Average percentage dry basis MC of four samples of rubber sheets is shown in Fig. 4.35. The MC decreased from an initial 27% db to a final 0.4% db in 38 hours. The dried samples of rubber sheets have bubbles developed in them.

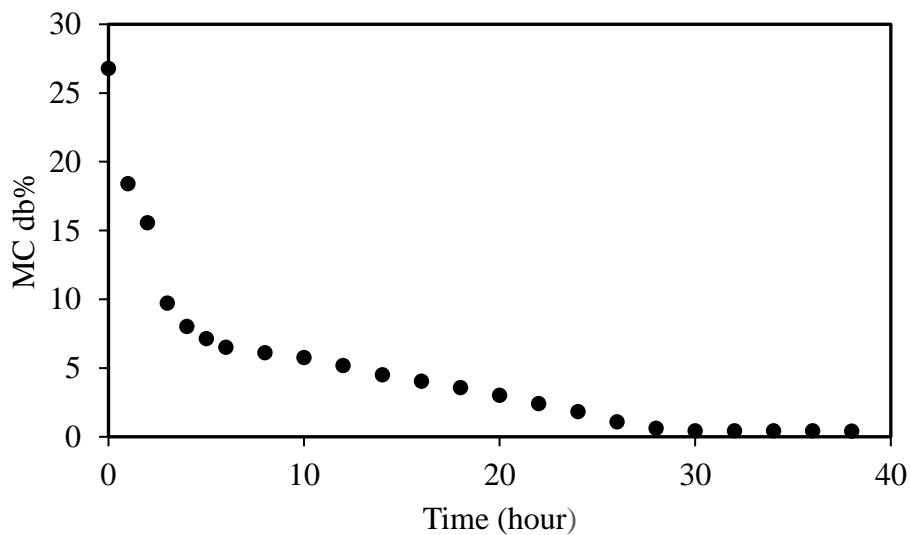


Figure 4.35 Moisture content evolution with time at 2.5 m/s, 40% RH, and 65°C.

### #3.2 Velocity at 3.0 m/s.

The temperature distribution, relative humidity and moisture content profile are presented in Figs. 4.36, 4.37, and 4.38, respectively. The average temperature (Fig. 4.36) at the top, middle and bottom plane were 58.9°C, 59.5°C and 60.0°C, respectively. However, the differences in the of average temperatures between any planes were negligible. The total average temperature was 60°C.

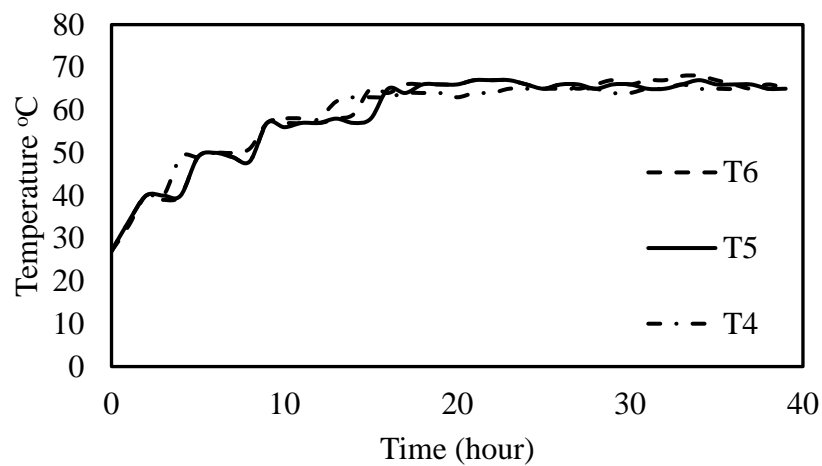


Figure 4.36 Temperature distribution in the chamber at 3.0 m/s, 40% RH and 65°C.

The relative humidity in the forced convective dryer (RH1) and ambient (RH2) are shown in Fig. 4.37. Average RH1 is 18.5%. The heated water and the recirculation duct were used in regulating the RH1. Average RH2 was 67.8%.

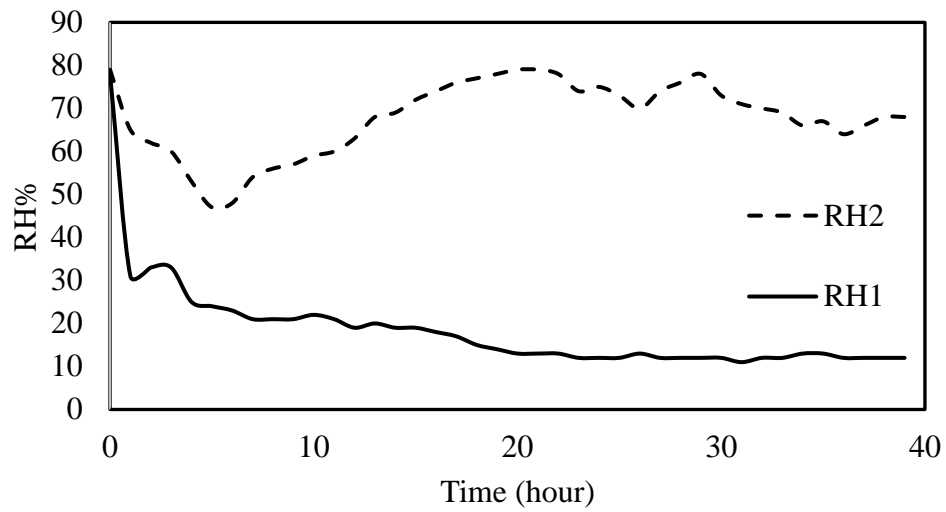


Figure 4.37 Inside (RH1) and ambient relative humidity (RH2) at 3.0 m/s, 40% RH and 65°C.

Average percentage dry basis MC of four samples of rubber sheets is shown in Fig. 4.38. The MC decreased from an initial 28 % db to a final 0.4% db in 39 hours. The dried samples of rubber sheets have bubbles developed in them.

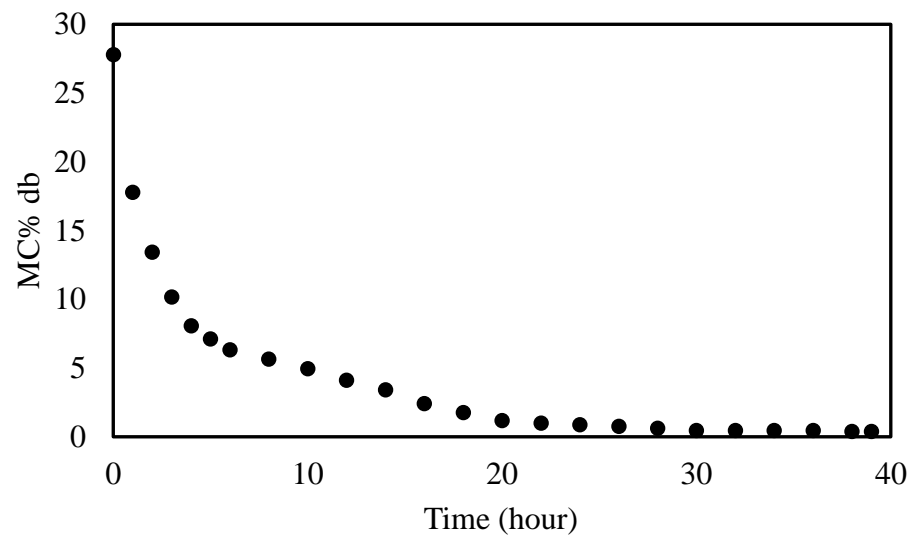


Figure 4.38 Moisture content evolution with time at 3.0 m/s, 40% RH and 65°C.

### #3.3 Velocity at 3.5 m/s.

The temperature distribution, relative humidity and moisture content profile are presented in Figs. 4.39, 4.40, and 4.41, respectively. The average temperature (Fig. 4.39) at the top, middle and bottom plane were 55.8°C, 56.6°C and 57.7°C, respectively. However, the differences in the of average temperatures between any planes are negligible. The total average temperature was 57°C.

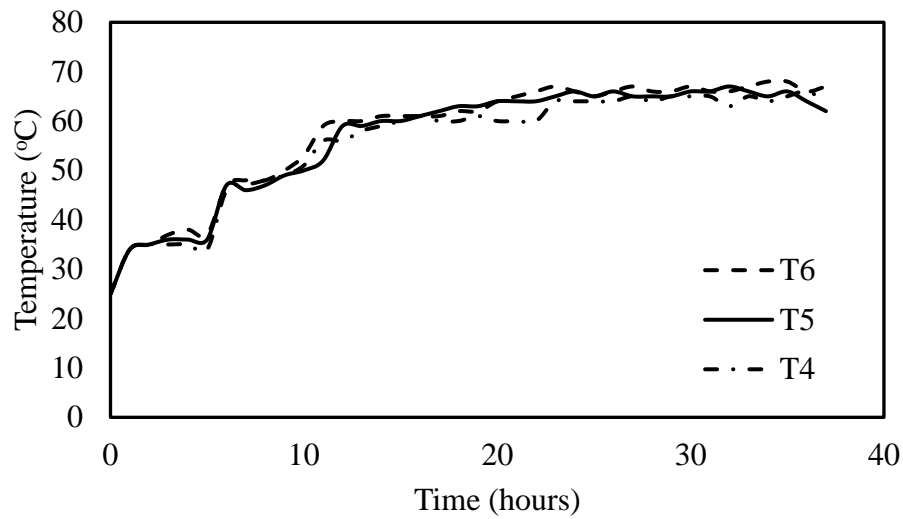


Figure 4.39 Temperature distribution in the chamber at 3.5 m/s, 40% RH and 65°C.

The relative humidity in the forced convective dryer (RH1) and ambient (RH2) are shown in Fig. 4.40. Average RH1 was 18.8%. The heated water and the recirculation duct were used in regulating RH1. Average RH2 was 68.3%.

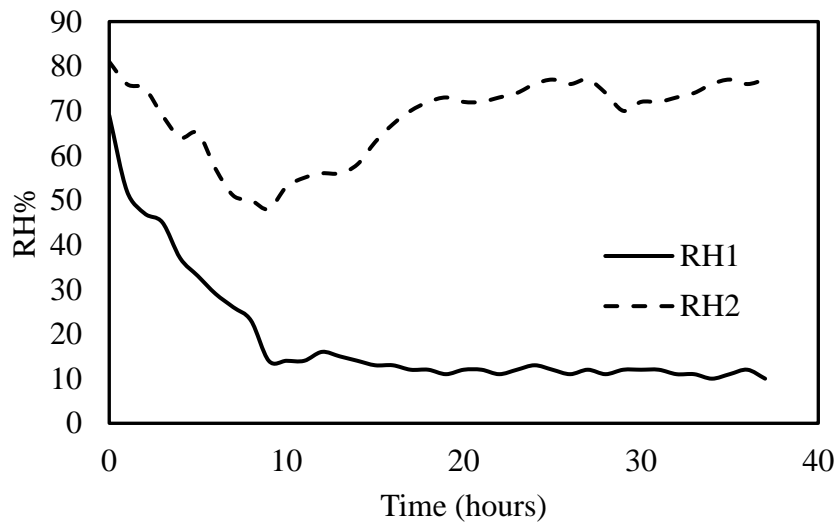


Figure 4.40 Inside (RH1) and ambient relative humidity (RH2) at 3.5 m/s, 40% RH and 65°C.

Average percentage dry basis MC of four samples of rubber sheets is shown in Fig. 4.41. The MC decreased from an initial 30% db to a final 0.4% db in 40 hours. The dried samples of rubber sheets have bubbles developed in them.

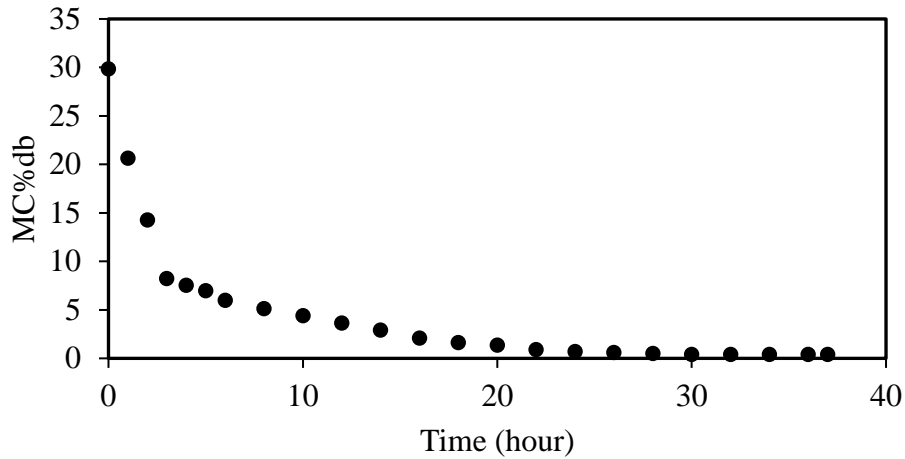


Figure 4.41 Moisture content evolution with time at 3.5 m/s, 40% RH and 65°C.

### #3.4 Velocity at 4.0 m/s.

The temperature distribution, relative humidity and moisture content profile are presented in Figs. 4.42, 4.43, and 4.44, respectively. The average temperature (Fig. 4.42) at the top, middle and bottom plane are 60.3°C, 60.6°C and 60°C, respectively. However, the differences in the of average temperatures between any planes were negligible. The total average temperature was 60°C.

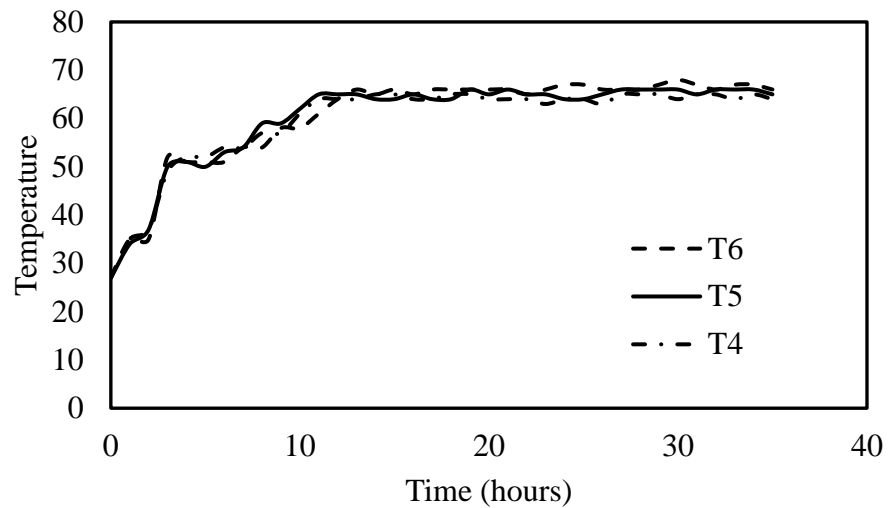


Figure 4.42 Temperature distribution in the chamber at 4.0 m/s, 40% RH and 65°C.

The relative humidity in the forced convective dryer (RH1) and ambient (RH2) are shown in Fig. 4.43. Average RH1 is 19.2%. The heated water and the recirculation duct are used in regulating RH1. Average RH2 was 63.6%.

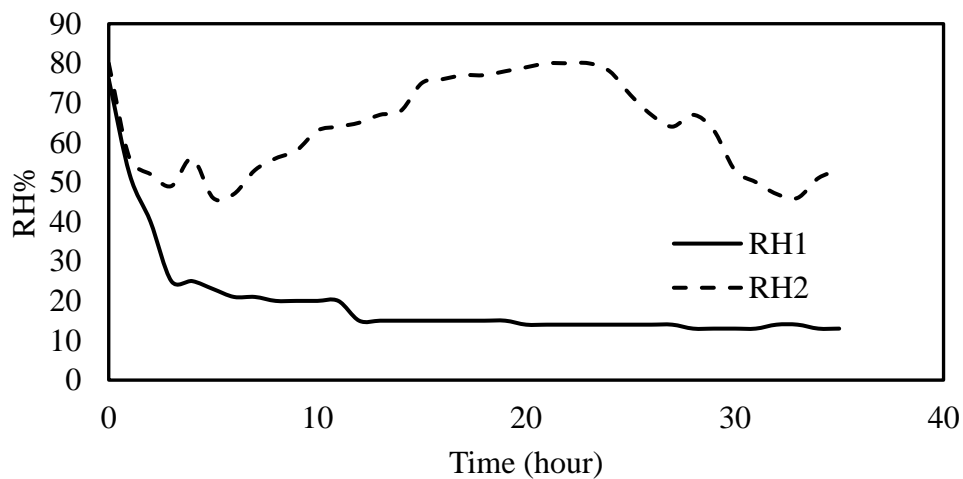


Figure 4.43 Inside (RH1) and ambient relative humidity (RH2) at 4m/s, 40% RH and 65°C.

Average percentage dry basis MC of four samples of rubber sheets is shown in Fig. 4.44. The MC decreased from an initial 27% db to a final 0.4% db in 35 hours. The dried samples of rubber sheets have bubbles developed in them.

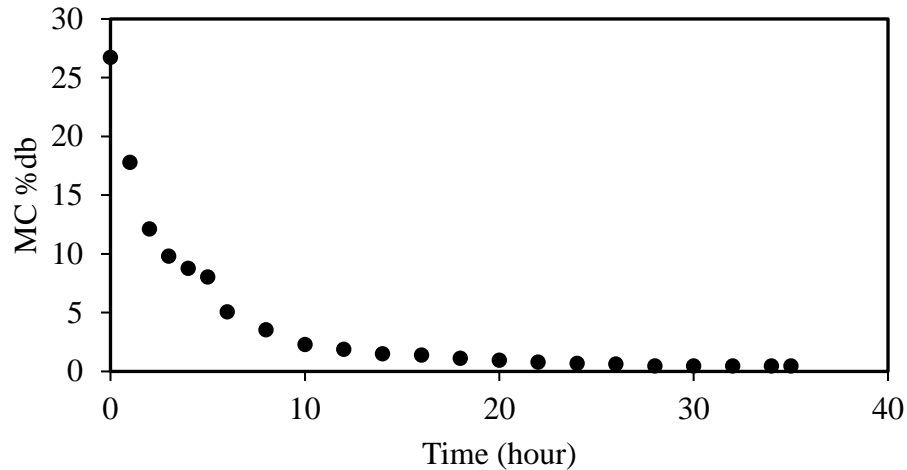


Figure 4.44 Moisture content evolution with time at 4m/s, 40% RH and 65°C.

Effects of the drying air velocity at 65°C and 40% RH are summarized in Table 4.5 and Fig. 4.45. High drying air velocity lower the drying time. However, from the quality of experiment 3.2 to 3.4, It was observed that there is formation of bubbles on the rubber sheets. The number of bad sheets for experiment 3.2, 3.3 and 3.4 were 1, 2 and 3, respectively. From Table 4.5, it was observed that the least drying time was 35 hours at the highest obtainable velocity of 4.0 m/s but the quality of the sheets was not good. The drying time of 38 hours though had good rubber sheet quality with no bubbles. Fig. 4.45 shows that the MC evolution was more drastic for velocity of 4.0 m/s compared to the lower values of velocities and hence, the least drying time. Thus, drying at velocity of 2.5 m/s is optimal drying in terms of the drying time and quality.



Table 4.5 Influence of velocity at 65°C and 40% RH on drying time.

Exp.	T °C	Ideal		Time (hours)	Realized		Quality
		inlet RH	Velocity (m/s)		Average Inlet RH%	Final MC db%	
3.1	65	40	2.5	38	18	0.4	Good
3.2	65	40	3.0	39	18	0.4	Not good (1 sheets)
3.3	65	40	3.5	37	19	0.4	Not good (3 sheets)
3.4	65	40	4.0	35	19	0.4	Not good (2 sheets)

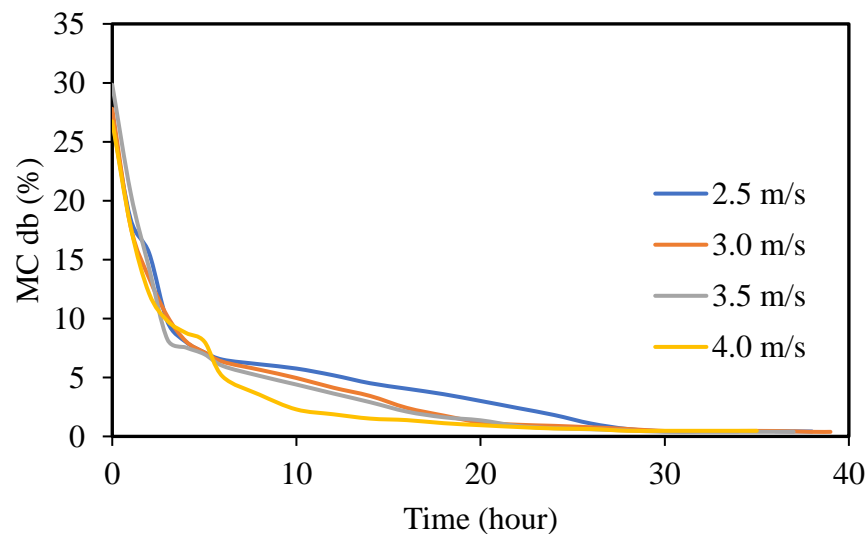


Figure 4.45 Moisture content variation with varying velocity at 65°C.

#### Experiment set 4: Effect of Relative Humidity at 60°C and 4.0 m/s

From all of experiments above, the fastest drying condition that maintains good quality of the rubber sheets is 65°C, 2.5 m/s and 40% RH. Drying time is 38 hours. However, higher velocity at 65°C affected the rubber quality. In this section, the temperature was kept at 60 °C and velocity was maintained at 4 m/s. Relative humidity was varied to determine its effect on the drying time and EMC of the rubber sheet.

##### #4.1 Relative humidity at 50%.

The temperature distribution, relative humidity and moisture content profile are presented in Figs. 4.46, 4.47, and 4.48, respectively. The average temperature

(Fig. 4.46) at the top, middle and bottom plane were 56.6°C, 56.9°C and 57.1°C, respectively. However, the differences in the average temperatures between any planes were negligible. The total average temperature was 57°C.

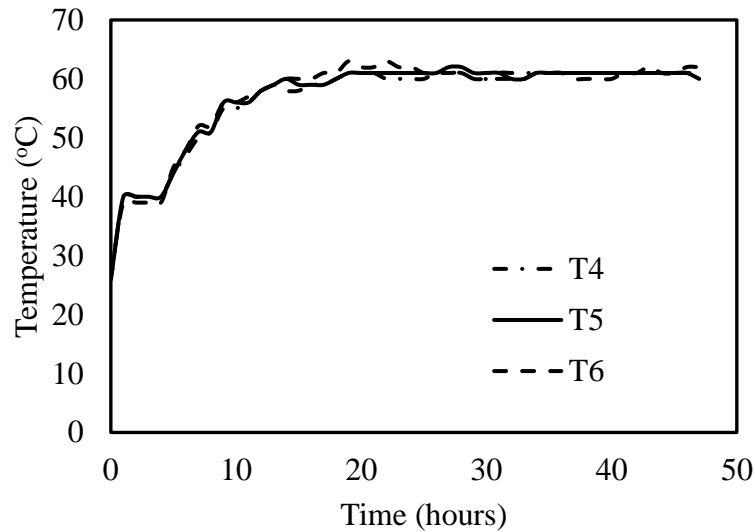


Figure 4.46 Temperature distribution in the chamber at 4.0 m/s, 50% RH, and 60°C.

Inside (RH1) and ambient relative humidity (RH2) are shown in Fig. 4.47. RH1 was set to 50% RH but with the limitation in keeping the relative humidity constant which can be seen from the wavelike profile of the RH, the average RH realized was 38%. The heated water and the recirculation duct were used in regulating RH1. Average RH2 was 76%.

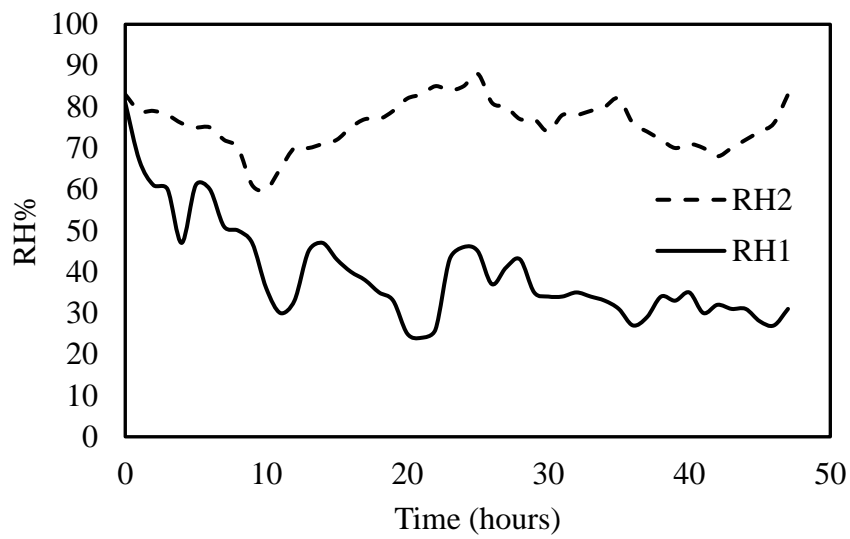


Figure 4.47 Inside (RH1) and ambient relative humidity (RH2) at 4.0m/s, 50% RH, and 60°C.

Average percentage dry basis MC of four samples of rubber sheets is shown in Fig. 4.48. The MC decreased in an exponential manner from an initial 34.2% db to a final 1.4% db in 47 hours. RH2 is one of the most important factors that determines the drying rate. The rubber sheet quality was good with no bubbles formed.

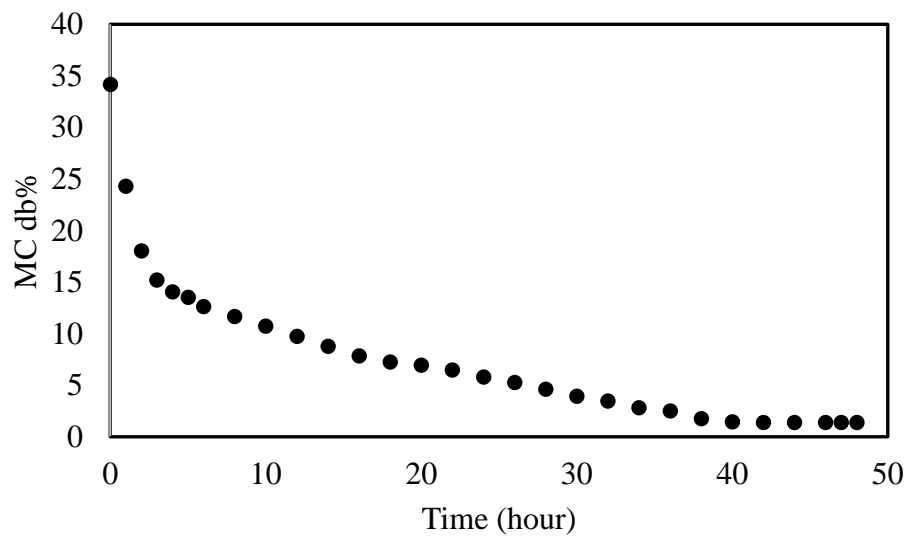


Figure 4.48 Moisture content evolution with time at 4.0 m/s, 50% RH, and 60°C.

#### #4.2 Relative humidity at 60% RH.

The temperature distribution, relative humidity and moisture content profile are presented in Figs. 4.49, 4.50, and 4.51, respectively. The average temperature at the top, middle and bottom plane are 57.4°C, 56.2°C and 57.9°C, respectively. Differences in the of average temperatures between any planes were negligible. The total average temperature was 57 °C.

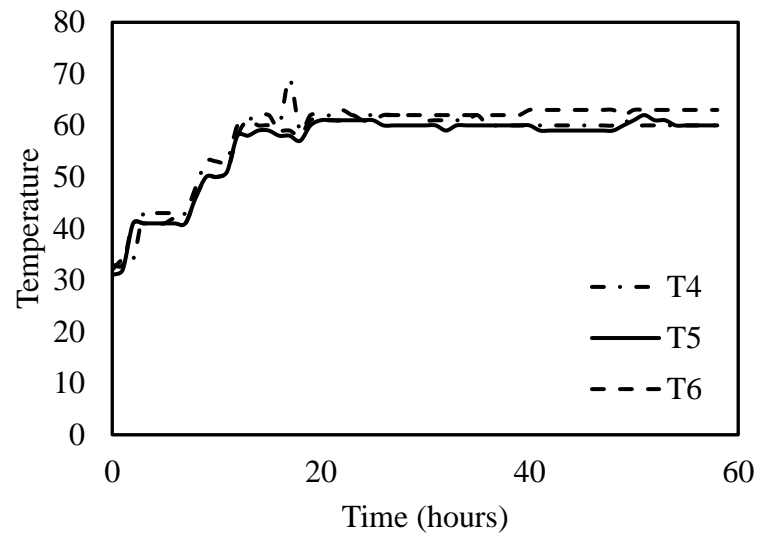


Figure 4.49 Temperature distribution in the chamber at 4.0 m/s, 60 RH, and 60°C.

Inside (RH1) and ambient relative humidity (RH2) are shown in Fig. 4.50. RH1 was regulated at 60% RH but an average of 45% was actually obtained. The heated water and the recirculation duct are used in regulating RH1. Average RH2 was 74%.

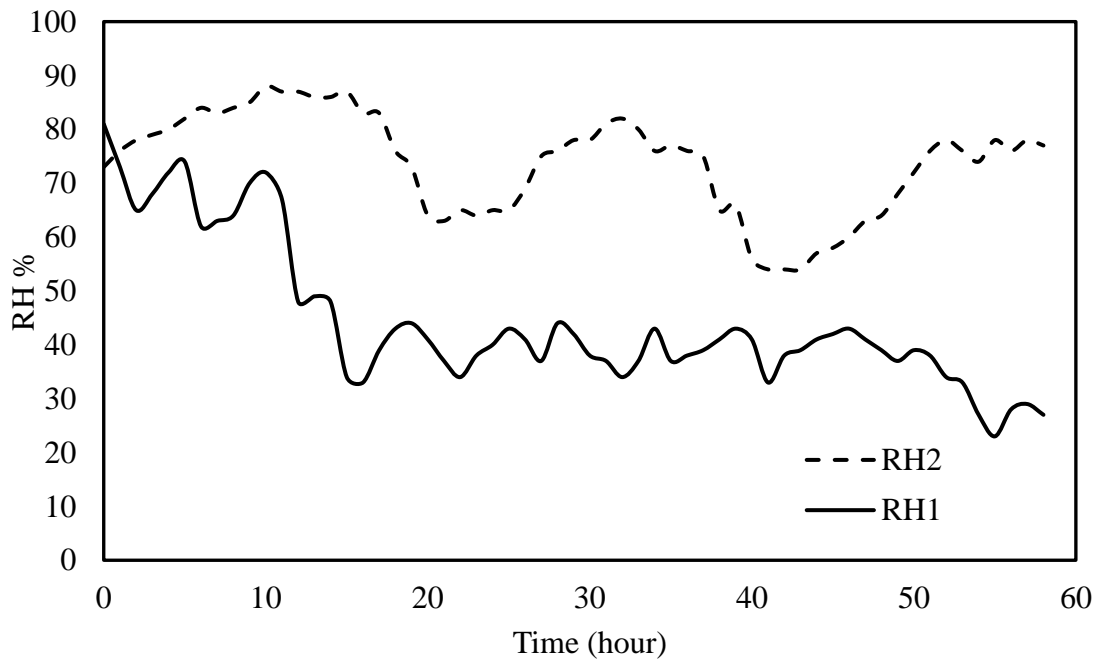


Figure 4.50 Inside (RH1) and ambient relative humidity (RH2) at 4.0 m/s, 60% RH, and 60°C.

Average percentage dry basis MC of four samples of rubber sheets is shown in Fig. 4.51. The MC decreased from an initial 36.2% db to a final 1.6% db in 58 hours. The longer drying time is likely due to the increased holding RH. The rubber sheet quality was good.

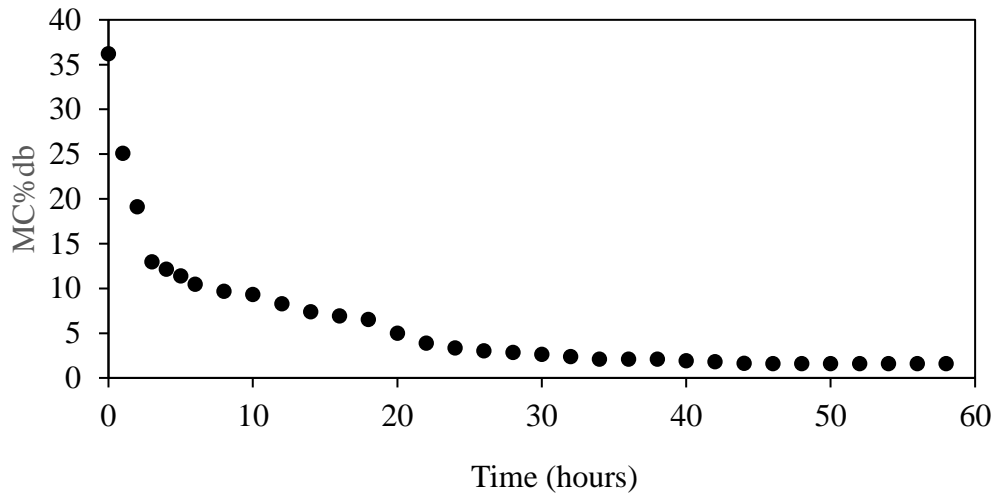


Figure 4.51 Moisture content evolution with time at 4.0 m/s, 60% RH, and 60°C.

The relative humidity influence on drying time at 60°C and 4.0 m/s is presented in Table 4.6 and Fig. 4.52.

Table 4.6 Influence of relative humidity on drying time.

Exp.	T °C	Ideal		Time (hours)	Realized		Quality
		inlet RH	Velocity (m/s)		Average Inlet RH%	Final MC db%	
4.1	60	50	4.0	47	38	1.4	Good
4.2	60	60	4.0	58	45	1.6	Good

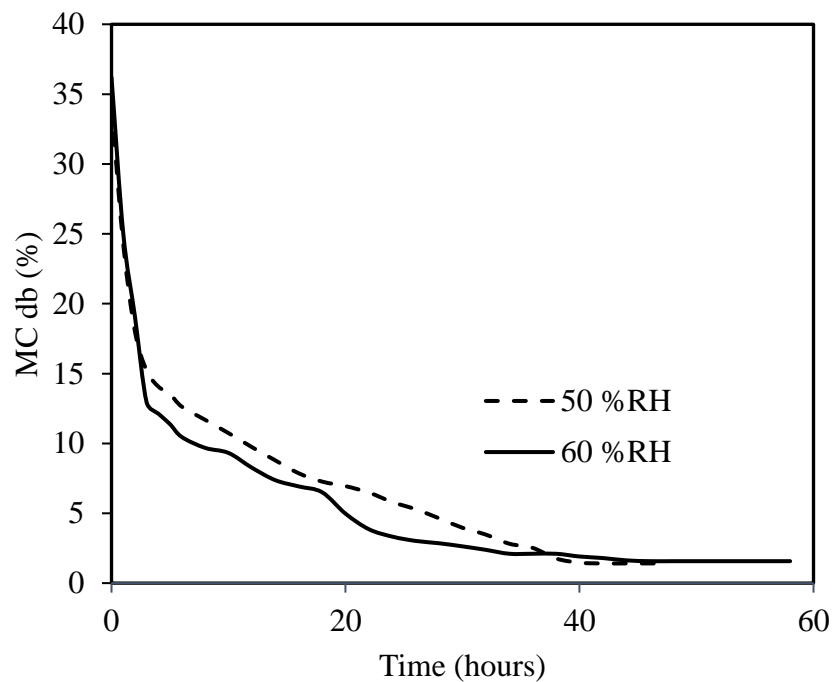


Figure 4.52 Moisture content variation at varying relative humidity.

The temperature and velocity in this set were kept constant at 60°C and 4.0 m/s, respectively. Because of the limitation in keeping the inside RH constant throughout the experiments, realized RHs were 38 % and 45%. For the case of RH at 45% drying rate was lower and the equilibrium moisture content was high at 1.6%. This is a result of the high holding RH in the system. For the case of 38%, the drying rate was increased and the EMC was lower at 1.4%. The lower EMC helps prevent microbial spoilage as a result of the reduced water activity in the rubber sheets. Hence, drying at the lowest possible RH is recommended for the best product and process optimizations.

The summary of all the experiments with their results are shown in Table 4.7. Regards to the effect of individual condition on the drying time, drying at the lowest possible relative humidity reduces both the drying time and the equilibrium moisture content of the sheets. However, in most cases, it is uncontrollable. Drying at higher temperature reduces the drying time. Also, drying at higher velocity reduces the drying time. Conclusively, in relation to all the experiment conducted as summarized

in Table 4.7, drying at temperature of 65°C with limit of 2.5 m/s was best for rubber sheet quality, as higher temperature and velocity affected the rubber sheets quality. The drying time was 38hours. For the second best condition, drying at temperature of 60°C and velocity of 4.0 m/s (the highest achievable velocity from experiment) was good for the rubber sheets quality. The drying time was 40 hours.

Table 4.7 Summary of all experimental results.

<b>Exp. No</b>	<b>T °C</b>	<b>Ideal inlet RH</b>	<b>Velocity (m/s)</b>	<b>Time (hours)</b>	<b>Realized Average Inlet RH%</b>	<b>Final MC db%</b>	<b>Quality</b>	
Exp.1	1.1	60	40	1.5	53	39	3	Good
	1.2	60	40	3.0	46	31	0.5	Good
	1.3	60	40	3.5	43	33	1	Good
	1.4	60	40	4.0	40	31	0.6	Good
Exp.2	2.2	65	40	3.0	39	18	65	Not good (2 sheets)
	2.1	65	40	2.5	38	18	65	Not good (3 sheets)
Exp.3	3.1	65	40	2.5	38	18	0.4	Good
	3.2	65	40	3.0	39	18	0.4	Not good (1 sheets)
	3.3	65	40	3.5	37	19	0.4	Not good (3 sheets)
	3.4	65	40	4.0	35	19	0.4	Not good (2 sheets)
Exp.	4.1	60	50	4.0	47	38	1.4	Good
	4.2	60	60	4.0	58	45	1.6	Good



## CHAPTER 5

### CONCLUSION AND RECOMMENDATION

#### 5.1 Conclusions

Numerical modelling and experiment to predict the shrinkage behavior of rubber sheets under convective drying using the finite element method have been carried out in the present study. Shrinkage percentage of about 9.1% was obtained for the operating condition. This proves that the shrinkage influence is significant and hence cannot be overlooked either in the real drying process or in the formulation of predictive models for natural rubber sheet drying. The predictive model can be used in quality index evaluation of the rubber sheet since the conjugate approach applied on the virtual work principle on the rubber sheet based on the operating parameter considered. Thus, the values and variation in the shrinkage stress and strain applied can provide insights on operating conditions that would predispose the rubber to formation of bubbles and damages. This can be better understood by using anisotropic shrinkage behavior. The experimental results are in good agreement with the simulation.  $R^2$  for moisture content and shrinkage are 0.9809 and 0.9991, while RSME are 0.0196 and 0.0091. The creation of a more realistic relationship between the free shrinkage strain and water concentration variation is important to improve the formulated model. The inference from the experimental studies show that drying at temperature of 65°C at 2.5 m/s is optimal for best rubber sheet quality as higher temperature and velocity affected the rubber sheets quality. The initial and final moisture content is 27% db and 0.4% db with drying time of 38 hours. For the second best condition, drying at temperature of 60°C and velocity of 4.0 m/s is also good for the rubber sheets quality with a drying time of 40 hours. The optimal RH cannot be accurately quantified because of the limitation of regulating the RH in the present study.

#### 5.2 Recommendations

To further improve the accuracy of the simulation, anisotropic shrinkage behavior needs to be considered for the rubber sheet drying. Viscoelastic model should be considered since it gives a more accurate model for rubber sheets. Also, the

Young modulus should be correlated to the variation in the moisture content for the time dependent study. Formulation of a variable dependent diffusion coefficient mathematical model should be considered instead of the constant used in Eq. (3.7). In regard to the drying system, the velocity should be increased by using a higher performance blower. Energy and exergy analysis of the system with recirculation ducts alongside the numerical analysis should be considered. Finally, 3D model would improve the simulation accuracy.

## REFERENCES

- [1] P. Arunmas, "Bankok post," in *Bangkok Post*, 2018.
- [2] Malaysian Rubber Board, "Natural rubber statistics 2016," pp. 26, 2016.
- [3] MREPC, "Rubber Industry Overview," *Malaysian Rubber Export Promot. Council.*, pp. 1-4, 2016.
- [4] T. Theppaya and S. Prasertsan, "Optimization of rubber wood drying by response surface method and multiple contour plots," *Drying. Technol.*, Vol. 22, No. 7, pp. 1637–1660, 2004.
- [5] K. Suntaro, S. Tirawanichakul, and Y. Tirawanichakul, "Determination of Isothermic Heat and Entropy of Sorption of Air Dried Sheet Rubber Using Artificial Neural Network Approach," *Appl. Mech. Mater.*, Vol. 541–542, pp. 374–379, 2014.
- [6] S. Tekasakul, M. Tantichaowan, Y. Otani, P. Kuruhingsa, and P. Tekasakul, "Removal of Soot Particles in Rubber Smoking Chamber by Electrostatic Precipitator to Improve Rubber Sheet Color," *Aerosol and Air Quality Research*, Vol. 6, No. 1, pp. 1-14, 2006
- [7] S. J. Kowalski and A. Pawłowski, "Intermittent drying of initially saturated porous materials," *Chem. Eng. Sci.*, Vol. 66, No. 9, pp. 1893–1905, 2011.
- [8] Q. Peng and W. Liu, "Inverse Analysis of Related Parameters in Calculation of Concrete Drying Shrinkage Based on ANSYS Design Optimization," *J. Mater. Civ. Eng.*, Vol. 25, No. 6, pp. 683–692, 2013.
- [9] M. Promtong and P. Tekasakul, "CFD study of flow in natural rubber smoking-room : I . Validation with the present smoking-room," *Applied Thermal Engineering*, Vol. 27, pp. 2113–2121, 2007.
- [10] B. Xia and D.-W. Sun, "Applications of computational fluid dynamics (CFD) in the food industry: a review," *Comput. Electron. Agric.*, Vol. 34, pp. 5–24, 2002.

- [11] P. S. Mirade, "Prediction of the air velocity field in modern meat dryers using unsteady computational fluid dynamics (CFD) models," *J. Food Eng.*, Vol. 60, No. 1, pp. 41–48, 2003.
- [12] E. Mathioulakis, V. T. Karathanos, and V. G. Belessiotis, "Simulation of air movement in a dryer by computational fluid dynamics: Application for the drying of fruits," *J. Food Eng.*, Vol. 36, No. 2, pp. 183–200, 1998.
- [13] P. Tekasakul and M. Promtong, "Energy efficiency enhancement of natural rubber smoking process by flow improvement using a CFD technique," *Appl. Energy*, Vol. 85, No. 9, pp. 878–895, 2008.
- [14] P. Tekasakul, R. Dejchanchaiwong, Y. Tirawanichakul, and S. Tirawanichakul, "Three-Dimensional Numerical Modeling of Heat and Moisture Transfer in Natural Rubber Sheet Drying Process," *Drying. Technol.*, Vol. 33, No. 9, pp. 1124–1137, 2015.
- [15] R. Dejchanchaiwong, Y. Tirawanichakul, S. Tirawanichakul, A. Kumar, and P. Tekasakul, "Conjugate heat and mass transfer modeling of a new rubber smoking room and experimental validation," *Appl. Therm. Eng.*, Vol. 112, pp. 761–770, 2017.
- [16] S. Curcio and M. Aversa, "Influence of shrinkage on convective drying of fresh vegetables: A theoretical model," *J. Food Eng.*, Vol. 123, pp. 36–49, 2014.
- [17] P. K. Mehta and P.J. M. Monteiro "Concrete: Microstructure, Properties, and Materials, Third ed., McGraw-Hill Companies, Inc New York, 2006.
- [18] R. Dejchanchaiwong, Y. Tirawanichakul, and S. Tirawanichakul, "Single-phase and multiphase models for temperature and relative humidity calculations during forced convection in a rubber-sheet drying chamber," *Maejo Int. J. Sci. Technol.*, Vol. 8, No. 2, pp. 207–220, 2014.
- [19] S. Sonthikun, P. Chairat, K. Fardsin, P. Kirirat, A. Kumar, and P. Tekasakul, "Computational fluid dynamic analysis of innovative design of solar-biomass hybrid dryer: An experimental validation," *Renew. Energy*, Vol. 92, pp. 185–

- 191, 2016.
- [20] The rubber manufacturers association, "International standards of quality and packaging for natural rubber grades RQPG (Green\_Book)." Rubber Manufacturers Association Inc., Washington, 1968.
- [21] F. O. Aguele, J. A. Idiaghe, and T. U. Apugo-nwosu, "A Study of Quality Improvement of Natural Rubber Products by Drying Methods," Vol. 3, pp. 7–12, 2015.
- [22] W. Versteeg, H. K., Malalasekera, *An Introduction to Computational Fluid Dynamics*, Second ed. John Wiley & Sons, Inc, New York, 2007.
- [23] E. K. Akpinar and Y. Bicer, "Modelling of thin layer drying kinetics of sour cherry in a solar dryer and under open Sun," *J. Sci. Ind. Res.*, Vol. 66, No. 9, pp. 764–771, 2007.
- [24] B. Wah, "Wiley Encyclopedia of Computer Science and Engineering" First ed., John Wiley & Sons, Inc, New York, 2008.
- [25] E. K. Akpinar, "Determination of suitable thin layer drying curve model for apple slices (variety-Golab)," *J. Food Eng.* 73, Vol. 73, No. 3, pp. 75–84, 2006.
- [26] T. Norton, B. Tiwari, and D. W. Sun, "Computational Fluid Dynamics in the Design and Analysis of Thermal Processes: A Review of Recent Advances," *Crit. Rev. Food Sci. Nutr.*, Vol. 53, No. 3, pp. 251–275, 2013.
- [27] T. Norton, D. W. Sun, J. Grant, R. Fallon, and V. Dodd, "Applications of computational fluid dynamics (CFD) in the modelling and design of ventilation systems in the agricultural industry: A review," *Bioresour. Technol.*, Vol. 98, No. 12, pp. 2386–2414, 2007.
- [28] J. D. Anderson, J. Degroote, G. Degrez, E. Dick, R. Grundmann, and J. Vierendeels, *Computational Fluid Dynamics: An Introduction.*, Springer-Verlag, Berlin, 2009.
- [29] D. M. Causon and C. G. Mingham, *Introductory Finite Difference Methods*

for PDEs. Ventus Publishing Aps., Frederiksberg, 2010.

- [30] W. F. Ames, *Numerical Methods for Partial Differential Equations*, 2nd ed. Academic Press, Inc., 1977.
- [31] B. Gustafson, H.O. Kreiss and J. Olinger, *Time dependent problems and difference methods.*, first ed., John Willey & Sons, Inc., New York, 1995.
- [32] J. M. Hyman, R. J. Knapp, and S. C. Scovel, "High order finite volume approximation of differential operators on nonuniform grids," *Phys. D*, Vol. 60, pp. 112–138, 1992.
- [33] H. Lomax, T. Pulliam, D. Zingg, and T. Kowalewski, "Fundamentals of Computational Fluid Dynamics," *Appl. Mech. Rev.*, Vol. 55, No. 4, p. B61, 2002.
- [34] Fluent, "*FLUENT 6.3 Getting Started Guide*," No. 5-8 , Fluent Inc. Lebanon, 2006.
- [35] J. Galindo, A. Tiseira, P. Fajardo, and R. Navarro, "Coupling methodology of 1D finite difference and 3D finite volume CFD codes based on the Method of Characteristics," *Math. Comput. Model.*, Vol. 54, No. 7–8, pp. 1738–1746, 2011.
- [36] A. Hrennikoff, "*The Finite Element Method in Application to Plane Stress*," First ed., ETH-Bibliothek, Zurich, 1968.
- [37] J. M. Meot, A. Briffaz, J. Jacquin, S. Rashidi, and Pruneau, "1D Axisymmetric Modeling of Shrinkage for Non- Porous Materials," COMSOL Conf.France, No. 1, pp. 2–5., 2015.
- [38] R. H. Pletcher, J. C. Tannehill, and D. A. Anderson, "Computational Fluid Mechanics and Heat Transfer 3rd ed., CRC Press, Boca Raton, pp. 2751, 2013.
- [39] K. J. Bathe and W. F. Hahn, "On transient analysis of fluid-structure systems," *Comput. Struct.*, Vol. 10, No. 1–2, pp. 383–391, 1979.

- [40] O.C.Zienkiewicz, R.L.Taylor, K. Morgan, O. Hassan, and N. P. Weatherill, "The Finite Element Method," *Acad. Eng. Polish Acad. Sci. Chinese Acad. Sci. Natl. Acad. Sci. Italy (Accademia dei Lincei)*, Vol. 35, No. 4, pp. 110–114, 1981.
- [41] K. J. Bathe, "Conserving energy and momentum in nonlinear dynamics: A simple implicit time integration scheme," *Comput. Struct.*, Vol. 85, No. 7–8, pp. 437–445, 2007.
- [42] T. Hughes, T ;Belytschko, *Computational methods for transient analysis.*, First ed., Elsevier Science publishing Inc. Amsterdam, 1983.
- [43] T. Kaewnok, Suttisak & Sirichai, "a Modeling of the Solar-Assisted for Rubber Smoked Sheets ( Rss ) System," *Engineering Journal of Siam Uiveristy*, Vol. 15. No. 9, pp. 27–30, 2007,
- [44] C. Tannehill, A. Anderson, and H. Pletcher, *Computational fluid mechanics and heat transfer*, Second ed., Taylor and Francis, Washington DC, 1997.
- [45] K. Jitjack, S. Thepa, K. Sudaprasert, and P. Namprakai, "Improvement of a rubber drying greenhouse with a parabolic cover and enhanced panels," *Energy and Building*, Vol. 124, pp. 178–180, 2016.
- [46] P. Tekasakul, R. Dejchanchaiwong, Y. Tirawanichakul, and S. Tirawanichakul, "Three-Dimensional Numerical Modeling of Heat and Moisture Transfer in Natural Rubber Sheet Drying Process," *Drying Technol.*, vol. 33, no. 9, pp. 1124–1137, 2015.
- [47] P. Somsila and U. Teeboonma, "Investigation of Temperature and Air Flow inside Para Rubber Greenhouse Solar Dryer Incline Roof Type by Using CFD Technique," *Adv. Mater. Res.*, Vol. 931–932, pp. 1238–1242, 2014.
- [48] L. P. Purba and P. Tekasakul, "Computational fluid dynamics study of flow and aerosol concentration patterns in a ribbed smoked sheet rubber factory," *Part. Sci. Technol.*, Vol. 30, No. 3, pp. 220–237, 2012.
- [49] Y. Pianroj, W. Werapan, S. Jumrat, P. Khongchana, and P. Rattanadecho, "A simulation study of drying kinetics for a natural rubber sheet by convective

- drying,” *Thammasat Int. J. Sci. Technol.*, Vol. 18, No. 4, pp. 9–16, 2013.
- [50] S. Kaewnok, S. Thepa and P. Namprakai, “A CFD Modeling of the Solar-Assisted Smoking System,” ICEE Conf. Thailand, pp. 27–31, 2015.
- [51] G. T. Mase and G. E. Mase, *Continuum for Engineers*. Second ed., CRC Press, New York 1999.
- [52] E. Stein, R. Borst and Thomas J.R. Hughes. *Encyclopedia of Computational Mechanics*, Vol. 1, JohnWiley & Sons, Newyork, 2004.
- [53] M. S. Gadala and J. Wang, A Practical Procedure for Mesh Motion in Arbitrary Lagrangian- Eulerian, *Engineering with Computers* Vol. 14, No. 3, pp. 223–234, 1998.
- [54] L. I. Sedov and P. G. Hodge, “Introduction to the Mechanics of a Continuous Medium,” *J. Appl. Mech.*, Vol. 33, No. 1, pp. 238, 1966.
- [55] L. Braescu and T. F. George, “Arbitrary Lagrangian-Eulerian method for coupled Navier-Stokes and convection-diffusion equations with moving boundaries,” *Proc. 12th WSEAS Int. Conf. Appl. Math.*, pp. 31–36, 2007.
- [56] F. Ahamed, “The Fluid Structure Interaction Analysis of a Peristaltic Pump, *Masters Thesis*, Lappeenranta University of Technology, Finland, 2015.”
- [57] C. W. Hirt, A. A. Amsden, and J. L. Cook, “An Arbitrary Lagrangian–Eulerian Computing Method for All Flow Speeds,” *J. Comput. Phys.*, Vol. 135, No. 2, pp. 203–216, 1997.
- [58] M. Souli and D. J. Benson, *Arbitrary Lagrangian-Eulerian and Fluid-Structure Interaction*. Second ed., John Wiley & Sons, Inc. Newyork, 2013.
- [59] N. Mastorakis, J. Sakellaris, and R. E. D. Eds, *Advances in Numerical Methods*, First ed., Springer, London, 2009.
- [60] P. G. Smith, *Introduction to Food Process Engineering*, Second ed., Springer, London 2011.



- [61] S. Curcio, M. Aversa, S. Chakraborty, V. Calabria, and G. Iorio, "Formulation of a 3D conjugated multiphase transport model to predict drying process behavior of irregular-shaped vegetables," *J. Food Eng.*, Vol. 176, pp. 36–55, 2016.
- [62] S. Curcio, "A Multiphase Model to Analyze Transport Phenomena in Food Drying Processes," *Drying Technol.*, Vol. 28, No. 6, pp. 773–785, 2010.
- [63] E. N. L. R. Byron Bird, Warren E. Stewart, *Transport Phenomena*, second ed., John Wiley & Sons, Inc, New York, 1961.
- [64] David C. Wilcox, "Turbulence-Modeling-for-CFD." first ed., Griffing printing, Glendale, California, 1993.
- [65] J. R. Welty, C. E. Wicks, R. E. Wilson, and G. L. Rorrer, *Fundamentals of Momentum, Heat, and Mass Transfer*, fifth ed., John Wiley & Sons, Inc, New York, 2008.
- [66] Y. A. Algabri, S. Rookkapan, and S. Chatpun, "Three-dimensional finite volume modelling of blood flow in simulated angular neck abdominal aortic aneurysm," *IOP Conf. Ser. Mater. Sci. Eng.*, Vol. 243, No. 1, pp. 1–7, 2017.
- [67] S. Tirawanichakul, S. Sanai, C. Sangwichien, Y. Tirawanichakul. "Parameters for the analysis of natural rubber drying," *Songklanakarin J. Sci. Technol.* Vol. 29 pp. 335–46, 2007.
- [68] Cambridge University Engineering Department, "*Materials data book*," 2003 ed. Cambridge press, Cambridge, 2003.
- [69] S. J. Kowalski, J. Banaszak, and A. Rybicki, "Plasticity in materials exposed to drying," *Chem. Eng. Sci.*, Vol. 65, No. 18, pp. 5105–5116, 2010.
- [70] D. Mihoubi and A. Bellagi, "Drying-Induced Stresses during Convective and Combined Microwave and Convective Drying of Saturated Porous Media," *Drying Technol.*, Vol. 27, No. 7–8, pp. 851–856, 2009.
- [71] V. P. Valdramidis, A. H. Geeraerd, and J. F. Van Impe, "Stress-adaptive

responses by heat under the microscope of predictive microbiology,” *Journal of Applied Microbiology* Vol. 103, No. 5, pp. 1922–1930, 2007.

- [72] ASABE/ASAE, Moisture Measurement- Unground Grain and Seeds, ASAE Stand. pp. 551, 1998.
- [73] A. Ekphon, T. Ninchuewong, S. Tirawanichakul, and Y. Tirawanichakul, “Drying Model, Shrinkage and Energy Consumption Evaluation of Air Dried Sheet Rubber Drying System for Small Enterprise,” *Adv. Mater. Res.*, Vol. 622–623, pp. 1135–1139, 2012.
- [74] R. Dejchanchaiwong, A. Arkasuwan, A. Kumar, and P. Tekasakul, “Mathematical modeling and performance investigation of mixed-mode and indirect solar dryers for natural rubber sheet drying,” *Energy Sustain. Dev.*, Vol. 34, No. 5, pp. 44–53, 2016.
- [75] L. Mayor and A. M. Sereno, “Modelling shrinkage during convective drying of food materials: A review,” *J. Food Eng.*, Vol. 61, No. 3, pp. 373–386, 2004.

**APPENDICES**

**APPENDIX A**

**ADDITIONAL RESEARCH PHOTOGRAPHS**



*Plate A1:* CLSM scanning and measurement of rubber sheet thickness.

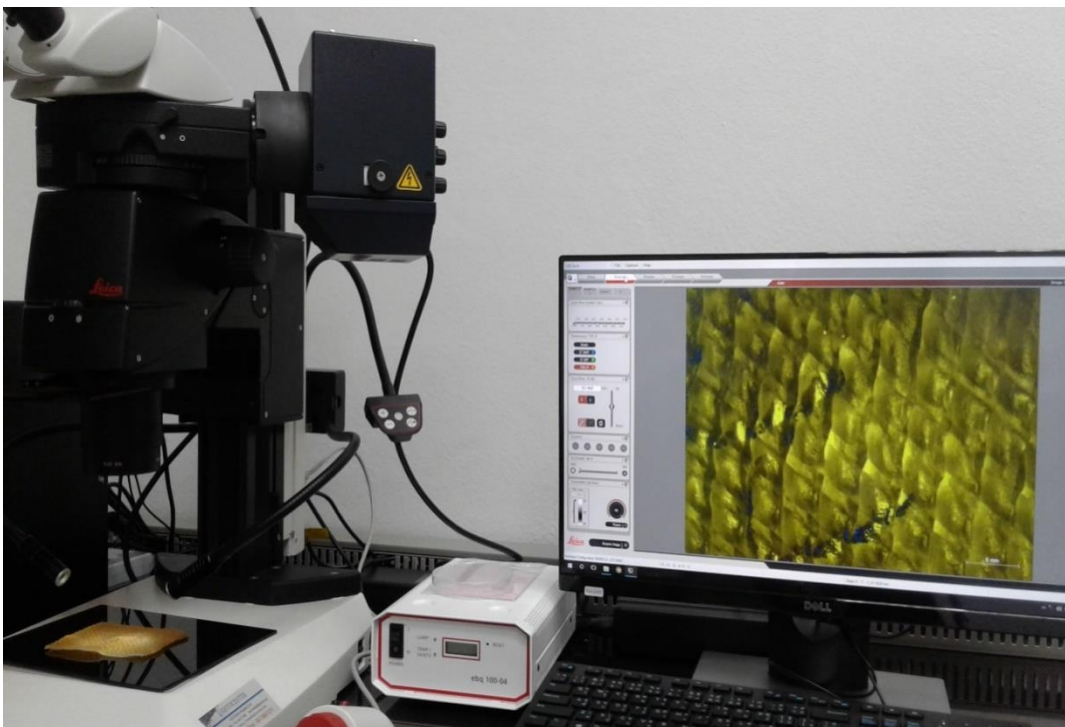


*Plate A2:* CLSM microstructural view of rubber sheet under analysis.



*Plate A4:* Fabricated rubber sheet drying system with the recirculation ducts.



*Plate A5:* Insulated rubber sheet dryer under experiments.

**APPENDIX B**  
**ABSTRACTS FOR PAPERS**

**Table E1.** Preview of papers and status

<b>S/N</b>	<b>Title</b>	<b>Type</b>	<b>Status</b>
1.	Historical and recent developments in natural rubber sheet drying technologies	Review paper	Rejected to repost to another journal; preparing for resubmission
2.	Applications of CFD Modeling in Natural Rubber Sheet Drying: A Review	Review paper	Final preparation stage. Not yet submitted to journal
3.	Influence of Shrinkage during Natural Rubber Sheet Drying: Numerical Modelling of Heat and Mass Transfer	Research Paper	Under review
4.	Parametric study and shrinkage modelling of natural rubber sheet drying using COMSOL multiphysics	Conference proceeding	Accepted for Oral Presentation at the 2 <sup>nd</sup> International Conference on Computational Fluid Dynamics in Research and Industry 3-4, Songkla, Thailand.
5.	Parametric study and shrinkage modelling of natural rubber sheet drying using COMSOL multiphysics	Research Paper	Accepted and published in IOP Conference series Elsevier (index in Scopus)



---

6.	Drying kinetics and parametric study of rubbers sheet drying optimization	Research Paper	Preparation stage. Not yet submitted to journal
7.	A Finite Element Analysis of Temperature and Moisture distributions in Rubber Sheet during Forced Convective Drying	Conference proceeding	Abstract submitted

---

## 1

**Historical and recent developments in natural rubber sheet drying technologies**

Clement Ajani<sup>a,c</sup>, Anil Kumar<sup>a,c</sup>, Racha Dejchanchaiwong<sup>b,c</sup> and Perapong Tekasakul<sup>a,c,\*</sup>

<sup>a</sup>Department of Mechanical Engineering,

<sup>b</sup>Department of Chemical Engineering,

<sup>c</sup>Energy Technology Research Center(ETRC),

Faculty of Engineering, Prince of Songkla University, Hatyai, Songkhla  
90112, Thailand

**Abstract**

Drying is essential part in the production of natural rubber sheet production . Different types of rubber drying systems have been developed for production of good quality rubber sheet and efficient energy utilization .Natural rubber sheet quality is affected as a result of unsteady operating conditions during drying .The rubber quality can be enhanced by designing drying systems to stabilize the operating conditions which also reduce the drying time and energy consumption .Therefore, there is a need for an updated bibliographic research on the rubber sheet drying systems .Air dried and smoked ribbed methods have been used for the drying of natural rubber sheets. Fire wood is burnt to generate hot smoke to dry rubber sheet in smoke house while solar energy is used air dried sheets\_Tremendous efforts have been put in by researchers to develop, design, and test these systems over the years .Major research breakthroughs and developments on the drying of rubber sheet systems and technologies is presented in this review .Relevant study on state and development in rubber sheet drying technology and drying systems around the world are also presented .

**Keywords** :Natural rubber sheet; Air drying; Smoked drying; Biomass; Solar energy; Rubber drying systems

## **Applications of CFD Modeling in Natural Rubber Sheet Drying: A Review**

Clement Ajani<sup>a,c</sup>, Anil Kumar<sup>a,c</sup>, Racha Dejchanchaiwong<sup>b,c</sup> and Perapong Tekasakul<sup>a,c\*</sup>

<sup>a</sup>Department of Mechanical Engineering,

<sup>b</sup>Department of Chemical Engineering,

<sup>c</sup>Energy Technology Research Center(ETRC),

Faculty of Engineering, Prince of Songkla University, Hatyai, Songkhla  
90112, Thailand

### **Abstract**

Computational fluid dynamics (CFD) is an important modelling technique used in handling complex drying systems and process. It is used for the analysis of heat, mass, energy and exergy transfers of the drying process. CFD is a veritable tool for natural rubber drying process and system optimization. The modelling technique is pertinent for the development, improvement, analysing and prediction of the efficiency of various rubber drying systems. The drying behavior of natural rubber sheets are tested and predicted using CFD modelling. Several parameters such as the temperature, flow field, moisture content of rubber sheets have been investigated using CFD with others such as quality, shrinkage, capillary effect, color degradation and microbial spoilage of natural rubber yet to be explored. CFD modelling techniques for the air-dried sheet and ribbed smoke sheet for Natural Rubber drying are reviewed in this paper. The finite difference, finite volume and finite element method in relations to NR drying are considered. The merits, future scope and prospects of CFD modelling of Natural rubber are also discussed.

**Key words:** Natural rubber, Drying, Review, CFD, ANSYS, COMSOL.

## 3

**Numerical Modelling of Heat and Mass Transfer: Influence of Shrinkage during Natural Rubber Sheet Drying**

Clement Ajani<sup>a,b</sup>, Stefano Curcio<sup>d</sup>, Racha Dejchanchaiwong<sup>a,c</sup> and  
Perapong Tekasakul<sup>a,b\*</sup>

<sup>a</sup>Energy Technology Research Center, Faculty of Engineering, Prince of Songkla University,  
Hatyai, Songkhla 90112, Thailand

<sup>b</sup>Department of Mechanical Engineering, Faculty of Engineering, Prince of Songkla  
University, Hatyai, Songkhla 90112, Thailand

<sup>c</sup>Department of Chemical Engineering, Faculty of Engineering, Prince of Songkla University,  
Hatyai, Songkhla 90112, Thailand

<sup>d</sup>Laboratory of Transport Phenomena and Biotechnology, Department of Computer Engineering,  
Modeling, Electronics and Systems, University of Calabria, 87036 Rende(CS), Italy

**Abstract**

A theoretical model describing the transport phenomena with the shrinkage effect involved in rubber sheet drying is presented. The conjugate approach involving the simultaneous transfer of momentum, heat and mass in the drying chamber and rubber sheet is investigated by a computational fluid dynamics method. An isotropic, linear elastic model is assumed, and the shrinkage is correlated with the moisture content evolution in the rubber sheet. The Arbitrary Lagrangian-Eulerian (ALE) method is used to solve the two-dimensional problem in accounting for the shrinkage effect. The shrinkage percentage is estimated at 9.1% and the moisture content is reduced from 0.4 db to 0.05 db at average holding relative humidity of 60% within 46 hours. The  $R^2$  for moisture content and shrinkage are 0.9809 and 0.9991, while RSME are 0.0196 and 0.0091, respectively. The formulated predictive model can be used as a quality index evaluation for rubber sheet and for drying process optimization. Water activity can also be used in locating regions that could be prone to microbial spoilage. The drying time is reduced compared to traditional drying of air dried sheet.

**Keywords:** Shrinkage; Computational fluid dynamics; Heat and mass transfer; Air dried sheet, Moisture content.

## **Drying kinetics and parametric study of rubbers sheet drying optimization**

Clement Ajani<sup>a,b</sup>, Stefano Curcio<sup>d</sup>, Racha Dejchanchaiwong<sup>a,c</sup> and Perapong Tekasakul<sup>a,b\*</sup>

<sup>a</sup>Energy Technology Research Center, Faculty of Engineering, Prince of Songkla University, Hatyai, Songkhla 90112, Thailand

<sup>b</sup>Department of Mechanical Engineering, Faculty of Engineering, Prince of Songkla University, Hatyai, Songkhla 90112, Thailand

<sup>c</sup>Department of Chemical Engineering, Faculty of Engineering, Prince of Songkla University, Hatyai, Songkhla 90112, Thailand

<sup>d</sup>Laboratory of Transport Phenomena and Biotechnology, Department of Computer Engineering, Modeling, Electronics and Systems, University of Calabria, 87036 Rende(CS), Italy

Natural rubber is one of the major exporting products in Thailand. However, a few researches have been carried out on the operating parameters to ensure fast drying of this product. Design and fabrication of a laboratory scale, rubber drying chamber of 0.7m×0.2m×2.0 m dimension, with a capacity of 4 rubbers in 2 rows and 2 columns was carried out. Experimental work was set to vary the velocity, temperature, and relative humidity from 1.5 to 4.0 m/s, 60 to 70°C and 20 to 60% respectively. The inference from the experimental studies showed that drying at temperature of 60°C is optimal for best rubber sheet quality, as higher temperature affected the rubber sheets quality. Drying at high velocity of 4.0m/s gave the optimal result in terms of the time reduction. Lastly, drying at the lowest possible relative humidity reduces both the drying, the equilibrium moisture content and consequently reduces the water activity that could result in microbial spoilage while in storage. The optimal operating condition from the experiment was 65°C, 2.5 m/s and 31% for the temperature and velocity. The initial and final moisture content is 0.27db (%) and 0.6db (%) with drying time of 38 hours. The drying time was reduced compare to traditional drying of air dried sheet.

## 5

## A Finite Element Analysis of Temperature and Moisture distributions in Rubber Sheet during Forced Convective Drying

Clement Ajani<sup>1,2</sup>, Stefano Curcio<sup>4</sup>, Racha Dejchanchaiwong<sup>1,3</sup> and Perapong Tekasaku<sup>1,2,\*</sup>

<sup>1</sup> Energy Technology Research Center,

<sup>2</sup>Department of Mechanical Engineering,

<sup>3</sup>Department of Chemical Engineering,

Faculty of Engineering, Prince of Songkla University, Hatyai, Songkhla 90112, Thailand

<sup>4</sup>Laboratory of Transport Phenomena and Biotechnology, Department of Computer Engineering, Modeling, Electronics and Systems, University of Calabria, 87036 Rende(CS), Italy

### Abstract

The present work is aimed at formulating a theoretical model of the heat and mass developed in rubber sheet under forced convective drying. The simultaneous heat and mass transfer of rubber sheet along with the momentum of flow under laminar conditions was investigated by a computational fluid dynamics (CFD) simulation. Half size of the drying room with a single rubber sheet is used in the 2D analysis. The velocity, and temperature is regulated at of 4.0 m/s and 60°C respectively. The system of non-linear time dependent partial differential equations is solved by Finite Elements Method. The expressions of physical and transport properties (air and rubber sheet) is formulated as functions of the local values of moisture content and temperature. The Velocity, temperature of the fluid, and moisture content profiles of rubber sheets is presented. Moisture content of the rubber sheets is accurately predicted, and agreement between the experimental and simulated results is acceptable. The proposed model therefore, represents a general tool capable of describing the behavior of rubber sheet under a wide range of process and fluid dynamic conditions.

**Keywords:** Computational fluid dynamics; Rubber sheet drying; Moisture content; Momentum

**APPENDIX C**

**VITAE**

## VITAE

**Name** Ajani Clement Kehinde

**Student ID** 5910120003

### **Educational Attainment**

Degree	Name of Institution	Year of Graduation
Bachelor of Engineering (Mechanical Engineering)	Federal University of Technology Minna, Nigeria.	2014

### **Scholarship Awards during Enrolment**

- Thailand Education Hub for ASEAN Countries (TEH-AC) award for Master's study year 2016-2017 (Grant No. TEH-AC 16/2016).
- Graduate School Dissertation Funding for Thesis.
- Natural Rubber Innovation Research Institute Funding, Prince of Single University (Grant No. ENG590305S)

### **List of Publication and Proceeding**

- Ajani, C., Kumar, A., Curcio, S., and Tekasakul, P. (2017). Parametric study and shrinkage modelling of natural rubber sheet drying using COMSOL multiphysics, IOP Conf. Ser.: Mater. Sci. Eng. 243 012012, doi:10.1088/1757899X/243/1/012012.
- Olugboji, O.A., Onuoha, O.J., Ajani, K.C. and Ogbor, M. A. (2017). Design and Construction of Polyvinyl Chloride Pipe Extrusion Machine, Nigeria Journal of Engineering and Applied Sciences (NJEAS) Vol. 4.
- Olugboji, O.A., Onuoha, O.J., Ajani, K.C. and Ogbor, M. A. (2017). External reliability and quality control analysis of Polyvinyl Chloride Pipe Produced Using Job Production Technique, Nigeria Journal of Engineering and Applied Sciences (NJEAS) Vol. 3.
- Abdulrahman, A.S., Ajani, K.C., Abubakar, I.A. (2016). Moringa Oleifera Root Extract as Green Corrosion Inhibitor of Mild Steel in Sulphuric Acid Environment, Nigeria Journal of Engineering and Applied Sciences (NJEAS) Vol. 2.
- Ajani, K.C., Abdulrahman, A.S., and Mudiare, E. (2014). Inhibitory Action of Aqueous Citrus aurantifolia Seed Extract on the Corrosion of Mild Steel in



- H<sub>2</sub>SO<sub>4</sub> Solution, World Applied Sciences Journal (WASJ), 31 (12): 2141-2147, DOI: 10.5829/idosi.wasj.2014.31.12.711.
- Olugboji, O.A., Yisa, J.J., and Ajani, K.C. (2015). Problem of calculating time delay between pulse arrivals, American Journal of Engineering Research (AJER) Volume-4, Issue-4pp-132-142.
  - Olugboji, O.A., Abolarin, M. S., Ohiemi, I.E., and Ajani, K.C. (2015). Modelling and Design of an Auto Street Light Generation Speed Breaker Mechanism. American Journal of Mechanical Engineering, vol. 3, no. 3: 84-92. doi: 10.12691/ajme-3-3-3.
  - Olugboji, O.A., Abolarin, M. S., Owolewa, M.O., and Ajani, K.C. (2015). Design, Construction and Testing of a Poultry Feed Pellet Machine, International Journal of Engineering Trends and Technology (IJETT), V22 (4), 168-170, 2015. ISSN: 2231-5381.
  - Olugboji, O.A., Abolarin, M.S., Yisa, J.J., Olaoluwa, P. S., and Ajani, K.C. (2015). Effect of Cutting Speed and Feed Rate on Tool Wear Rate and Surface Roughness in Lathe Turning Process", International Journal of Engineering Trends and Technology (IJETT), V22(4),171-173, ISSN: 2231-5381.
  - Abolarin, M. S., Olugboji, O.A., Yisa, J.J., Idoo, N R., and Ajani, K.C. (2015). Design Fabrication and Testing of a Motorized Paper Perforation Machine International Journal of scientific research and management (IJSRM) Volume 3 Issue 4 PP. 2619-2623.
  - Olugboji, O.A., Abolarin, M. S., Yisa, J.J., Muftau, A. G., and Ajani, K.C. (2015).Design and Construction of a Spring Stiffness Testing Machine, American ournal of Engineering Research (AJER) Volume-4, Issue-4, pp- 79-84.
  - Ajani, C., Kumar, A., Curcio, S., and Tekasakul, P. (2017). Parametric study and shrinkage modelling of natural rubber sheet drying using COMSOL multiphysics, 2<sup>nd</sup> Int. Conf. on Computational Fluid Dynamics in Research and Industry (CDFRI) 2017, pp.3.  
[http://cfdri.uthm.edu.my/images/Abstract\\_Book\\_V2-Final.pdf](http://cfdri.uthm.edu.my/images/Abstract_Book_V2-Final.pdf)
  - Abdulrahman, A.S., Ajani, K.C., and Augustine, J.J. (2015). Investigation of impressed current protection of underground steel pipeline, 1st International Engineering Conference Proceedings, SEET, pp. 226-232, <http://http://dSPACE.futminna.edu.ng/jspui/handle/1/4410>
  - Olugboji, O.A., Hale, J., Yisa, J.J., and Ajani, K.C. (2015) Application of Inverse method to Reconstruct the form of Pulse During Impulsive damage to Pipelines, 1st International Engineering Conference Proceedings, SEET pp. 415-423. <http://http://dSPACE.futminna.edu.ng/jspui/handle/1/4418>

- Oluyemi, O.D., Olugboji, O.A., Ekuase, L., Adewuyi, B.O., Oladele, I.O., and Ajani, K.C. (2016). Comparism on the reinforcing effect of Silica Gel Powder and Rice Husk Ash on the mechanical properties in high density polyethylene (HDPE) polymer composite, 4<sup>th</sup> International Conference on Natural Resources Development and Utilization, RMRDC.
- Olugboji, O.A., Abolarin, M. S., Ohiemi, I. E., Ajani, K.C. (2016). Development of a speed breaker mechanism for generating electrical energy by compression method, SEET Annual Conference.